ELECTRICAL CELL MANIPULATION IN MICROFLUIDIC SYSTEMS

Urban SEGER

diplômé en électronique physique de l'Université de Neuchâtel
de nationalité suisse et originaire d'Ermatingen (TG)

EPFL

ÉCOLE POLYTECHNIQUE
FÉDÉRALE DE LAUSANNE

Lausanne, EPFL
2006

Für d'Mama und de Papa.

Acknowledgements

I would like to acknowledge the following people who contributed to this work:

in suspension.

Special thanks to Martin Jordan. You have spent much time teaching me various aspects of cell biology - and thanks for the brainstorming sessions.

Marilia Panayiotou, David Calabrese, Juan-Carlos "Floyd" Sarria at EPFL or University of Lausanne. You were other external biologists who provided me with smart polymers, porating equipment and confocal gear. Thanks a lot.

Staff of the EPFL Centre of MicroNanoTechnology (CMI), particularly Georges-André Racine et Irène Magnénat. Thank you for the help in the clean-room production of the microfluidic devices.

Pascal Zbinden at the EPFL Atelier de l'Institut de Production et Robotique. There is no piece of equipment that this man could not fabricate - and improve. You're a genius.

Semesterwork and Diploma Students: Vincent Gfeller, Nicolas Demierre, Abdelaziz Hmamda, Frédéric Declercq, Marc Tonteling, Sylvan Schnydrig, Raphael Tornay. I really appreciate the help of each one of you during various phases of my thesis and I enjoyed having you around.

Rose-Mary Apothéloz. I don't know how you do that: always smiling and in good mood, but all requests and problems treated and solved in no-time. Thank you Rose-Mary!

Shady Gawad. You introduced me to the fascinating world of *the lab on a chip*, but I'd like to thank you also for the time spent out of work.

Arnaud Bertsch. Probably the hardest man in the world. (And one of the most useful.) Ta.

Pontus Linderholm, Thomas Braschler and Nicolas Demierre. That brainstorm-and-nail-down experience we shared was one of the richest I've had in my life so far. Thank you boys!

Matteo Leonardi and Mario Schlund. Keep on improving the world, mates - each one in his style ;-)

Mina Todorova and Raphael Tornay. Thank you for your thoughts and inspiration while sharing office and/or drinks.

Everybody (past and present) at LMIS4, but also at LMIS 1/2/3. Thank you all who helped me in any way during my period on BM's 3rd floor.

My friends in Lausanne and elsewhere. Thank you for your support and understanding, particularly in the last phase of my thesis.
Invaluable latest-phase support came from Jorge Bauzà. Thank you hombre!

My family in Bischofszell and St. Gallen. You have encouraged and supported me over the years. Without you, this work would not even have started. Thank you very much!

Isa. TmS.

The present document has been typeset in LaTeX using the free editor TeXShop by Richard Koch.

Abstract

This dissertation reports on the development of devices and concepts for electrical and microfluidic cell manipulation. In the present context, the term cell manipulation stands for both cell handling and cell modification.

The combination of microfluidic channels with micropatterned electrodes allows for the definition of highly localised chemical and electrical environments with spatial resolution comparable to the size of a cell. The devices fabricated in the frame of this thesis employ dielectrophoretic particle handling schemes such as deflection and trapping in pressure-controlled laminar flows to bring cells to - or immobilise them at - locations where cell altering electric fields or chemicals are present.

The two concepts of dielectrophoretic cell dipping and cell immersion are introduced and experimentally shown for erythrocytes dipped into Rhodamine in flow, and for individually immobilised Jurkat cells immersed by Trypan Blue.

Also, *in-situ* membrane breakdown in high intensity AC electric fields is optically assessed by efflux of haemoglobin (haemolysis) and by influx of nucleic stains or fluorescence-enhancing ions.

The most advanced experiments are on-chip medium exchange followed immediately by electropermeablisation or electrodeformation.

The majority of assays presented in this thesis are carried out in microfabricated glass-polymer-glass chips featuring top-bottom electrodes. The devices are fluidically controlled by external gas pressure bridging circuits.

Experimental evidence of the unmatched precision of pressure bridging is given in the case of micrometric xy positioning of cells at the intersection of two perpendicular microfluidic channels.

Further shown in this document are two methods of optical *in-situ* temperature measurements, important for bioinstrument characterisation. The two concepts of thermoquenching of a fluorescent dye and the original thermoprecipitation of "smart polymers" are used.

The last part of this work deals with the innovative, conceptual engineering tool *Liquid Electrode*. The general concept and its advantages over solid-state electrodes are given, followed by numerical particle tracking in the case of the novel lateral nDEP particle deflection. The chapter on liquid electrodes concludes with preliminary experimental results of buffer swapping of cells in flow and of AC electropermeabilisation of erythrocytes at frequencies far below the cut-off frequency of corresponding solid-state microelectrodes.

Résumé

Ce travail de doctorat présente le développement de dispositifs et de concepts pour la manipulation électrique et microfluidique de cellules. Dans ce contexte, le terme de manipulation de cellules se réfère à la manipulation ainsi qu'à la modification de cellules.

La combinaison de canaux microfluidiques et de microélectrodes permet de définir des environnements chimiques et électriques hautement localisés, de résolution spatiale comparable à la taille d'une cellule. Les dispositifs réalisés dans le cadre de cette thèse se fondent sur des méthodes de manipulation diélectrophorétique de particules (telles que la déflection et le piégeage en flux laminaire sous contrôle de pression), afin de guider les cellules - ou de les immobiliser - à des endroits spécifiques où des champs électriques ou composés chimiques altérants sont présents.

Les deux concepts de "cell dipping" diélectrophorétique et d'immersion de cellules sont présentés et démontrés expérimentalement pour des érythrocytes trempés dans de la Rhodamine en flux, ainsi que pour des cellules Jurkat immobilisées individuellement, immergées par du Trypan bleu.
De plus, la perméabilisation membranaire *in-situ*, provoquée par des champs électriques AC de haute intensité est évaluée optiquement par afflux d'hémoglobine (hémolyse) et par influx de colorant nucléique ou d'ions promoteurs de fluorescence.
Les expériences les plus avancées sont l'échange de milieu sur puce, suivi aussitôt par une électroperméabilisation ou une électrodéformation.

La majorité des essais présentés dans cette thèse sont réalisés sur des micropuces en verre-polymère-verre comprenant des électrodes en haut et en bas des canaux. Le contrôle fluidique de ces dispositifs se fait par des circuits externes de division de pression de gaz.

La précision inédite du système de contrôle par pression est mise en évidence dans le cas de positionnement planaire micrométrique de cellules à l'intersection de deux canaux microfluidiques perpendiculaires.

Ce document présente de plus deux méthodes pour la mesure optique de température *in-situ*, dont l'application est importante pour la caractérisation d'instruments biomédicals. Les deux concepts de thermoextinction (quenching) d'un colorant fluorescent et la précipitation de "smart polymers" sont utilisés.

La dernière partie de ce travail se concentre sur l'outil d'ingénierie innovateur qu'est *L'Electrode Liquide*. Le concept général et ses avantages par rapport aux électrodes solides sont présentés, ainsi que des simulations numériques de trajectoires de particules déviées par diélectrophorèse latérale. Le chapitre sur les électrodes liquides se conclut avec les résultats expérimentaux préliminaires de cellules passées en flux d'une solution tampon à une autre, et d'électropérméabilisation AC d'érythrocytes à des fréquences bien inférieurs à la fréquence de coupure d'électrodes solides de taille correspondante.

mots-clés: lab-on-a-chip, flux équilibré par pression, positionnement de cellules, diélectrophorèse, piégeage de cellules, cell dipping, resuspension, électroperméabilisation, lyse cellulaire, électrodéformation, fluorescence, effet Joule, thermoprécipitation, électrodes liquides

Contents

CONTENTS

Chapter 1

Introduction

Microtechnology allows for the fabrication of microfluidic devices with integrated channels and electrodes of dimensions that are comparable to the ones of biological cells. The widely promoted advantages of miniaturisation are high surface-to-volume ratio, fast response, potential for parallelism, disposability, etc. [Reyes DR 2002, Auroux PA 2002]. Additionally, the capability of producing small structures allows for novel experiments to be carried out. This is the playground on which this thesis took place: creating instruments for the research on a small number cells.

The resulting tools allow biologists to position still cells in an xy plane, to observe cells while changing their liquid environment or/and applying electric pulses, to deform cells by electric fields, and to expose or wash flowing cells to/from media.

1.1 Motivation

Nature was (and luckily still is) capable to bring up living organisms of inimaginable complexity. But no matter how large or small, all living organisms are assemblies of subunits, of which the smallest living

1

element is the cell.

Cells are tiny, and they may experience their microenvironment as extremely viscous [Purcell EM 1977]. With today's technologies, humans are capable of making systems that are as small (or even much smaller than) cells. It is therefore a natural approach to probe cells within their environment, or in systems that mimic the latter.

It is from this need that the community of technology specialised in microtool fabrication has evolved. So far, many biotechnology applications have benefitted from using miniaturised systems [Brody JP 1996, Voldman J 1999, Beebe DJ 2002]. In general, however, biologists make only moderate use of emerging tools. This is partly due to the lack of communication between engineers and life scientist, partly because the proposed tools are simply not yet versatile enough to carry out complex biological protocols.

The present thesis is a contribution to the field of advanced cell manipulation, meaning both handling and modification. *In-situ* cell manipulation is one of the building blocks required to get a cellular lab into a chip.

1.1.1 Cell Handling

If an object is handled (in the physical meaning), its position or orientation in respect to a geometrical reference system is changed; forces have to be applied on that object.

In our macrosopic everyday world, this is done by grabbing the object, bringing it somewhere and releasing it. We use the tool "hand" to exert forces on the object, part of the force is used to keep the object in contact with the tool, part is used for the actual displacement. If the object is delicate, the contact force should be as little as possible. Ideally, there should be no contact with the tool at all. In our macroscopic world, the use of contact-less object handling is limited. It only works for force fields that have an extended reach and it works only on "light" objects with a large surface-to-volume ratio (*e.g. autumn*

leaves handled by a gardener's blower).

In the microscopic world, inertia is of minor importance *and* a number of short-range forces become available. This makes the use of contactless object handling convenient. Cells in suspension can be handled by numerous types of external force fields ([Chiou PY 2005] and the references cited therein). Biological particle handling in microfluidics reviewed in section 1.2.

1.1.2   Cell Modification

Cells are modified when the composition of their membrane or interior is changed. Cell membranes have the role to separate the cytoplasm from the surrounding environment, but selectively let pass nutrition, metabolic byproducts and messenger molecules. Foreign (xeno)molecules do not spontaneously penetrate across the membrane into cells.

Viruses are natural cell modifiers, they have mechanisms to inject foreign material into cells and to use the cellular replication machinery to multiply that material.

Man is also interested in modifying and exploiting cells, be it for biotechnological production of proteins, be it for drug research. One possibility is to "misuse" biological mechanisms such as viral shuttles [Cepko CL 1984] or fusing liposomes [Schneider H 1980]. Membranes are also somewhat permeable to charge neutral complexes (DNA with added cations) [McCutchan JH 1968] and calcium-phosphate coprecipitated DNA [Graham FL 1973]. Other man-made cell modification mechanisms are rather "heavy duty" methods: they temporarily destabilise the cell membrane using detergents [Holz RW 1985], shear forces [McNeil PL 1989], laser pulses (optoporation) [Tsukakoshi M 1984] or electric field pulses (electroporation) [Neumann E 1982], or they use gene-guns [Klein TM 1987] or penetrate cells with micropipettes [Graessmann M 1983].

3

All of the methods cited above have their advantages and drawbacks in terms of efficiency, cost, biological side effects and health risks. They are therefore preferably applied for specific tasks [Hapala I 1997]. Cheaper, commercially available techniques with relatively low transfection rates such as the calcium phosphate method [Jordan M 1996] and in-cuvette electroporation are used for large scale transfection of yeast or bacteria cultures, whereas both the tedious manual microinjection and the hazardous viral methods [Micka B 2000] are employed for treating rare primary cells due to their high efficiency.

Electroporation relies on pore formation due to an applied external *electric* field, followed by diffusion of species and cell resealing. Electrical cell manipulation techniques are reviewed in section 1.4 and discussed in more detail in chapter 2.

1.1.3   Cell Deformation

Viscoelastic properties of cells yield information on the state of the cell membrane and the cytoskeleton, they are indicators of ageing, metabolic defects and other diseases [Elson EL 1988]. For instance, hereditary erythrocyte diseases such as Spherocytosis [Jacob H 1972] or Ovalocytosis [Mohandas N 1992] as well as metastatic competence of eukaryotes [Guck J 2005] change the elasticity of cells.
Numerous experimental methods assessing cell deformability have been developed in the past 50 years.

The two methods still most widespread today are filtering [Schmid-Schönbein H 1973, Reid HL 1976, Koutsouris D 1988] (including its sibling, the microfabricated lattice method [Brody JP 1995]) and micropipette aspiration [Mitchison JM 1954, Rand RP 1964, Hochmuth RM 2000]. Filtering is heavily size-dependent and micropipette aspiration is labour-intensive.
Single cell membranes can be indented locally by microneedles [McConnaughey WB 1980] and by scanning AFM tips [A-Hassan E

1998]; or they can be squeezed and pulled by microplate manipulation [Thoumine O 1997]. These methods poke adherent cells, or they contact suspended cells.

Other methods rely on supplementary particles to test the deformability of cells: either optically held beads attached to the membrane exterior [Sleep J 1999] or magnetically actuated beads priorly infiltrated into the interior of cells [Wang N 1993]. Both methods are labour-intensive and heavily invasive.

Shear stress methods in rheoscopes (cone-plate viscometers) are able to analyse populations of cells, if they rely on light scattering [Groner W 1980] or fast image acquisition [Dobbe JGG 2002].

The vast majority of contact-less methods rely on radiation and polarisation, they can either be of optical [Bronkhorst PJH 1995, Guck J 2001], acoustic [Kundu T 2000] or electrical [Friend AW 1975, Bryant G 1987, Engelhardt H 1988] nature.

1.2 Microfluidic Particle and Cell Handling

1.2.1 Pressure-Driven Flow

The most "intuitive" way of moving liquids in tubes is applying a pressure difference between in- and outlets, thus inducing a pressure-driven flow (PDF). In microchannels, the no-slip condition at walls limits flow rates and results in a parabolic flow profile following the law of J. Poiseuille (1797-1869). On one hand, this is an unwanted effect causing dispersion of sample plugs in the case of several separation techniques, on the other hand, the specific flow profile allows for microscopic applications of the field-flow fractionation technique (FFF) originally introduced by J. C. Giddings in the late 1960s [Giddings JC 1989]. In PDF, controlling flow rates or even switching flows between different in- and outputs is rather cumbersome, some experimental setups use hydrostatic pressure and valves, or active pressure

gauges. Optionally, negative pressure can be applied on outlet ports. A particular application of PDF is Sheath Flow: the addition of lateral buffer flow confines the sample and deviates/centres it. Sheath Flow centring is used as well in traditional as in microfluidic FACS (fluorescence activated cell sorting).

1.2.2 Electroosmotic Flow

At charged surfaces in contact with conductive liquids, electric double-layers are induced due to charge separation. While one charge unit is immobilised at the surface, the opposite charge can move freely within its layer. If an external E-field with components parallel to the surface is applied, this second layer of charges migrates in an electrophoretic manner and nearby liquid is dragged in the same direction by shear forces. If the surface-volume ratio is favourable (i.e. in small channels), a net flow occurs. This electroosmotic flow (EOF) has – in contrast to PDF – a flat "plug flow" profile [Manz A 1994]. EOF is well established in microfluidics, as flow directions can easily be switched by simply changing the driving E-field. Numerous applications include: separation of species in capillary electrophoresis (CE) where ions and molecules of different charges and sizes are separated by competing electrophoretic and EOF-driven hydrodynamic forces [Manz A 1992]; particle sorting in devices where an EOF is deflecting [Duffy DC 1999] or switching [Fu AY 1999] flows to specific outlets; or free flow particle trapping in nozzle/diffuser structures with competing EOF and PDF [Lettieri GL 2002].

1.2.3 Electrophoresis

Charged particles undergo electrostatic forces in an electric field. At a given DC field strength, they migrate at a certain velocity, depending on their polarity (i.e. net charge) and on their mobility (which is a function of their size (i.e. effective cross-sectional area) and of the

obstacles (i.e. viscosity) of the medium). The most popular biotechnology application of electrophoresis is the separation of DNA-fragments in slab-gel [Sugden B 1975]. Applications in the LOC-field include single-cell positioning for on-chip patch-clamping [Schmidt C 2000], DNA extraction from cell lysate [Prinz C 2002] and free flow electrophoresis in a so-called DNA prism [Huang LR 2002].

1.2.4 Dielectrophoresis

While electrophoresis is used to move *charged* particles in electric fields, dielectrophoresis (DEP) is employed to induce forces on *dielectric* (i.e. insulating) particles: In an inhomogeneous alternating E-field, particles can be attracted to (positive DEP) or repelled from (negative DEP) field-fringes regardless of their intrinsic charge. The direction of that force is given by the sign of the real part of the so-called Clausius-Mossotti factor (CM), which depends itself on the frequency-related properties of the particle and the surrounding medium. Due to its importance for our applications, DEP theory is treated separately in chapter 2.

Dielectrophoresis has first been thoroughly described in the landmark monograph by H.A. Pohl in 1978. In the early days of dielectrophoresis, only macroscopic manipulations were experimentally performable. Typical achievements are in the area of particle separation and preconcentration of suspended particles (see references cited in [Pohl HA 1978]). Two decades later, DEP has seen a true revival; MEMS technologies allow for producing small electrode structures thus for creating very fringing, high fields at low absolute voltages [Pethig R 1992, Schnelle T 1993, Huang Y 1991]. At the same time, electrochemical processes are of minor importance for AC signals whereas heating is an issue [Seger U 2005]. Under certain experimental conditions, even cell culturing in DEP-fields is reported [Glasser H 1998, Fuhr G 1994, Müller T 2003]. Microfluidic DEP applications for particle and cell handling should be divided into different sub-groups:

1. Introduction

DEP-Attraction Positive Dielectrophoresis (pDEP) can be employed to concentrate and collect particles suspended in low conductive media at specific locations in microfluidic devices [Pethig R 1992].

DEP-Deflection Negative Dielectrophoresis (nDEP) can repel particles in highly conductive media from electrode edges of parallel line-electrode configurations [Schnelle T 1999]. In particular, nDEP allows for the specific deflection of liposomes and cells within an unaffected buffer flow, thus for the establishment of funnels and switches [Fiedler S 1998], barriers [Docoslis A 1997] and semi-open traps [Gawad S 2002].

Fieldcages More complex 3D electrode configurations (e.g. octocages [Schnelle T 1993, Schnelle T 2000]) can be supplied with electric potentials in a way that a field gradient minimum is established in the centre of the cubic volume. At that location, individual particles – down to the size of viruses or single molecules [Muller T 1996] – can be trapped, held, and rotated (refer also to paragraph 1.3.3).

Travelling-Wave-DEP / Moving Particle Traps Electrode pairs can be used to create particle-repellent zones. If they are activated alternatively, particles can be moved in a peristaltic fashion, even in non-flow situations. One- and two-dimensional setups have been [Fuhr G 1991] / are being [Fuchs A 2002] developed, respectively.

Electrodeless pDEP-Trapping A "softer" way of trapping delicate particles by local gradients at pDEP conditions is to provoque field fringing by inserting isolating membranes with orifices in homogeneous electric fields, one possible application is the concentration of DNA [Chou CF 2002].

Electrodeless nDEP-Deflection Field concentration across small diameter structures in microchannels may also be employed in conjunction with negative DEP conditions. Very recently, particle deflection from insulating ridges at an angle in respect to the flow direction has been shown [Barrett LM 2005].

1.2.5 Standing Acoustic Waves

If a channel containing liquid and particles is acoustically excited at certain frequencies, standing acoustic waves (SAW) with nodes and anti-nodes are formed. These sites are preferably occupied by the particles, as they represent energetic minima, depending on the acoustic impedance of the latter. By adjusting the frequency, these trapping zones can be shifted in the direction of the acoustic radiation [Coakley WT 1989] and if a perpendicular flow is superimposed, particles can be separated and/or sorted [Johnson DA 1995, Yasuda K 2000, Nilsson A 2002].

1.2.6 Optical Tweezers

Another contact-less approach for trapping (dielectric) particles is using "optical forces" as shown by Ashkin *et al.* in 1986. Tiny objects can be held in the waist of a laser beam by negative light pressure [Ashkin A 1986]. If the beam is moved laterally, the particle is dragged with the moving spot and can be placed freely on an xy plane. Furthermore, when a highly condensed laser beam is used, the position of the particle can also be controlled in the z direction. Optical tweezers gives rise to many applications in biology [reviews] [Ashkin A 2000, Grier DG 2003]. They can be interferelessly combined with other cell handling methods, in particular with AC electric tools [Fuhr G 1998, Reichle C 2000].

1.2.7 Mechanical Tweezers

Microtechnology lends itself to fabricate micromanipulators having tips of the size of biological cells. Such mechanical tweezers – working in aqueous media – can be actuated thermally [Chan HY 2002], optically [Shoji M 2002], or electrochemically [Jager EWH 2000].

1.2.8 Cell Docking

Several concepts for immobilising cells with the help of particular channel structures can be employed. They are summarised in three categories:

Suction   A vertical or a horizontal channel constriction (e.g. hole) is constructed. Buffer containing cells is drawn in until a particle or cell occupies the site and remains there by suction (*e.g.* on-chip patch-clamp [Fertig N 2001] or drug injection [Yun KS 2002]).

Overpressure   Like in a filter, buffer is pressed through constrictions, which will eventually be blocked by particles. Clogging is a problem that can be addressed, an interesting approach is cell-docking on a dam between two adjacent parallel channels [Yang MS 2002].

Gravity   In some particular designs, sedimentation helps keeping cells in place. For instance, a miniaturised well improves stability of long-term positioning [Daridon A 2002].

1.2.9 Cell Adhesion

Other methods for immobilising biological cells take profit of or mimic intrinsic cell properties: Membrane proteins make cells adhere to surfaces, and/or selective receptors link to antibodies. These caracteristics have been employed to pattern cells on substrates as summarised

by numerous articles and reviews: cell adhesion depending on topography [Curtis A 1997], cell functionality regulated by photolithographically patterend macromolecules [Ito Y 1999], or direct cell patterning by soft lithography [Kane RS 1999] or microfluidics [Takayama S 1999, Chiu DT 2000].

1.2.10 Cell Casting

Cells may also be immobilised by casting them into an alginate hydrogel grown in a microchannel [Braschler T 2005].

1.3 Electrical Cell Characterisation

1.3.1 DEP Spectroscopy

In a given electric field, DEP forces depend alone on cell characteristics such as size, membrane capacitance and cytoplasmic conductivity (chapter 2). In particular, one type of cells might undergo pDEP whereas another one is subjected to nDEP. This means that by choosing such an environment (thus the buffer, the electrode geometries, and the frequency), two (electrically) very different cell types can be discriminated and separated by selective attraction of one and repulsion of the other [Becker FF 1995]. There are several limitations to cell discrimination based on pure DEP affinity [Gascoyne PRC 2002]. The process can for example be rendered more sensitive by combining nDEP force fields with field-flow fractionation [Giddings JC 1989], a technique termed DEP-FFF [Huang Y 1997]. Another concept of cell chromatography makes use of small differences in pDEP forces [Holmes D 2002]: Different cells in a constant flow follow different trajectories and accumulate at places which are specific for their dielectric properties and for their size.

1.3.2 DEP Levitation

A special case of DEP measurement methods is levitation [Kaler VIS 1990]. It allows acquiring dielectric spectra of *single cells* by suspending them by pDEP in a vertically inhomogeneous field against gravitation and keeping them in equilibrium. This permits to draw conclusions on the membrane capacitance as the real part of the CM-factor is assessed over a certain frequency domain. Refer to the book by Jones [TB 1995, p. 83] and the references cited therein for more detail.

1.3.3 Electrorotation

Electrorotation (ROT) has been first observed in 1892 by Arno and in 1893 by Weiler for rotating and static electric fields, respectively (source: [Jones TB 1995]). First modern experiments have been carried out in the early 1980s [Holzapfel C 1982, Arnold WM 1998]. Nowadays, ROT is extensively used for electrical *single-cell* (membrane) characterisation. The power of this technique – somewhat the twin brother of DEP, but often treated independently – has been underestimated for some time. ROT measurements are undertaken on dielectric particles in suspension subjected to rotating electric AC fields: a torque is induced on the particle which in turn will rotate in the same (co-field) or in the opposite (anti-field) sense of the external field, depending on the phase lag between the field and the induced dipole. As this torque is proportional to the imaginary part of the CM factor, important information on dielectric characteristics of single cells can be retrieved. Experimental setups with four [Huang Y 1991, Hughes MP 1998] or three [Arnold WM 1998] independent electrodes have been presented. ROT spectra of different cell types [Arnold WM 1982, Holzel R 1997,Yang J 1999, Muller T 1998], of live/dead cells [Engel J 1988, Huang Y 1992], of cells with ion enriched membranes [Kürschner M 1998 / 2000] and of osmotically swollen [Kiesel M 2006] cells have been assessed.

1.3.4 Coulter Counter

In a Coulter Counter [Coulter WH 1953], as proposed in the 1950s, suspended particles flow through an aperture from one fluidic reservoir to another: The presence of each particle on the orifice modifies its electrical resistance as a function of the liquid's conducitvity, the surface of the opening and the particle's volume. By assessing the electrical response of the system, counting and sizing of particles independently of their shape and optical properties is possible. Several micromachined implementations have been reported [Koch M 1999, Saleh OA 2001], one of them relying on apertures tuneable by sheath-flow [Nieuwenhuis JH 2003].

1.3.5 Impedance Measurements

Dielectric properties of particles may also be assessed via direct impedance measurements over a large range of frequencies. Instead of fitting levitational or rotational data with one of the corresponding models, the impedance of particles suspended in a known buffer medium and situated in a known detection zone can be assessed in a direct manner. Traditionally, mixtures of a large number of particles suspended in large volumes were characterized [Asami K 1996].

On single particle level, direct impedance measurement are achieved by modeling electric current pathways around and across the particle under question. A basic equivalent electrical model of a biological cell suspended in buffer reveals that a finite number of measurement points at discrete frequencies is sufficient to identify different types of cells having characteristic impedance signatures. Therefore, a cell in a detection zone may be identified using multiple frequency modulated signal injection, paired with signal retrieval and demodulation. This approach is intrinsically faster than complete frequency sweeps, it allows for particle detection and identification in a fraction of milliseconds.

Gawad [S 2001 / 2004] *et al.* have successfully implemented discrete frequencies impedance measurements in a micromachined flow-through device allowing for a cell recognition based on dielectric properties of the latter. In the same device, Cheung [K 2005] has demonstrated a label-free distinction between RBCs fixed with different levels of glutaraldehyde. If sorting capability and real-time decision algorithms are added to the existing method, a micromachined dielectricity-activated cell sorter (μDACS) will be able to isolate individual cells from mixed populations without the use of specific markers.

1.4 Electrical Cell Modification

1.4.1 Electrical Cell Lysis

There are several approaches to lyse cells (i.e. to destroy their membranes in order to liberate their content) that are employed in macroscopic devices on populations. Some methods have been adapted to microfluidics, in particular for flow-through or single cell lysis. This can be done chemically (membranes dissolved in a detergent [Li PCH 1997]), osmotically (cells bursting in low ionic strength buffer [Prinz C 2002]) or mechanically (cells passed in an array of sharp blades [DiCarlo D 2002]). The most currently used method in MEMS is however *electrical cell lysis*: cell membranes break down in high electric fields [Crowley JM 1973]. In 1999 a first micromachined cell lysis device with planar interdigitated sawtooth electrodes was presented [Lee SW 1999], today's chips are enhanced with other functionalties, such as DNA binding to beads [Ramadan Q 2006]

1.4.2 Electroporation

In an electroporating process, a biological cell is exposed to high electric field pulses that temporarily destabilize the cell membrane and render it highly permeable by the creation of transient pores. Molecules

can freely enter and leave the cell basically by diffusion [Chang DC 1992b]. Table 1.1 summarises major advances towards modern electroporation.

period	achievements, discoveries
1950s / 1960s	induction of large *membrane potentials* at poles of a cell in an external electric field
late 1960s	excessively high fields can cause *cell lysis*
early 1970s	dielectric breakdown of the cell membrane has a *threshold value*, demonstrated on RBCs and model membranes
late 1970s	establishment of the concept of *resealing membrane pores* preventing cell death
early 1980s	"explosion" of the electroporation technique as a transfection method: *introduction of a variety of molecules into a broad array of cell types*
late 1980s	utilisation of *symmetric electric pulse trains* at radio frequencies

Table 1.1: The early days of electroporation (source: [Chang D 1992b] and references therein)

Up to today experimental and industrial *in vitro* applications of electroporation encompass the insertion of virtually any biological or chemical entity (dyes, peptides, inhibitors, antibodies, or other macromolecules) into cells [Zimmermann U 1996] and of DNA into bacteria [Taketo A 1996]. The traditional main application is gene transfer (electrotransfection) [Neumann E 1982, Lurquin PF 1997].

Relatively new is the important trend of *in vivo* electroporation of tissues (e.g. specific drug delivery, local gene therapy, etc.). See [Dev SB 2000] for a review of and [Jaroszeski MJ 2000] for further information on that subject.

A novelty in the field of electric cell manipulation was reported by

Schoenbach [KH 2001] *et al.*: They observed that ultrashort high electric pulses can be tailored in order to target intracellular substructures – such as granules, organelles and the nucleus – without harming the outer cell shell.

Sukhorukov [VL 2005] *et al.* found that there are relationships between osmolar cell swelling vs. electrotransfection efficiency and cell volume regulation vs. survival rate.

Of particular interest with respect to this work are publications on single cell electroporation. Nolkrantz [K 2001] *et al.* as well as Rae [JL 2002] *et al.* used patch clamp techniques either with electrolyte-filled or with electrode-enhanced capillaries. Haas [K 2001] electroporated single neurons in-vivo with a similar method. Single-cells electroporation has been assessed [Ryttsen F 2000] and reviewed [Olofsson J 2003].

From the instrumentation point of view, today's researchers and operators face situations similar to the ones encountered by their colleagues of the early days when experimental setups consisted mainly of custom-made prototypes. [This hardware (such as cuvettes, electrical connectors, pulse-generators, etc.) evolved and became commercially available from start-up companies in the 1980/90s.] In today's research, when more specific detail is demanded, many experiments - in particular on tissues and single cells - require special material, which is again built by or in collaboration with the operator. Examples are the microporator presented by Teruel [MN 1999] *et al.* and the aluminium oxide filter by Müller [KJ 2001] *et al.*.

In the MEMS/Lab-on-a-Chip field, electroporation is the first choice for an in vitro transfection method for it has great potential for miniaturization (lower voltage, better joule heat dissipation, etc.). Several micromachined solutions have been presented: They either electroporate locally cultured cell populations [Lin YC 2001b / 2004] or sediments [He H 2006], they work as flow through devices for suspended cells [Lin YC 2001, Sarkar A 2004], or they perform patch clamp of individual cells on chip [Huang Y 1999 / 2001]. Shin [YS 2004] and

Khine [M 2005] use casted PDMS channels and external macroelec-
trodes.
Electroporation in microfluidic devices has recently been reviewed by
Fox [MB 2006] *et al.*

1. Introduction

Chapter 2

Electrical Cell Manipulation Theory

The underlying principle of both cell handling and cell alteration by electric fields is based on charge displacements inducing polarisations. In this chapter, an introduction to dielectrophoresis and electropermeabilisation is given.

2.1 Effective Dipole Moments of Spherical Particles

In this section, the induction of effective dipole moments on lossless and lossy dielectric spherical particles and shells by external electric fields will be discussed.

This approach – thoroughly described by T.B. Jones in *Electromechanics of Particles* [1995] – will allow the calculation of the dielectrophoretic force on polarised particles as well as the transmembrane voltage induced on biological cells.

2.1.1 The Dipole

Net Force on a Dipole A small dipole of charges $+q$ and $-q$, and of charge separation $\vec{d}$, is submerged in an electric field $\vec{E}(\vec{r})$. It has a net force

$$\vec{F} = q\vec{E}(\vec{r} + \vec{d}) - q\vec{E}(\vec{r}) \tag{2.1}$$

exerted on it (see Fig. 2.1).
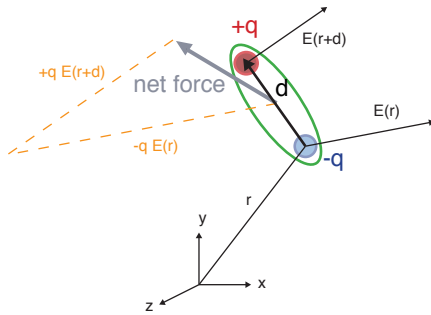
Figure 2.1: Force on a small dipole due to an electric field. The net force is the result of the vector addition of $+q\vec{E}(\vec{r}) - q\vec{E}(\vec{r} + \vec{d})$.

The infinitesimal dipole approximation

$$\vec{F}_{dipole} = q\vec{d} \cdot \nabla \vec{E} \equiv \vec{p} \cdot \nabla \vec{E} \tag{2.2}$$

can be obtained by developing the net force expression as Taylor series and by taking the limit $|\vec{d}| \to 0$, assuring that $q\vec{d}$ remains finite. $\vec{p} \equiv q\vec{d}$ is defined as the dipole moment.

Net Force occurs if the gradient of $\vec{E}$ is non-null, *i.e.* if the electric field is inhomogeneous.

Torque on a Dipole   A same dipole (charges $+q$ and $-q$, charge separation $\vec{d}$) submerged in a homogegeous electric field $\vec{E}$ experiences the net electrostatic torque

$$\vec{T}_\varepsilon = \frac{\vec{d}}{2} \times q\vec{E} + \frac{-\vec{d}}{2} \times (-q\vec{E}) \qquad (2.3)$$

Fig. 2.2 depicts this situation schematically.
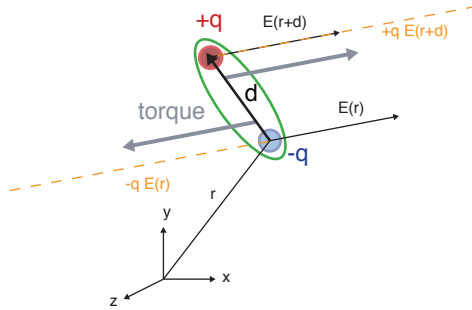
Figure 2.2: Torque on a small dipole due to an electric field.

This torque on a dipole may be rewritten in terms of the dipole moment $\vec{p}$:

$$\vec{T}_\varepsilon = q\vec{d} \times \vec{E} \equiv \vec{p} \times \vec{E} \qquad (2.4)$$

Torque occurs if $\vec{p}$ and $\vec{E}$ are not aligned.

Polarisation of Dielectric Material   Apart from acting electro-statically on charges, electric fields exert forces on polarised and po-larisable particles having no net charge. An example of a polar particle is the water molecule H_2O. As the two O-H bonds are at an angle, the H_2O molecule possesses a dipolar moment. As a result, exposed to a homogeneous electric field, water molecules do not move, but they will

orient themselves.

An *additional* electric field of inverse direction is superimposed to the original one; this is where the term *di*electricity comes from. Materials exhibiting dielectric properties are characterized by their relative permittivity or dielectric constant $\kappa_{\varepsilon i}$, which can take values between 1 (for vacuum) and 78 (for water).

Absolute permittivitty is expressed as $\epsilon_i \equiv \kappa_{\varepsilon i} \cdot \epsilon_0$, where $\epsilon_0 = 8.85 \cdot 10^{-12}$ F/m is the permittivitty of free space.

Dielectrics influence the frequency behaviour of the conductivity of a material submitted to alternating fields at angular frequency ω

$$\sigma_{AC} = \sigma_{DC} + j\omega\epsilon_1\epsilon_0 \ . \tag{2.5}$$

Dipole Induction in an External Electric Field A dipole moment of magnitude p in a dielectric medium of permittivity ϵ_1 gives rise to an electrostatic potential

$$\Phi_{dipole} = \frac{p\cos\theta}{4\pi\epsilon_1 r^2} \ , \tag{2.6}$$

where r and θ are the spherical coordinates.

The same way a permanent dipole is generating an electrostatic potential around it, an external potential can provoque a displacement of charges in/on a dielectric particle, hence *induce* an "effective" dipole itself.

2.1.2 Effective Dipole Moments of Lossless Dielectric Particles

Lossless Dielectric Sphere in an Electric Field A non-charged spherical particle of radius R and permittivity ϵ_2 is suspended in a medium of permittivity ϵ_1 and a uniform external electric field of

magnitude E_0 is applied. As only polarisation occurs, Laplace's equation $\mathrm{div}(\mathrm{grad}\Phi) = 0$ must be satisfied. The assumed solutions outside (uniform external field *plus* induced dipole field) and inside (uniform internal field) the particle are of the forms:

$$\text{outside}\ :\ \Phi_1(r, \theta) = -E_0\, r \cos\theta + \frac{A \cos\theta}{r^2},\ r > R \qquad (2.7)$$

$$\text{inside}\ :\ \Phi_2(r, \theta) = -B\, r \cos\theta,\ r < R \qquad (2.8)$$

The coefficients A and B depend on the boundary conditions at $r = R$:

- The radial component of the displacement flux vector ϵE_{radial} is continuous, i.e. $\epsilon_1(-\partial\Phi_1/\partial r) = \epsilon_2(-\partial\Phi_2/\partial r)$

- The electrostatic potential is continuous across the boundary, i.e. $\Phi_1 = \Phi_2$

Resolving the above equation yields

$$A = \frac{\epsilon_2 - \epsilon_1}{\epsilon_2 + 2\epsilon_1} R^3 E_0 \quad\text{and}\quad B = \frac{3\epsilon_1}{\epsilon_2 + 2\epsilon_1} E_0 \qquad (2.9)$$

If we replace p with p_{eff} in (2.6) and if we compare it with the induced dipole field term of (2.7), we find the relationship

$$p_{eff} = 4\pi\epsilon_1 A = 4\pi\epsilon_1 \Big(\frac{\epsilon_2 - \epsilon_1}{\epsilon_2 + 2\epsilon_1}\Big) R^3 E_0 \equiv 4\pi\epsilon_1 K(\epsilon_1, \epsilon_2) R^3 E_0 \quad (2.10)$$

The factor $K(\epsilon_1, \epsilon_2)$ is known as the Clausius-Mossotti function. Its numerical value range is $-0.5 < K \leq +1.0$, therefore the magnitude of the effective moment $|p_{eff}|$ is limited. The maximum possible value of p_{eff} for a single sphere is thus $p_{max} = 4\pi\epsilon_1 R^3 E_0$.

As long as the particle is perfectly dielectric, i.e. as long as no losses occur, the permittivities ϵ_1 and ϵ_2 as well as the Clausius-Mossotti factor are scalar quantities.

2. Electrical Cell Manipulation Theory

Lossless Dielectric Shell(s) in an Electric Field Placed in an external field of magnitude E_0, the electrostatic potentials of a layered sphere made of a core and a shell (Fig. 2.3) may be described by:

$$\text{outside} \; : \; \Phi_1(r,\theta) = -E_0 \, r \cos\theta + \frac{A \cos\theta}{r^2}, \; r > R_2 = R \qquad (2.11)$$

$$\text{shell} \; : \; \Phi_2(r,\theta) = -B \, r \cos\theta + \frac{C \cos\theta}{r^2}, \; R_2 > r > R_3 \qquad (2.12)$$

$$\text{inside} \; : \; \Phi_3(r,\theta) = -D \, r \cos\theta, \; r < R_3 \qquad (2.13)$$

By imposing continuity of the electric potential Φ and radial displacement flux $\epsilon(\partial\Phi/\partial r)$ at the two boundaries, the familiar expression for A is found:

$$A = \frac{\epsilon_2^{eff} - \epsilon_1}{\epsilon_2^{eff} + 2\epsilon_1} R^3 E_0 \qquad (2.14)$$
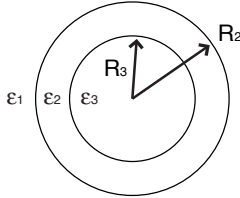
Figure 2.3: Layered Sphere made of a core with permittivity ϵ_3 and a shell with permittivitty ϵ_2, suspended in a medium of permittivitty ϵ_1, and submitted to an electric field E_0.

For calculations with shelled spheres, the same Clausius-Mossotti factor as for homogeneous spheres can be kept, and only the permittivity of the particle must be replaced by the effective permittivity ϵ_2^{eff} "seen

from the outside":

$$\epsilon_2{}^{eff} = \epsilon_2 \left\{ \frac{\left(\dfrac{R_2}{R_3}\right)^3 + 2\left(\dfrac{\epsilon_3 - \epsilon_2}{\epsilon_3 + 2\epsilon_2}\right)}{\left(\dfrac{R_2}{R_3}\right)^3 - \left(\dfrac{\epsilon_3 - \epsilon_2}{\epsilon_3 + \epsilon_2}\right)} \right\} \tag{2.15}$$

For multi-shelled spheres, this substitution procedure can be repeated at will, starting with the innermost shell.

Again, all permittivities and CM factors are scalar constants, the moment induced on the particle may be either negative or positive, but invariant.

2.1.3 Clausius-Mossotti Factors of Dielectric Particles with Loss

Lossy Dielectric Particle in an AC Electric Field If the particle under investigation is not perfectly "insulating" (= dielectric) a frequency dependent conductivity term σ has to be added to the description of the electric permittivity. Using the below definitions, the dielectric constants become complex:

$$\underline{\epsilon_i} \equiv \epsilon_i - j\frac{\sigma_i}{\omega} \ , \quad i = 1, 2, \dots, n \tag{2.16}$$

In the same manner, the Clausius-Mossotti function becomes complex, too:

$$\underline{K}(\underline{\epsilon_1}, \underline{\epsilon_2}) = \frac{\underline{\epsilon_2} - \underline{\epsilon_1}}{\underline{\epsilon_2} + 2\underline{\epsilon_1}} \tag{2.17}$$

The loss introduced by the conductivity term results in a phase lag of the dipole polarisation in an alternating field; it takes a certain amount of time to build up the charge displacements while being induced.

Therefore the complex Clausius-Mossotti factor contains information on magnitude *and* phase of the effective dipole moment, this information is frequency-dependent.

Application: Homogenous Spherical Particle in a Conducting Medium As a first practical example, we look at the frequency-dependent CM factor of a homogeneous, spherical particle as polystyrol beads are commonly used to test microfluidic devices.

The real and the imaginary part of the complex Clausius-Mossotti function $\underline{K}(\underline{\epsilon}_1, \underline{\epsilon}_2)$ for the frequency range of $f = 100\ \mathrm{Hz} \ldots 1\ \mathrm{GHz}$ are represented in Fig. 2.4.

One observes that positive values of the real part only occur in conjunction with poorly conducting solutions. In the case of PBS ($\sigma_{PBS} = 1.4\ \mathrm{S/m}$), the real part of the CM factor remains negative for all frequencies.
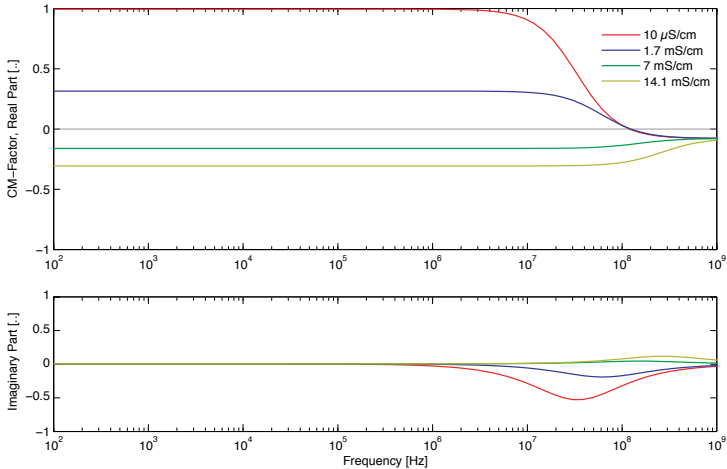
Figure 2.4: CM spectra (real and imaginary parts) of homogeneous beads in different suspension media.
(media: $\epsilon_1 = 78\,\epsilon_0$; $\sigma_1 = 0.001,\ 0.17,\ 0.7,$ or $1.4\ \mathrm{S/m}$ // beads: $\epsilon_2 = 60\,\epsilon_0$; $\sigma_2 = 0.4\ \mathrm{S/m}$)

Lossy Dielectric Sphere in an AC Electric Field, Charge Relaxation When loss is present, the dipole moment of the particle in a suddenly switched on field is delayed. Or, in a harmonically oscillating field, the dipole moment exhibits a phase lag.

This delay or lag depends, on the ratio between polarisability and depolarisation ability, generally expressed as:

$$\text{charge relaxation time} \ : \ \tau = \frac{\epsilon}{\sigma} \ : \ \frac{\text{permittivity}}{\text{conductivity}}$$

The depolarisation behaviour is ruled by an exponential relaxation law, $e^{t/\tau}$.

By the substitutions [Jones TB 1995]

$$\tau_{MW} = \frac{\epsilon_2 + 2\epsilon_1}{\sigma_2 + 2\sigma_1} \quad \text{and} \quad \tau_0 = \frac{\epsilon_2 - \epsilon_1}{\sigma_2 - \sigma_1} \tag{2.18}$$

the complex CM factor of the previous paragraph becomes:

$$\underline{K}(\underline{\epsilon}_1, \underline{\epsilon}_2, \omega) = \left(\frac{\sigma_2 - \sigma_1}{\sigma_2 + 2\sigma_1} \right) \left[\frac{j\omega\tau_0 + 1}{j\omega\tau_{MW} + 1} \right] \tag{2.19}$$

τ_{MW} is the relaxation time constant of the Maxwell-Wagner surface polarisation, is associated with the accumulation of free charge at the at the particle-medium interface.

Lossy Dielectric Shell in an AC Electric Field The approach of representing shelled spheres by homogeneous spheres having an apparent permittivity, as seen in the paragraph for lossless shells, remains valid for lossy ones. Again by taking the complex values $\underline{\epsilon}_i \equiv \epsilon_i - j\sigma_i/\omega$ the effective permittivity is given by

$$\underline{\epsilon}_2^{eff} = \underline{\epsilon}_2 \left\{ \frac{\left(\dfrac{R_2}{R_3} \right)^3 + 2\left(\dfrac{\underline{\epsilon}_3 - \underline{\epsilon}_2}{\underline{\epsilon}_3 + 2\underline{\epsilon}_2} \right)}{\left(\dfrac{R_2}{R_3} \right)^3 - \left(\dfrac{\underline{\epsilon}_3 - \underline{\epsilon}_2}{\underline{\epsilon}_3 + \underline{\epsilon}_2} \right)} \right\} \tag{2.20}$$

2. Electrical Cell Manipulation Theory

The scalar values of apparent permittivity ϵ_{eff} and conductivity σ_{eff} may be extracted from the above relationship using the inverse definition of the complex permittivity. They are dependent upon frequency:

$$\epsilon_2^{eff}(\omega) \equiv \Re\{\underline{\epsilon_2}^{eff}\} \text{ and } \sigma_2^{eff}(\omega) \equiv -\omega\Im\{\underline{\epsilon_2}^{eff}\} \qquad (2.21)$$

Lossy Dielectric Thin Shell in an AC Electric Field, Equivalent Electric Circuit Shells with thicknesses $\Delta \ll R$, able to support a certain electropotential drop across them, may be modelled in terms of capacitance $c_m = \epsilon_m/\Delta$ and conductance $g_m = \sigma_m/\Delta$, both per unit surface. The index m stands here for membrane, as biological cells are typical examples of thin shell particles.

For the current passing through the thin shell, electrostatic potential solutions may be obtained by using the same set of equations as for homogeneous spheres (2.7) / (2.8), but with adapted current continuity conditions at the interface at $r = R$:

- The radial component of the displacement flux vector $\underline{\epsilon}E_{radial}$ is continuous,
  i.e. $\underline{\epsilon}_1(-\partial\underline{\Phi}_1/\partial r) = \underline{\epsilon}_2(-\partial\underline{\Phi}_2/\partial r)$

- The electrostatic potential drops across the boundary,
  i.e. $(\underline{\Phi}_1 - \underline{\Phi}_2)(j\omega c_m + g_m) = -j\omega\underline{\epsilon}_1\underline{E}_{1,radial}$

The resulting effective permittivity of the thin-shelled particle is

$$\underline{\epsilon}_2^{eff} = \frac{\underline{c}_m R\,\underline{\epsilon}_2}{\underline{c}_m R + \underline{\epsilon}_2} \text{ , with } \underline{c}_m \equiv c_m - j\,\frac{g_m}{\omega} \qquad (2.22)$$

A sketch of the situation and the equivalent electric circuit are given in Fig. 2.5.
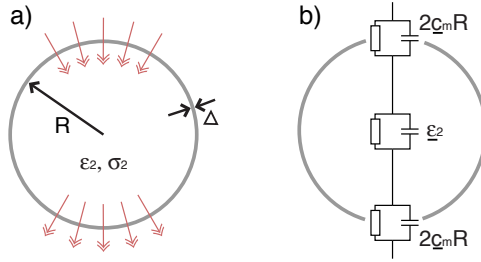
Figure 2.5: Schematic of series current paths across the membrane and cytoplasm of a cell (a) and its equivalent electric circuit (b).

2.1.4 Clausius-Mossotti Factors of Biological Cells

Application: Lossy Spherical Cell in Saline Solution, The Protoplast Model For illustration of the Clausius-Mossotti factor of a biological cell or vesicle, a spherical volume of cytoplasm delimited by a thin capacitive membrane is considered (see illustration in Fig. 2.6).
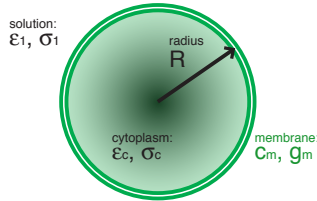
Figure 2.6: Electrical parameters for the protoplast model featuring a thin membrane of bilipid layer capacitance c_m and conductance g_m.

The expression for the cytoplasm's permittivity, given by $\underline{\epsilon}_c = \epsilon_c - j\sigma_c/\omega$ is complex, whereas the membrane capacitance stays scalar if the conductance g_m is supposed to be null: $\underline{c}_m = c_m + j0$.

According to the protoplast model by Kaler [KVIS 1990] and Jones,

the apparent effective permittivity of a soft-walled cell $\underline{\epsilon}_p^{eff}$ is given by

$$\underline{\epsilon}_p^{eff} \approx c_m R \frac{j\omega\tau_c + 1}{j\omega(\tau_m + \tau_c) + 1} \ , \ \text{with} \ \ \tau_m \equiv \frac{c_m R}{\sigma_c} \ \text{and} \ \tau_c \equiv \frac{\epsilon_c}{\sigma_c} \quad (2.23)$$

where c_m is the membrane capacitance per unit surface, R the radius of the cell, τ_m and τ_c are respectively the relaxation times of the membrane and the cytoplasm, and σ_c and ϵ_c are respectively the conductivity and permittivity of the cytoplasm. The above expression assumes a membrane thickness of small dimension compared to the cell radius and a transmembrane conductance of negligible magnitude. Introducing $\underline{\epsilon}_p^{eff}$ as $\underline{\epsilon}_2$ into the general expression of the Clausius-Mossotti factor (2.17) yields an analytical solution:

$$\underline{K}(\omega) = -\frac{\omega^2(\tau_1\tau_m - \tau_c\tau_m') + j\omega(\tau_m' - \tau_1 - \tau_m) - 1}{\omega^2(\tau_c\tau_m' + 2\tau_1\tau_m) - j\omega(\tau_m' + 2\tau_1 + \tau_m) - 2} \quad (2.24)$$

with $\tau_1 = \epsilon_1/\sigma_1$ and $\tau_m' = c_m R/\sigma_1$. It is important to note that the CM factor of a protoplast depends on the cell size R.

As an illustration of the above formula, its real part is plotted in Fig. 2.7 as a function of frequency as well as conductivity of the solution. The plot shows important negative values for frequencies below 10 kHz and a weak negative values for frequencies above 100 MHz. The amplitude of positive values at intermediate frequencies vanishes with increasing conductivity σ_1 of the solution.

2.2 Dielectrophoresis on Spherical Particles

In the previous section, polarisation of spherical particles has been discussed using Jones' effective dipole moment induction methodology. In the present section, dielectrophoresis is introduced, the establishment of *time averaged net forces*.
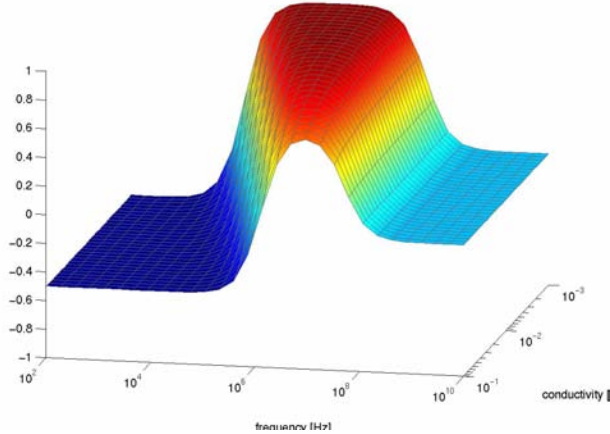
Figure 2.7: Real part of the Clausius-Mossotti function for the protoplast model plotted as a function of frequency and medium conductivity.
(frequency: $f = 100$ Hz ... 10 MHz // suspension medium: $\epsilon_1 = 78\,\epsilon_0$; $\sigma_1 = 0.001$ ... 0.1 S/m // cytoplasm: $\epsilon_c = 78\,\epsilon_0$; $\sigma_c = 0.5$ S/m // membrane: $c_m = 1\ \mu F/cm^2$, $g_m = 0$ // dimension: $R = 2\mu m$)

2.2.1 Dielectrophoretic Phenomenology

The force generated by the interaction of a dipole with an electric field is described in the dipole approximation $\vec{F}_{dipole} = \vec{p} \cdot \nabla \vec{E}$ from page 20. Using the effective dipolar moment of (2.10) and the product rule of derivatives and gradients $\nabla(f \cdot g) = \nabla f \cdot g + f \cdot \nabla g$, the net forces formula becomes the classic expression for DC dielectrophoresis force on a lossless dielectric sphere

$$\vec{F}_{DEP} = 2\pi\epsilon_1 R^3 (\frac{\epsilon_2 - \epsilon_1}{\epsilon_2 + 2\epsilon_1})\nabla E_0^2 \ . \tag{2.25}$$

2. Electrical Cell Manipulation Theory

If we consider a time-dependent form $\vec{F}_{dipole}(t) = \vec{p}(t) \cdot \nabla \vec{E}(t)$ and a general expression for the CM factor, the time-averaged DEP force on a lossy particle in a slightly inhomogeneous alternating field becomes

$$\langle \vec{F}_{DEP}(t) \rangle_t = 2\pi\epsilon_1 R^3 \, \Re\{\underline{K}(\omega)\}\nabla E_{rms}^2 \tag{2.26}$$

The dissymmetry of the external electric field (see Fig. 2.8) is necessary because the DEP force vector is aligned in the direction of the *electric field intensity's gradient* ∇E_0^2.
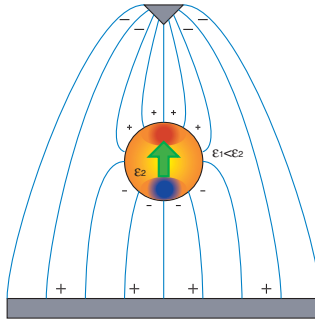
Figure 2.8: A polarisable particle in an inhomogeneous electric field is inhomogeneously polarised and a net force following the field gradient occurs. In the present schematic, the particle is more polarisable than the medium, resulting in positive dielectrophoretic behaviour.

Equations (2.25) and (2.26) suggest furthermore that the DEP force vector is proportional to the particle's volume ($\sim R^3$) and to the permittivity ϵ_1 of the surrounding medium. The sign of the direction is given by the *real part* of the Clausius-Mossotti factor; in fact, the following convention arises:

- $\Re\{\underline{K}(\underline{\epsilon}_1, \underline{\epsilon}_2, \omega)\} > 0$
  pDEP, *positive* dielectrophoresis, force *towards* higher field strengths,

- $\Re\left\{\underline{K}(\underline{\epsilon}_1, \underline{\epsilon}_2, \omega)\right\} < 0$
  nDEP, *negative* dielectrophoresis, force *away from* higher field strengths.

2.2.2 DEP-Crossover Frequency

Whether a lossy particle experiences positive or negative dielectrophoresis is a function of the particle's and medium's electric properties *and* of frequency.

In particular, for a given particle, there exists a frequency at which no dielectrophoretic forces are present, *i.e.* the frequency at which the real part of the CM factor changes sign. This crossover frequency is easily observable experimentally. Theoretically it can be calculated imposing $\Re(\underline{K}) = 0$. Expanding the complex Clausius-Mossotti factor of expression (2.17) with the conjugate of its denominator, the crossover frequency f_c of a lossy homogeneous particle can be calculated analytically. (The "inverted" term $(\sigma_1 - \sigma_2)$ in the numerator is due to j^2.)

$$f_c = \frac{1}{2\pi} \sqrt{\frac{(\sigma_1 - \sigma_2)(\sigma_2 + 2\sigma_1)}{(\epsilon_2 - \epsilon_1)(\epsilon_2 + 2\epsilon_1)}} \tag{2.27}$$

This property of null force may be employed to separate a mixture of two or more cell types in stationary and flow-through devices.

2.3 Electrodeformation

Electrodeformation forces on spherical shells are governed by the Clausius-Mossotti factor $\underline{K}$, which is a measure of polarisability. Charge accumulation induced by an external field E leads to electrostatic stress on elastic particles. For small deformations, it can be shown [Sukhorukov VL 1998] that the elastic stain $\Delta l/l$ is

$$\Delta l/l = \alpha E^2 \Re(\underline{K}) , \tag{2.28}$$

33

where the proportionality factor α depends on the particle or cell type. Electrodeformation occurs - unlike DEP - also in homogeneous electric fields. AC cell deformation is frequency-dependent: following the positive or negative sign of the real part of $\underline{K}$, cells are streched or compressed, respectively.

2.4 Electropermeabilisation

2.4.1 Electroporation

Until today, the electroporation (EP) process is not yet fully understood [Teissie J 2005]. Numerous theories have been proposed on this subject. They vary in terms of creation explanations and resealing kinetics but all agree on the concept of transient pores. Spectacular evidence of such pores and their disappearance in electroporated RBCs has been revealed by the rapid deep freezing experiments of Chang *et al.* [DC 1990, 1992c].

Fundamental research topics focus on four different areas according to Ho [SY 1996] and Mittal:
(A) Measurements of transmembrane potentials (TMP)
(B) Dynamics of electroporation such as time sequence, properties of electropores such as size, structure, and population
(C) Membrane permeabilisation and breakdown theory
(D) The effects of secondary factors such (ion type, cell growth stage, temperature, chemicals) on electroporation

(A) Transmembrane potentials   TMPs are measured by staining the cell membrane with a voltage-sensitive fluorescent dye. The change of colour induced by the electric field is recorded by high-speed video microscopy [Gross D 1986, Hibino M 1993].
Experiments have shown that membrane rupture is induced when the

TMP – physiologically between -60 and -100 mV – is raised to values in the range of 1 Volt.

(B) Dynamics of electroporation   Straightforward control of EP is carried out on cell populations with gene expression assays, with turbidity changes in cell suspensions, or with FACS measurements (detecting the incorporation of fluorescent molecules). Individual cell responses are assessed with charge-relaxation studies in patch clamp experiments [Ryttsen F 2000].

In (A) described image analysis and rapid freezing methods allow for the characterisation of dynamics (i.e. the time sequence of electropores), they are summarised in Table 2.1.

time elapsed	events
0.01 ns	molecular collision within lipid membrane
0.1 to 1 μs	cell and cell membrane charging times
0.1 to 1 μs	membrane discharging times: reversible
1 to 10 μs	membrane discharging times: membrane rupture
0.1 ms to 2.8 h	membrane recovery; metastable pore

Table 2.1: Electroporation time scales (source: [Ho SY 1996])

Another aspect of EP dynamics is the study of population densities of electropores [Sowers AE 1986]. It is believed that they reflect the distribution of membrane inhomogeneities due to the cell skeleton and to membrane proteins. Theories are based on energy considerations [Smith KC 2004], the same is valid for pore disappearance kinetics [Saulis G 1997].

(C) Permeabilisation theory   The most widely accepted *Molecular Reorientation Theory* [Benz R 1979, Zimmermann U 1982, Glaser

RW 1988, Weaver JC 1996] claims that thermally induced hydrophobic pores are enlarged by the presence of an E field and thus rendered hydrophilic by an energetically more favourable reorientation of the bilipids of the membrane (Fig. 2.9). Recent molecular dynamics simulations support the molecular reorientation theory [Tarek M 2005].

(D) Secondary factors A last research branch concentrates on the investigations of other parameters (such as medium conductivity [Djuzenova CS 1996] and osmolarity [Barrau C 2004], cell density and arrangement [Pavlin M 2002], growth phase of the cells [Hojo S 2003], etc.) on the electroporation process.

2.4.2 DC Transmembrane Voltage

Polarisation of cells leads to voltage drops across the membrane. If a certain threshold voltage is exceeded, there is membrane integrity breakdown. Transmembrane voltage $\Delta\psi$ induction is locus-dependent:

$$\Delta\psi = 1.5 \cdot R \cdot E_0 \cdot \cos\theta + \text{Resting Potential} . \qquad (2.29)$$

It depends on the cell radius R, the external field strength E_0, and on the polar angle θ in respect to the field direction (Fig. 2.10, top). As a consequence of the intrinsic negative cell resting potential, the voltage drop across the membrane at the pole facing the anode is higher than the drop at the cathode pole (Fig. 2.10, bottom) [Saulis G 1993c]. This effect is experimentally measurable [Golzio M 2002].

2.4.3 AC Transmembrane Voltage

Dipole inductions on cells in time-varying fields also lead to voltage drops over their membranes, but they are frequency dependent. As the cell membrane acts as a capacitor between the cytosol and the

suspension medium, transmembrane voltages can only be built up below a cut-off frequency. In the case of a spherical cell of radius r, the AC transmembrane voltage $\Delta\psi$ is given by [Holzapfel C 1982]:

$$\Delta\psi = \frac{1.5 \cdot R \cdot E_0 \cdot \cos\theta}{\sqrt{1 + (\omega\tau)^2}} \; , \tag{2.30}$$

where ω is the pulsation of the field, and the τ the time constant given by [Jeltsch E 1979]:

$$\tau = r \cdot C_m \cdot (\rho_{int} + \rho_{ext}/2) \; . \tag{2.31}$$

C_m is the specific cell membrane capacitance, and ρ_{int} and ρ_{ext} are the cytosol and suspension medium resistivities, respectively.

The frequency behaviours of the AC transmembrane voltage for red blood cells in suspension media of different resistivities are plotted in Fig. 2.11 a). In low conductive media such as sugar water ($rho_{ext} = 10\mu\text{S/cm}$), the transmembrane voltage drops at frequencies in the kHz range whereas in highly conductive media such as PBS ($rho_{ext} = 14.1$ mS/cm), it drops in the MHz range.

The transmembrane voltages plot is directly comparable to the Clausius-Mossotti factors plot of (Fig. 2.11 b). The CM-factors plot is calculated with the protoplast model of paragraph 2.1.4. Comparing the plots a) and b) side-by-side reveals that high transmembrane voltages are only present under nDEP conditions. This is the effect of the membrane getting more "transparent" to electric current with increasing frequency.

2.4.4 Electrotransfection

One of the main goals of electropermeabilisation is the insertion of foreign DNA into a cell. Once pores are established, the principle driving force is the concentration difference between the inside and the outside of the cell [de Gennes PG 1999], fighting against electrostatic repulsion (both the cell interior and the DNA are negatively charged). DNA

concentration in vicinity of plated cells can be increased by accumulation prior to pulsing [Lin YC 2004], the same as active DNA transport (electrophoresis) enhances transfection efficiency [Klenchin VA 1991]. Ion leakage is best prevented if cells are permeable on one side only (see above).

2.5 Summary

In this chapter, the two main tools for AC cell manipulation were introduced: The protoplast model for the Clausius-Mossottti factor, which is directly applicable for dielectrophoretic cell handling and electrodeformation, and the frequency-dependent transmembrane voltage relationship, for electropermeablisation.
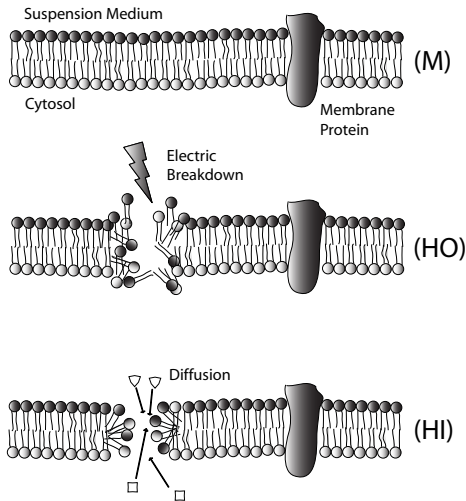
Figure 2.9: Schematic representation of electropermeabilisation of a bilipid membrane (M): according to the electric breakdown and molecular reorientation model, hydrophobic pores are created as a critical transmembrane voltage is reached (HO). The size and the lifetime of hydrophobic pores are too small for an exchange of species. Upon reorientation of the lipids, hydrophilic pores may be created (HI). These pores are metastable and eventually reseal. During the resealing process from (HI) to (M), the molecules have to pass through the energetically less favourable (HO) state. Therefore the resealing kinetics are temperature-dependent.
Graph adapted from [Tornay R 2004/2005].
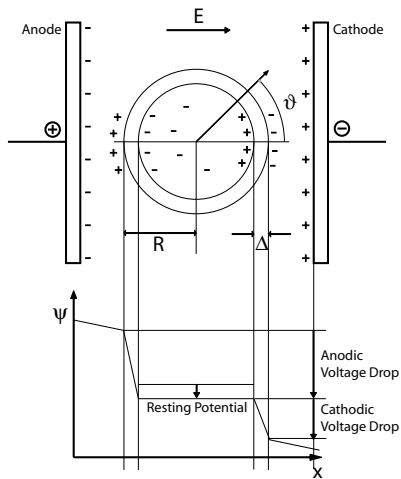
Figure 2.10: DC transmembrane voltage induction depending on the angle in respect to the electric field (top). The potential drop accross a cell is asymmetric due to the resting potential (bottom). As a result, electric membrane breakdown is more likely at the pole facing the anode [Neumann E 1999].
Graph adapted from [Tornay R 2004/2005].
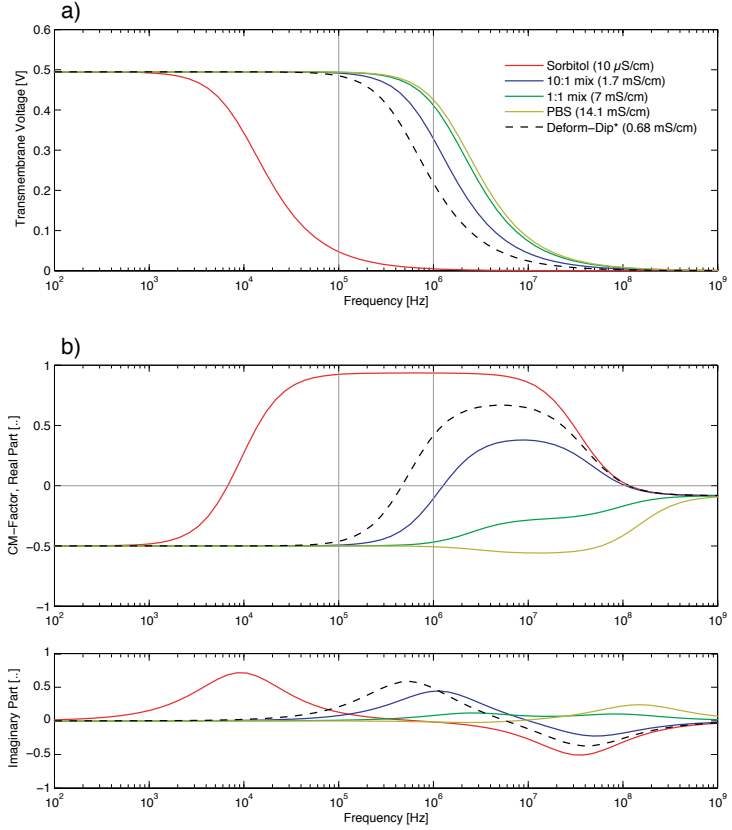
Figure 2.11: AC transmembrane voltages on red blood cells in different suspension media according to Jeltsch and Holzapfel (a). CM spectra (real and imaginary parts) of red blood cells according to Kaler and Jones (b). The graphs a) and b) are linked via the membrane capacitance.
(field: 10 kV/cm // media: $\epsilon_1 = 78\,\epsilon_0$; $\sigma_1 = 0.001,\ 0.17,\ 0.7,$ or 1.4 S/m // RBC: $\epsilon_2 = 60\,\epsilon_0$; $\sigma_2 = 0.4$ S/m)
Note: The CM factors of the protoplast model (b) can also be compared to the homogeneous sphere model of Fig. 2.4, where the same electrical characteristics were used.

Chapter 3

Miniaturised Cell Manipulation Devices

This is the chapter is about the design and operation cell manipulation devices. The applied concepts are based on the particularities of microfluidics, electric field development and external pressure bridging.

3.1 Drag and Laminar Flows

Reynolds Number With the size reduction of channels goes an increase of the surface-to-volume ratio: one passes from the inertia dominated regime into the viscosity dominated regime. For a flow speed v, as a function of fluid density ρ and fluid viscosity η, the Reynolds number Re is defined as the ratio

$$Re = \frac{\rho \cdot v \cdot d}{\eta} \ . \tag{3.1}$$

d is the characteristic length of the system (the diameter for circular conduits, the smaller dimension of flat rectangular conduits).
Flow is turbulent for Reynolds numbers > 2300 and laminar below. In microfluidic systems of characteristic lengths of some tens of microns,

water at some mm/s is well in the laminar regime.

Flow Profile Incompressible fluids are governed by the Navier-Stokes equation

$$\rho[\frac{\partial \vec{v}}{\partial t} + (\vec{v} \cdot \nabla)\vec{v}] = -\nabla p + \eta \nabla^2 \vec{v} \ , \qquad (3.2)$$

where ∇p is the pressure gradient. At low Reynolds numbers, the inertial terms on the left hand side of the N-S equation vanish and equation (3.2) simplifies [Brody JP 1996] to

$$\eta \nabla^2 \vec{v} = \nabla p \ . \qquad (3.3)$$

The above expression for laminar flow does not contain time derivatives, this means that laminar flow is independent of time, *i.e.* flow lines are the same whether a channel is actuated from one end or the other.

If equation (3.3) is applied for a circular conduit of radius r with no-slip conditions at the walls ($v(R) = 0$) and a fixed pressure gradient $G = -\partial p/\partial z$ between the ports, pipe flow with a parabolic flow profile occurs:

$$v(r) = \frac{G}{4\eta}(R^2 - r^2) \ . \qquad (3.4)$$

For rectangular conduits, things are a little more difficult, but basically the flow profile remains parabolic along the short semi-axis in the the case of a flat channel.

Flow Resistance The flow resistance of a channel depends on its cross-section and on its length. In channels fabricated with planar technology of constant height, the flow resistance is therefore proportional to length/width.

Diffusion   The time t_D required for a particle du diffuse across a distance l depends on its diffusion constant D,

$$t_D = \frac{l^2}{D} \; .$$ (3.5)

The diffusion constant of a Brownian sphere is a function of its radius R, of the Boltzmann constant and the temperature T, and of the viscosity η of the surrounding medium,

$$D = \frac{k_B T}{6\pi\eta R} \; .$$ (3.6)

Stokes Drag   A laminar flow of velocity $\vec{u}$ exerts a force on a particle of speed $\vec{v}$ if their relative movement is non-zero. This force depends on the particle shape and size. In the case of a sphere of radius R, the resulting drag force is

$$\vec{F}_{Stokes} = 6\pi\eta R \cdot (\vec{u} - \vec{v}) \; .$$ (3.7)

3.2   Electrical Cell Manipulation Concepts

3.2.1   Cell Handling: DEP-Barriers and Traps

Dielectrophoresis requires an inhomogeneous field. The stronger the gradient of the field intensity, the stronger the developed force. The research group around Prof. Günter Fuhr was the first to use the fringing effect of the field between two parallel line electrodes to create repulsing field barriers in microfluidic devices. Such barriers can deflect cells in flow (Fig. 3.1, left), or curved barriers can trap cells against flow (Fig. 3.1, right).
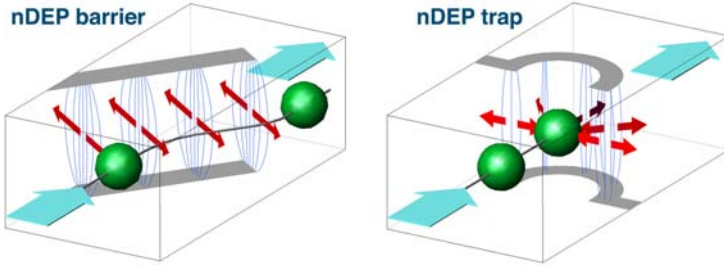
Figure 3.1: Artist's views of two structures for particle handling in flows. A dielectric particle flowing against an energised field barrier. The fringing field between a facing pair of line electrodes created a dielectrophoretic force. Under nDEP conditions, the particle is repelled from the barrier whereas the fluid path is remains unaffected. If the barrier is positioned at an angle in respect to the flow, the particle is shifted laterally (left). The field generated by a pair of curved horseshoe line electrodes also repels the particle

DEP vs. Stokes   The dielectrophoretic force is perpendicular to the axis of the barrier. Using a dipole approximation, Schnelle [T 1999] *et al.* calculated that the maximum force on a spherical particle is

$$F_{nDEP} = \frac{27}{32}\pi^2 \epsilon_1 (\frac{R}{a})^3 \Re(\underline{K}) V^2 \ , \tag{3.8}$$

where a is the separation between the electrodes and V the applied voltage.

Particles are retained by a barrier if its DEP force is superior to the Stokes drag. At an inclined barrier of an angle α in respect to the flow direction (Fig. 3.2), particles are deviated if

$$\sin(\alpha)F_{nDEP} > F_{Stokes} \ . \tag{3.9}$$

3.2.2   Cell Modification: Electropermeabilisation

One of the major intrinsic drawbacks of electroporation is the narrow band of successful permeabilisation and resealing of individual cells
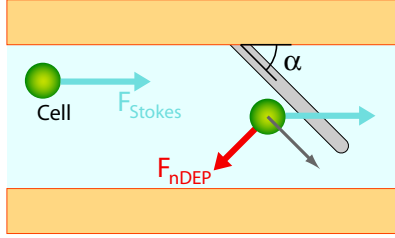
Figure 3.2: Schematic top view of the force balance of spherical cells flowing towards an inclined dielectrophoretic barrier.

within a broadly spread population [Weaver JC 1992]. The effect of the electroporating treatment ranges from "not responding" to "cell death due to permanent membrane disruption" when applied to a large number of cells. Besides the direct influence of cell size on the trans-membrane voltage, other sources for EP heterogeneity within a cell population have been identified (Table 3.1).

source	significance
cell orientation	the E field is directional
cell-cell separation	perturbation of local field by nearby cells
E field heterogeneity	field fringing
membrane composition	composition variation within a cell population
pore statistical behaviour	electroporation is fundamentally stochastic

Table 3.1: Possible sources of heterogeneity in cell electroporation (source: [Weaver JC 1992])

The second point of the above table is one of the main reasons for

microfluidic electropermeabilisation experiments: if cells are flowing
one-by-one through a zone of well defined electric field, there is no
perturbation induced by neighbouring cells. A possible configuration
in shown in Fig. 3.3. The openings in the electrodes serve for optical
observation.
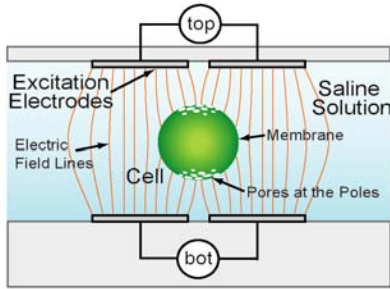
Figure 3.3: Schematic side view of a cell between a pair of micro-
electrodes. The electrodes' separation and each electrode's width are
comparable to the size of the cell.

3.3   Chip Fabrication and Connectivity

Both particle handling by negative dielectrophoretic barriers and and
miniaturised electropermeabilisation in homogeneous fields require
facing electrode pairs. For our microfluidic applications of individual
cell handling, electrode patterns should have a resolution of some
μm. Electrodes must be made of a material of no corrosion and low
erosion. Other requirements on the chip are optical transparency and
chemical inertia to solutions.

3.3.1 Fabrication

The devices are designed at LMIS4 and microfabricated under cleanroom conditions in the facilities of the EPFL Centre of MicroNanoTechnology, CMI.

Clean Room   0.7 mm thick float glass wafers (Schott Guinchard EPLDQ Float) are Piranha cleaned and HDMS primed before a 1.35 μm layer of a reversible photoresist (Microresist MA-N1440) is spun on. After exposure and development, the patterned photoresist serves as a sacrificial mask defining the electrodes. A 20 nm Ti seed layer and a 200 nm thick Pt film are deposited in a sputtering machine (Balzers BAS 450 or Pfeiffer Vacuum Spider-600), the resulting electrode patterns are revealed by lift-off. 10 to 30 μm (depending on the desired channel height) of photosensitive polyimide (HD Microsystems PI 2731) is spin coated, pre-baked, exposed and developed. Two identical wafers are flip-chip assembled (Süss MicroTec BA-6 bonding aligner), the bonding and final PI curing (Süss MicroTec SB-6 vacuum bonder) is obtained by thermal treatment at 300 °C under N_2 atmosphere. The chips are partially diced from both sides (Disco Corp. DAD 321 rotating blade dicer). Access-holes are drilled by electrochemical discharge machining of glass in NaOH.

A schematic of the microfabrication process is given in Fig. 3.4.

Flip-Chip Mask Design   Chips featuring top-bottom electrodes have different layouts of the lower and the upper half. If the designs and arrangement of lower and upper chips are distributed symmetrically about an axis at the centre of a wafer, one instead of two sets of masks can be used. Wafer level flip-chip mask design bears also the advantage of better yield of prototype cleanroom fabrication.
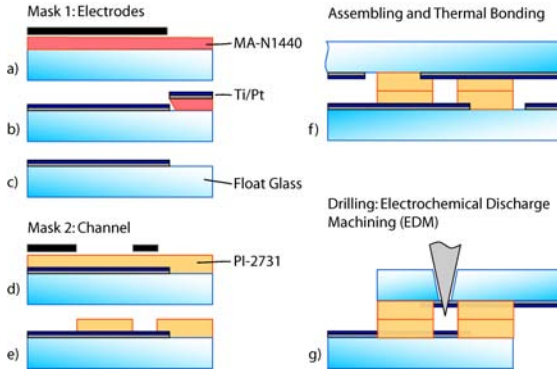
Figure 3.4: Schematic side-view of the microfabrication steps of two polymer layers sandwich chips. In a planar two masks process, electrodes are defined by photolithography (a), thin film deposition (b) and lift-off (c), channels are defined by photosensitive polymer structuring (d, e) and bonding (f). Outside the clean room, the wafer is diced and access holes are drilled through the top glass layer (g).

3.3.2 Connectivity

Device interfacing and external control is developed at LMIS4, in collaboration with the EPFL Atelier de l'Institut de Production et Robotique, ATPR workshop.

The released chips have double-sided connector pad exposure; seen from the side, they have a kind of a Z-shape (see Fig. 3.4, g)). They need to be contacted once from underneath, once from above. During operation, they are mounted into a combined fluidic and electric interface, where they are held tightly between a polymer block and a printed circuit board (PCB). Nitrile o-rings and spring-loaded contacts assure fast fluidic and electrical connections, without the need for gluing tubing or bonding wires (Fig. 3.6).
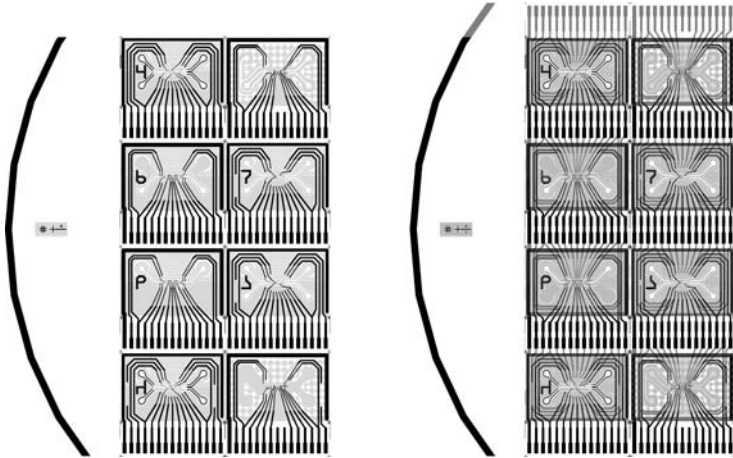
Figure 3.5: Detail view of a wafer design for wafer level flip-chip design. Single side wafer (left) and assembled wafer sandwich (right). The horizontal symmetry axis is situated across the alignment marks at the left wafer edge.

3.4   Microfluidic Actuation

3.4.1   Volume vs. Pressure Control

If tubing is used to supply microfluidic chips with liquids, flow control by volume displacement (*i.e.* syringe pump) has the disadvantage of poor response times and inaccurate control (due to the combination of compliances in the system's tubing and interconnection with the high fluidic resistance of the microchannel): such a setup acts like an RC electric circuit.

Driving liquids through the fluidic system by controlled overpressures minimises unwanted flows and backflows in the chip itself: pressure and flow balancing occurs "backward" *via* the low resistive connection into the reservoir.
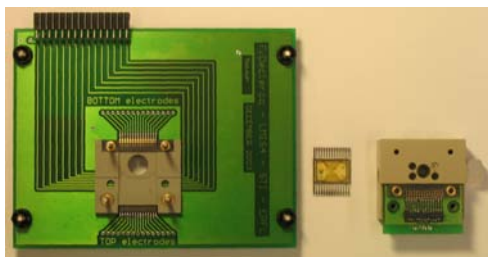
Figure 3.6: Chip, printed circuit board and chip holder open before assembly. The sealing between the polymer block and the flat glass surface of the chip is assured by o-rings.
PCB design and picture by Declercq [F 2003/2004].
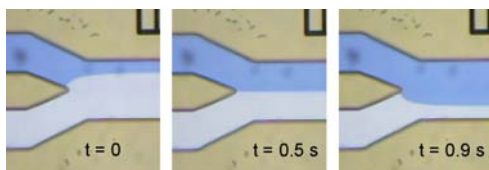
Figure 3.7: Laminar flow control. Top views of a two-liquids flow, controlled by regulating slight overpressures independantly at the two inlets. Changing flow patterns is fast (time delay between the pictures: 0.5 s). The estimated in the 300 μm wide channel is 2 mm/s.

The performance of pressure controlled fluid control gets better with smaller distance to the fluid reservoir. In the latest incarnation of the present setup reservoirs are directly built into the fluid connector block. Using fine gel electrophoresis pipette tips, liquids can be dispensed right onto the chip, through the nitrile o-rings. This makes the setup a low dead-volume system and very small amounts of liquid (less than 10 μl) are used per experiment.

3.4.2 Pressure-balanced Particle Positioning in the xy Plane

The concept of pressure bridging by an external gas flow circuit was developed at LMIS4 [Braschler T 2005]. As an example of an extension and direct application of the method, particle positioning is shown.

Concept   The prerequiste for planar particle positioning by fluid control is that the liquid must be enabled to flow back and forth independently in both the x and the y directions. If this is done at the intersection of two channels, perpendicular leakage / crosstalk can be prevented by keeping the pressure at the cross section of the two axis must constant. This is achieved if the pressure rise in one branch is compensated by a pressure drop in its counterpart (Fig. 3.8), i.e. if a differential pressure is applied.
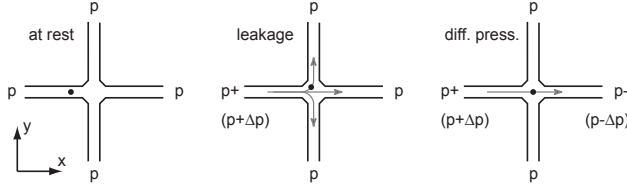
Figure 3.8: Schematic representation of an independently pressurised channel cross and a cell that has to be centred. At equilibrium state all pressures are equal. No fluid flow occurs. (left) The pressure is raised to p+ in the left hand branch. Liquid is leaking to all other branches and the cell escapes through the top branch. (centre) The pressure is raised to p+ on the left and lowered to p- on the right. No leakage in the vertical direction occurs and the cell passes about the centre of the cross. (right)

As shown by Braschler [T 2005] *et al.*, pressures can be controlled manually by an external gas network having fixed and variable restrictions/flow resistances over which pressure drops occur. Such networks

can be treated as equivalent electric resistor networks, where the gas flow is represented by I, the pressure by V, and restrictions by R. The requirement of varying p by $\pm \Delta p$ to $p+$ and $p-$, respectively, is translated to $V \pm \Delta V$. This differential behaviour is fulfilled by the Wheatstone bridge configuration, with two resistors varied in parallel (Fig. 3.9). Translated back to the gas network, this means that two variable restrictions (valves) have to be manipulated at the same time. In our setup, this is solved by mechanically squeezing two silicone tubes by the same amount. The high-pressure knot of such a gas flow Wheatstone bridge is supplied by a manual pressure regulator, the low-pressure knot is kept at atmospheric pressure (ground).
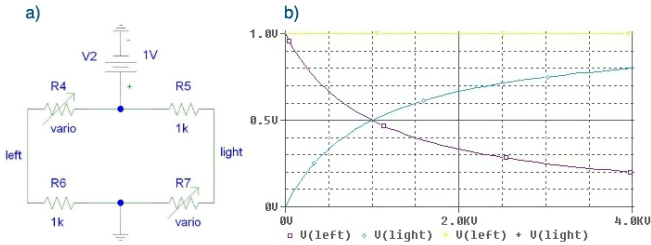
Figure 3.9: A Wheatstone bridge configuration for pressure divider circuits: Two flow resistances (R4 and R7) must be varied in parallel in order to get a symmetrical variation in the branches "left" and "light". The resulting pressure differences are 100 % of full scale in both the inverted and the direct modes.

Experimental Results   The system was primed with the test particles suspension and the four outputs of two differential pressure bridges were connected to the chip reservoirs. Initial flow induced by hydrostatic pressures due to different filling levels was equilibrated as the system was balanced by adjusting the working points of the two pressure bridges; the difference between the controlled overpressures being inferior to the millibar (i.e. the hydrostatic pressure of 1 cm water).

Starting with a stabilised system, particles in the region of interest can be positioned by decoupled x-y movements, as shown in Fig. 3.10.
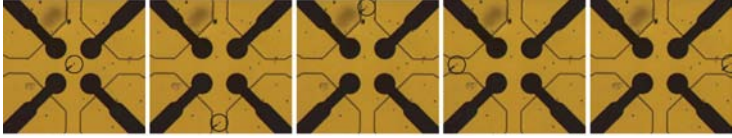
Figure 3.10: Video screenshots of a suspended 5 μm bead at the intersection of two perpendicular 50 μm large microchannels. The central pool measures 250 x 250 μm^2. The black areas are electrorotation electrodes. The bead (marker) initially centred is brought down and up, then left and right. The difference between the controlled overpressures is well below the millibar (the hydrostatic pressure of 1 cm water).

Conclusion When no relative movement between particle and suspension medium is required, differential pressure bridging might represent a welcome alternative to more costly ways of particle positioning. A potential application is cell positioning prior to and during electrorotation in a planar four-electrodes structure. The pressure balancing approach has the advantage that it does not bear any risk of damaging fragile objects such as mammalian cells, because forces are exerted on the suspending medium, and not on the object itself.

3.5 Electric Chip Characterisation

The impedance between a facing pair of electrodes and the bandwidth of efficient current injection are linked to the electrolyte in the channel. The electrical properties of a typical top-bottom nDEP barrier are shown in Fig. 3.11. For a pair of 8 μm wide and 500 μm long Ti/Pt electrodes separated by 20 μm, the plateau is about two decades wide.
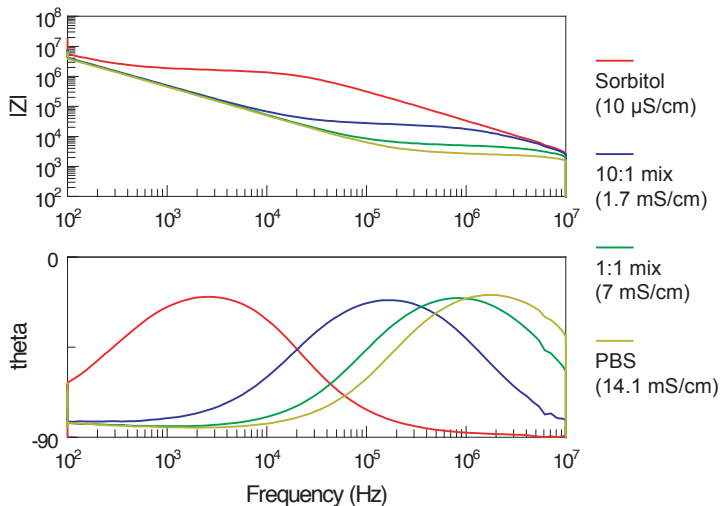
Figure 3.11: Bode plot showing the impedance of a top-bottom nDEP barrier of 500 μm length for different medium conductivities. For PBS, the lower end of the plateau is situated at 200 kHz.

For highly conductive media such as PBS, the double-layer capacitance is only fully bypassed above 200 kHz.

Chapter 4

Optical *in-situ* Temperature Measurements

4.1 Abstract

The manipulation of living biological cells in microfluidic channels by a combination of negative dielectrophoretic barriers and pressure driven flows is widely employed in lab-on-a-chip systems. However, electric fields in conducting media induce Joule heating. This study investigates if the local temperatures reached under typical experimental conditions in miniaturised systems cause a potential risk for hyperthermic stress or cell damage.
Two methods of optical *in situ* temperature detection have been tested

and compared: The exposure of the thermo-dependent fluorescent dye Rhodamine B to heat sources situated in microfluidic channels, and the use of thermoprecipitating *N*-alkyl substituted acrylamide polymers as temperature threshold probes.

Two-dimensional images of temperature distributions in the vicinity of active nDEP-barriers have been obtained and local temperature variations of more than 20 °C have been observed at the electrode edges. Heat propagation via both buffer and channel walls lead to significant temperature increases within a perimeter of 100 μm and more. These data indicate that power dissipation has to be taken into account when experiments at physiological temperatures are planned.

4.2 Introduction

Among numerous methods for handling individual biological cells in solution – such as optical or mechanical tweezers, standing acoustic waves, pressure differences (suction), or gravity (sedimentation) – positive and negative dielectrophoresis (pDEP and nDEP) [Pohl HA 1978] cell handling schemes are implemented with great success in microfluidic systems. One advantage is that dielectrophoretic forces scale well with size reduction [Jones TB 1995, Morgan H 2003]. Another advantage is that the specific electrode patterns and the microfluidic channels can be fabricated using the same photolithographic tools.

When employing dielectrophoresis for cell handling, the useful range of electric field strengths depends on the type of experiment and the physiology of the cells. Very high fields lead to a dielectric breakdown of the lipid bilayer of cellular membranes (electropermeabilisation) [Neumann E 1989, Zimmermann U 1996] and may result in electrical cell lysis. Cell damage can also be caused at lower field strengths due to

Joule heating. Cell death can be induced by a short, sharp increase in temperature (e.g. to 60 °C and more) or by a sustained, lower increase (e.g. 5.5 °C above physiological temperature for 30 min) [van Rijn J 1995]. Cellular responses might also occur at lower temperature shifts: it has been reported that a temperature increase of only a few degrees for 10 minutes is already sufficient to induce the production of cellular heat shock proteins [Higaki S 2003]. In order to avoid exposing cells to any kind of hyperthermic stress, the buffer temperature should not exceed the physiological value by more than 3 °C for prolonged times. Glasser *et al.* showed that for the electric field strengths typically required to immobilise cells in planar multipolar traps under no-flow conditions, the temperature of the buffer rises by less than 3° C during electrode activation [Glasser H 1998, Glasser H 1999]. In thermostabilised systems which are accessible from the top, two different measurement techniques were employed: first, they used the thermodependency of the electrical conductivity of the buffer to determine the temperature indirectly by measuring impedance variations; second, they inserted a small thermal resistor into the buffer, thus measured the temperature directly.

Recently, Müller *et al.* confirmed these measurements in similar devices by using liquid-crystal beads [Muller T 2003]. These beads disappear optically when heated above a critical temperature.

In the present flow-through cell handling devices [Gawad S 2001, Seger U 2004] higher electric field strengths than the ones reported by Glasser *et al.* and Müller *et al.* are used (up to 4 kV/cm compared to 1 kV/cm) and thus more extreme temperature increases are expected. These Joule heating effects should be quantified under normal working conditions in order to define operation ranges with little risk of exposing cells to hyperthermic stress. In the frame of the present study, field strengths up to 4.5 kV/cm are applied to top-bottom electrode configurations in microfluidic channels, and two methods for *in situ* temperature measurements are used: (A) the temperature dependency of the fluorescence intensity emitted by Rhodamine B, a technique that was

first successfully employed by Ross *et al.* to measure longitudinal temperature distributions in microchannels under DC electric fields [Ross D 2001, Erickson D 2003]. And (B) the temperature dependency of the conformal (folding) state of *N*-alkyl substituted acrylamides resulting in solubility below and precipitation above distinct (critical) temperatures. This easily implementable technique is here applied to microfluidics for the first time. We present the results of the two independent methods A and B, both of which permit optical temperature measurements of the liquid itself. Temperature gradients near active electrode pairs are visualised within the microfluidic chip under normal operation conditions.

4.3 Materials and Methods

4.3.1 Microfabrication and Dielectrophoresis

The microfabricated devices used for this study consist of a 20 μm thick polymer spacer that defines the fluidic paths between two 700 μm thick float glass plates. The spacer material is photosensitive polyimide [Metz S 2001]. At the top and the bottom of such channels, Ti/Pt thin film electrodes of 200 nm thickness are patterned by lift-off. Pairwise, they define nDEP-barriers which are used to manipulate cells flowing through the microchannel.

Negative dielectrophoresis barriers [Schnelle T 1999, Durr M 2003] are known to repel biological cells in electrically polarisable suspension media by forces that depend on the size of the cells, the gradient of the electric field strength, the frequency of the applied signal and the difference in polarisability between the cells and the buffer.

An active nDEP-barrier is depicted in Fig. 4.1. It deflects yeast cells in PBS with a sinusoidal signal of 7.4 V_{rms} at 1 MHz. At a flow speed of 400 μm/s, the cells are deflected about 5 μm upstream of the electrode pair. In the frame of this study, amplitudes from 5.5 to 9 V_{rms} were used.
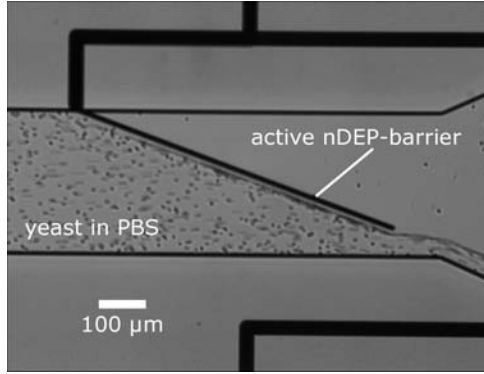
Figure 4.1: Top view of an active nDEP-barrier in a 300 μm wide and 20 μm high channel (electrode width: 8 μm). Baker's yeast cells suspended in PBS flow from left to right at a maximum speed of 400 μm / s (parabolic flow profile). The cells are deflected laterally by the inhomogeneous electric field of the electrode pair supplied with 7.4 V$_{rms}$ at 1 MHz.

4.3.2 Heat Generation and Conduction

The temperature distribution near an active nDEP-barrier can be predicted by balancing heat generation and heat conduction. Considering two long parallel line electrodes as axisymmetric at mesoscopic scale, cylindrical heat conduction can be assumed: Heat generated in the volume between the electrodes flows radially outwards.

The heat flow $\dot{Q}$ through a coaxial cylinder of radius r and surface $A(r)$ is given by [von Bockh P 2004]:

$$\dot{Q} = -\lambda \cdot A(r) \cdot \frac{dT}{dr} \tag{4.1}$$

where λ is the thermal conductivity coefficient and T is the temperature at r.

After integrating (4.1), and imposing a given temperature T_{ext} (room

temperature) at the outer boundary r_{ext} (chip thickness) the temperature decay $T(r)$ is expressed by:

$$T(r) = \frac{\dot{Q} \cdot ln(\frac{r_{ext}}{r})}{\lambda \cdot 2\pi l} + T_{ext}, \; r_{int} \leqslant r \leqslant r_{ext} \; . \tag{4.2}$$

The validity of this logarithmic temperature decay towards T_{ext} at r_{ext} has an inner limit r_{int} given by the channel height.

At steady-state the heat flow matches the electrical power $P = UI = U^2/Z$ dissipated in the channel. The electrical impedance Z of the buffer volume between the electrode pair depends on the specific conductivity ρ of the buffer, and on the electrode width w, length l and separation h. It is assumed that at nDEP frequencies (here: 1 MHz), any superficial double layer capacitance is bypassed by a short. The apparent resistance R is then a real number:

$$R = \frac{1}{1.4}\rho\frac{h}{w \cdot l} \; . \tag{4.3}$$

The shape factor 1.4 has been calculated by conformal mapping at typical electrode dimensions [Gawad S 2004]. R is in the range of 5-15 kΩ for typical nDEP-barriers ($l = $ 100-300 μm, $w = 8$ μm, $h = 20$ μm) and $\rho_{PBS} = 0.8\Omega m$.

Introducing (4.3) into (4.2) yields an expression for T, independent of the length l of the parallel line electrodes:

$$T(r) = 0.7\frac{U^2 \cdot w \cdot \ln\left(\frac{r_{ext}}{r}\right)}{\lambda \cdot h\pi \cdot \rho} + T_{ext} \; . \tag{4.4}$$

The thermal conductivities λ of glass and PBS are 1.4 and 0.6 W / (m °C), respectively. Note that this model neglects aspects such as heat evacuation by buffer flow, temperature dependence of the buffer conductivity and particularly heat flow parallel to the cylinder's axis. Nevertheless, this model permits rough estimations: Inserting a voltage of 7.4 V_{rms} (corresponding to a power dissipation of 8 mW)

predicts a temperature rise of 21 °C at r_{int} =10 μm (in respect to room temperature at $r_{ext} = 700$ μm).

General observations should be added to the above: The Joule heat produced in the chip is proportional to the square value of the applied voltage. Heat production can most efficiently be controlled via this voltage. Heat dissipation occurs mainly via conduction through the chip bulk material. Lowering room temperature will permit lower temperatures within the chip. It is also important to note that at micrometer channel dimensions, heat evacuation by volume displacement (i.e. liquid cooling) is negligible even for high flow speeds (e.g., for liquid velocities of 300 μm/s, heat evacuation by flow is in the order of 5 % of the heat generated by 7.4 V_{rms}).

4.3.3 Fluorescence Decrease of Rhodamine B

In the first method of *in situ* thermometry, a temperature-dependent fluorescent dye is used. This technique can be implemented using a standard fluorescence microscope. It is possible to measure fluid temperatures with micrometer spatial resolution and millisecond time resolution [Ross D 2002].

Generally, a rise in temperature results in a decrease in fluorescence due to the increased efficiencies of non-radiative processes related to thermal agitation (e.g. collisions with solvent molecules or intramolecular vibrations and rotations). The change in fluorescence is typically -1 %/°C. However, in some compounds, such as Rhodamine B, it can be as high as -5 %/°C [Lou JF 1999].

In this work, the property of fluorescence decrease with temperature is used to visualise the local heat distribution near nDEP-barriers.

1mM Rhodamine B (Standard Fluka, Sigma-Aldrich) solution was prepared in PBS buffer (pH 7.4, Sigma-Aldrich). Rhodamine B was chosen because its fluorescence is temperature-, but not pH-dependent [Coppeta J 1998]. PBS was chosen because it is a standard solution when working with living cells.

In situ fluorescence imaging of the Rhodamine B dye was performed using an inverted fluorescence microscope (DM IL, Leica Microsystems) equipped with a long working distance 20x objective, a mercury lamp, an appropriate filter set, a CCD camera (Qicam, QImaging) and a lab PC.

Within the microfluidic chip itself, an I versus T calibration curve was assessed by recording fluorescence intensities at different temperatures. Placed in an airtight hood, the entire experimental setup was heated externally, the air temperature was controlled with a Pt100 thermocouple. A second temperature probe was cast in thermoconductive gel in intimate contact with the surface of the chip. Measurements were taken after half an hour of stabilisation time, when the internal and external thermocouples indicated differences less than 0.5 °C. Reference points in the range of 30 to 50 °C were assessed. In order to minimise photo bleaching, the dye was renewed between consecutive experiments.

The measured curve is shown in Fig. 4.2. The data was fitted with an exponential function, yielding an intensity decay of -1.2 %/°C. This value will be used to link the intensity decreases of the dye to temperature variations induced by Joule heat.

4.3.4 Thermo-precipitation of *N*-alkyl Substituted Acrylamides

In a second method of *in situ* thermometry, water-soluble polymers exhibiting thermo-precipitating properties are used to detect temperature thresholds near nDEP-barriers in microfluidic channels. It is possible to sense temperature variations of a few degrees with this method. Such polymers have promising potential for applications in drug delivery, bioseparation, artificial muscles, chemo-mechanical systems, sensors etc. [Galaev IY 1993, Garret-Flaudy F 2000, Panayiotou M 2004].
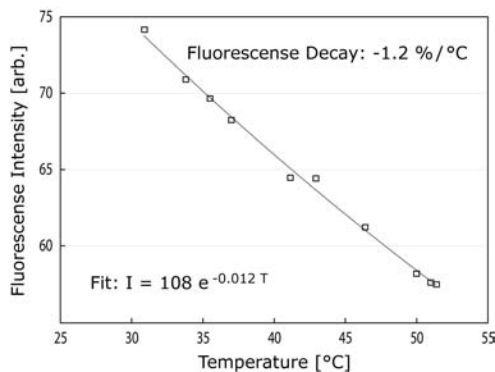
Figure 4.2: Fluorescence intensity of 1 mM Rhodamine B (ex: 560 nm, em: 585 nm) in PBS as a function of temperature. This calibration curve was assessed within an externally heated microfluidic chip. The exponential fit reveals an intensity decrease of -1.2 %/°C.

Environmentally sensitive polymers exhibit sharp changes in behaviour in response to an external stimulus. They can be classified according to the stimuli to which they respond: temperature-, pH-, ionic strength-, light-, electric- and magnetic field-sensitive. Some polymers respond to a combination of two or more stimuli.

Stimulus-responsive or "smart" polymers undergo fast, reversible changes in microstructure from a hydrophilic to a hydrophobic state. These changes are triggered by small changes in the environment but are apparent at the macroscopic level as precipitate formation from a solution [Galaev IY 1999]. These macroscopic changes are usually reversible and the system returns to its initial state when the trigger is removed.

Thermosensitive polymers show thermoreversible hydration-dehydration changes in response to external temperature changes. They are soluble in water at low temperatures but separate from

solution when the temperature is raised above the Lower Critical Solution Temperature (LCST) [Gan LH 2001].

An appropriate balance of hydrophobicity and hydrophilicity in the molecular structure of the polymer is required for the phase transition to occur. The phase transition phenomenon is associated with the temperature dependence of hydrogen bonding and hydrophobic interactions. Below the LCST the polymer molecules exist in solution as extended coils, surrounded by ordered water molecules. This shell of hydration causes a decrease in the entropy of the system. Thus, the free energy of solution is lowered by the formation of hydrogen bonds but is raised by the loss of entropy. At temperatures above the LCST the entropy term dominates and the thermoresponsive polymer chains are observed to undergo a transition to more compact globular states having hydrophobic properties [Idziak I 1999].

In this work, *N*-isopropylacrylamide and *N,N*-dimethylacrylamide were used for the synthesis of a thermoresponsive copolymer. Poly(*N*-isopropylacrylamide) in pure water has an LCST of 32-34 °C and poly(*N,N*-dimethylacrylamide) is soluble at any temperature. Copolymerization of the two monomers shifts the critical temperature to values above 34 °C due to the hydrophilicity of poly(*N,N*-dimethylacrylamide). The chemical structure of poly(*N*-substituted acrylamides) is given below. The thermosensitivity can vary depending on the R-group.
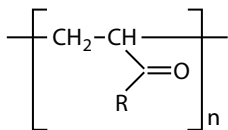
R= NH-CH2-(CH3)2: Poly(*N*-isopropylacrylamide)
N-(CH3)2: Poly(*N*-dimethylacrylamide)

Poly(isopropylacrylamide-co-dimethylacrylamide) was prepared by chain transfer polymerization (telomerization): 1 g of monomers,

with a molar proportion of 80 % *N*-isopropylacrylamide and 20 % *N,N*-dimethylacrylamide, was dissolved in 15 ml methanol at room temperature and transferred to a three-necked flask at 70 °C. Afterwards, 13.4 mg of the starter (AIBN: 2,2-azoisobutyronitrile) and 71 μl of the chain transfer agent (MPA: 3-mercaptopropionic acid) were added. The mixture was refluxed for 3 h under argon. After removal of the solvent by distillation (rotary evaporator), the residue was dissolved in acetone (solvent), precipitated from *n*-hexane (non solvent) and filtrated under vacuum.

For the on-chip measurements presented here, two probe liquids were prepared: 10 mg of poly(isopropylacrylamide) or 10 mg of poly(isopropylacrylamide-co-dimethylacrylamide) were diluted in 1 ml PBS buffer. The solutions' LCSTs of 29 $\pm$ 1 °C and 40 $\pm$ 1 °C were optically determined in a thermocycled water bath.

4.4 Results and Discussion

4.4.1 Two-dimensional Fluorescence

Fig. 4.3 shows a microfluidic channel in which a parallel line electrode pair is used as an nDEP-barrier. The channel contains Rhodamine B dyed PBS buffer. Fig. 4.3a shows a calibration picture taken at room temperature (24.8 °C). Changing neither illumination nor camera settings, the nDEP-barrier is activated and the fluorescence intensity is reduced due to the local heat generation (Fig. 4.3b). The insets in Figs. 4.3a and 4.3b show intensity plots retrieved at the same location before and during activation of the nDEP-barrier. The dips in the plots correspond to the electrodes, which screen the fluorescence.

Fluorescence variations due to changes in pH are not expected: nDEP-barriers are driven by AC voltages and no DC electrochemical reaction should occur.
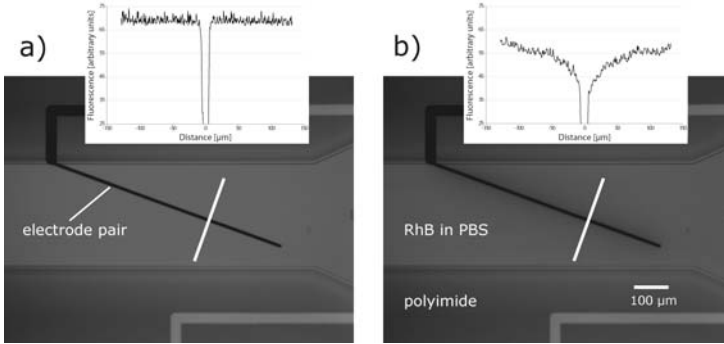
Figure 4.3: Fluorescence images of an nDEP-barrier in a microfluidic channel filled with 1 mM Rhodamine B in PBS. a) A reference image (exposure time: 500 ms) taken at room temperature (24.8 $^\circ$C) with no voltage applied to the nDEP-barrier. Fluorescence intensity levels are homogeneous. The white line perpendicular to the electrode pair indicates the location at which the intensity profile (inset) has been extracted. b) When a voltage is applied to the electrodes, the generated Joule heat dissipates and the temperature rise induces a loss in fluorescence intensity. This raw experimental picture has been taken 1 s after the activation of the nDEP-barrier supplied with 9 V_{rms} at 1 MHz, under the same conditions as the reference image. The inset shows the intensity plot obtained at the same location.

The decrease in fluorescence intensity is very fast once the voltage applied. Due to the small dimensions, thermal steady state is reached in less than 1 s; no fluorescence decrease due to photobleaching is observable in that timeframe. If the fluorescent dye is replaced between consecutive experiments, measurements under no-flow conditions are possible. However, increased temperature accelerates the effect of photobleaching drastically. Therefore, data retrieved more than 5 s after the activation of the nDEP-barriers are rejected.

Fig. 4.4a shows intensity profiles obtained for different voltages applied to the nDEP electrodes. The profile OFF is a reference profile taken at 24.8 $^\circ$C with no voltage applied; illumination is homogeneous and is only altered close to the electrodes. Using calibration data

(exponential decay -1.2 %/°C, Fig. 4.2), the intensity plots are converted to raw temperature plots as shown in Fig. 4.4b. The temperature profiles exhibit considerable noise, which is due to low levels of fluorescence and thus fluctuations from the CCD camera.

The dark grey vertical bar in Fig. 4.4a represents the 8 μm wide electrodes. All fluorescence profiles, including the calibration profile, drop to lower intensity levels at a distance between 4 and 6 μm from the electrodes edges; this is an indication of poor illumination and light collection in the zone next to the electrodes.

On the right side of Fig. 4.4b, the experimentally obtained temperature profiles were fitted by the logarithmic temperature decay behaviour arising from the cylindrical heat propagation 2D-model described above. The model fits the temperature profiles nicely, but it is not valid in areas less than 6 μm away from electrodes edges. (At 6 μm distance, the diameter of the limiting inner cylinder corresponds to the channel height.) This is indicated by the two vertical light grey bars.

In this zone with a total width of 20 μm, no conclusion on temperature is drawn, neither from the present measurements, nor from the present model. The plots of Fig. 4.4b show that at a distance of 6 μm from the electrodes of a chip at room temperature, buffer temperatures of 50 °C and higher are reached. Furthermore, it can be observed that thermal conduction leads to significant temperature increases in areas 100 μm and more away from the electrodes.
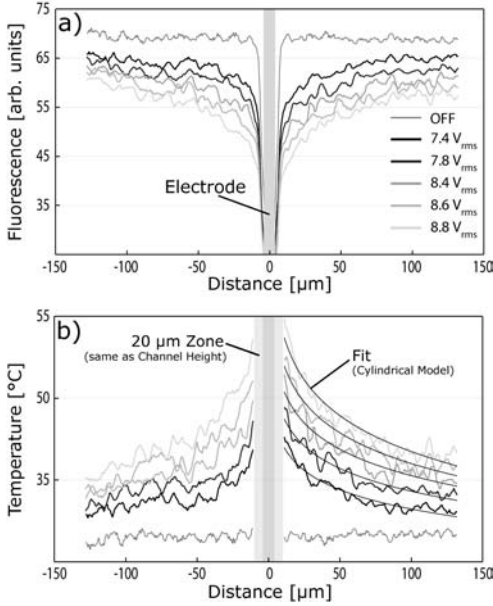
Figure 4.4: a) Fluorescence intensity profiles measured when applying sinusoidal signals of 1 MHz and variable amplitudes to an 8 μm wide electrode pair separated by 20 μm. The indicated distance is measured perpendicularly to the electrodes, the intensity is measured in arbitrary units. The dark grey zone indicates the electrode's masking. b) Temperature profile obtained by correlating calibration data to the above intensity profiles. Values within 10 μm of the centre line (i.e. 6 μm off electrodes edges, light grey zone) are not considered, as illumination is not satisfactory. The temperature data on the right are fitted by logarithmic decay curves. For supply voltages above 8 V$_{rms}$, temperature rises of up to 30 °C are observed.

4.4.2 Thermoprecipitation

The measurements with the two thermosensitive polymers poly(isopropylacrylamide) and poly(isopropylacrylamide-co-dimethyl-acrylamide) with LCSTs of 29 and 40 °C in PBS are made under working nDEP conditions. The heat generated in the volume between the electrode pair is traced by the formation of optically detectable precipitates if the medium locally reaches or exceeds the LCST. The effect of precipitation is reversible, and the interface between the zones of transparent solution and precipitation corresponds to an isotherm at LCST (see Fig. 4.5a). By changing the voltage applied to the electrodes during experiments, this isotherm can be shifted back and forth, the precipitation zone always indicating temperatures of 29 / 40 °C and above (see Fig. 4.5b).
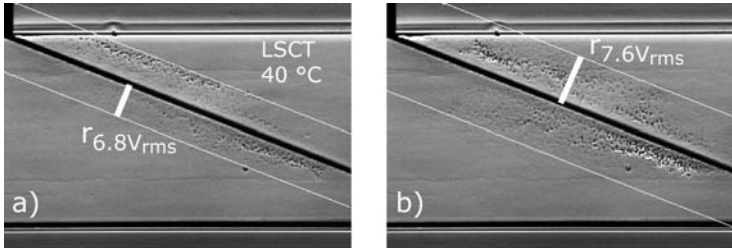
Figure 4.5: Top-views of a 300 μm large microchannel with an nDEP-barrier electrode pair reaching in from the side. Thermosensitive poly(isopropylacrylamide-co-dimethylacrylamide) in PBS buffer is present. This solution has an LCST of 40 °C. a) A sinusoidal signal of 6.8 V$_{rms}$ at 1 MHz is applied to the electrode pair, the gradient of the generated Joule heat induces a visible 40 °C isotherm between the precipitate close to the electrodes and the clear solution. The distance electrodes-isotherm is indicated by the white bars perpendicular to the electrode pair. b) The supply voltage is increased and so is the isotherm distance r. At greater distances, accuracy decreases. At lower polymer concentration, precipitation kinetics are slower because nucleation is diffusion limited. Typical delays are in the order of seconds.

With this kind of *in situ* temperature measurement it is not possible to obtain two-dimensional temperature distributions in one shot, but by sweeping through a range of supply voltages and correlating the distance r from the electrode pair to the isotherm, useful information can be retrieved. Such correlations are plotted in Fig. 4.6 for both polymers. Again, critical temperatures well above the physiological value of 37 °C are attained when too much power is applied to an nDEP-barrier of a chip at room temperature.

The main advantage of the thermosensitive polymer method lies in its intrinsic capability to locally probe absolute temperatures without optical intensity calibration. This is the case regardless of channel geometries and of heating mechanisms. Moreover, the LCST of the thermosensitive polymers can be tailored depending on the hydrophilic/hydrophobic balance of the polymer chains but also on the polymerisation method used for synthesis [Panayiotou M 2004]. This allows the user to explore different ranges of temperatures in microfluidic channels or in any other liquid containing system.

4.4.3 Comparison between the Two Experimental Methods

The temperature dependent fluorescence decrease has an excellent response time, and the information in Rhodamine B fluorescence pictures two-dimensional. When this method is employed to measure temperature distributions in homogeneously illuminated areas near active nDEP electrodes, perpendicularly extracted intensity profiles reveal a logarithmic temperature decrease. Optical information obtained with this method represents a vertical integration (averaging) of the fluorescence signal emitted by the dye filling the complete channel height. With standard transmission microscopy, no vertical temperature distributions can be retrieved. For the complete acquisition of 3D temperature distributions, more sophisticated methods such as sliced illumination or confocal microscopy must be employed.
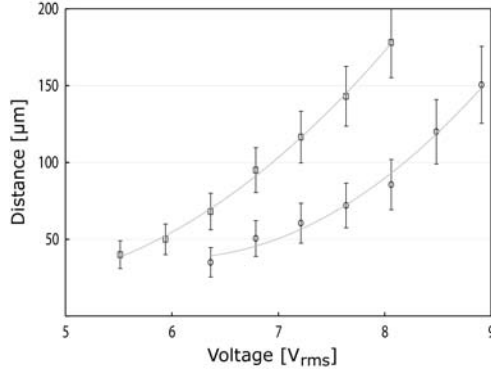
Figure 4.6: Distance-voltage relationship for polymers with LC-STs of 29 °C (left curve) and 40 °C (right curve), respectively. The distance between an active nDEP-barrier and the corresponding isotherms is plotted as a function of the applied voltage. Spatial uncertainty increases with growing distance as the contrast of the liquid-solid interface decreases. The lines are parabolic fits.

The raw information in thermo-responsive acrylamide precipitation pictures is one-dimensional and has a temporal resolution that is diffusion-limited. Due to short optical pathways, the interface between the precipitation zone and the clear solution is not easily detectable in microfluidic channels. In our system, the spatial resolution is estimated from ± 10 to ± 25 microns, depending on the distance from the heat source. Phase contrast microscopy should reduce some positional uncertainty.

The thermo precipitation method senses isotherms at predefined LC-STs; it does not require *in situ* calibrations. Since thermoresponsive polymers probe for threshold temperatures, no vertical averaging occurs. If a choice of polymers with different LCSTs is available, the precipitation method lends itself to quick temperature estimations or it can serve as a control in other temperature measurement methods. The absolute results independently obtained with the two experimen-

tal measurement methods are in agreement, the difference is in the range of 3 to 8 °C, depending on the applied voltage and the distance from the active nDEP-barrier. At the same time, the preliminary prediction obtained with the cylindrical model matches the experimental results quite well.

We suppose the discrepancy between the two experimental results arises to some extent from the uncertainty of the fluorescence intensity calibration and the overall low fluorescence signal levels, but mainly from the detection imprecision of the weak contrast between precipitation and clear solution of the LCST isotherm.

4.4.4 Impact of Joule Heating on nDEP Cell Handling

In situ temperature measurements with either method revealed temperature increases of several tens of degrees near nDEP-barriers supplied with 8 V_{rms} and more. The measurements also revealed significant peripheal heating at distances on the order of 100 μm. Heat evacuation by flow is small, so it cannot be used for cooling. When highly conductive buffers such as PBS or cell culture medium are used, lower voltages - with the drawback of smaller DEP forces and thus lower usable flow speeds - are the key to lower temperatures. For typical applications, such as cell dipping [Seger U 2004], small lateral DEP forces are sufficient to guide cells in flows. Moreover, in flow-through systems the residence time of cells in hotspots is short. For these reasons, we conclude that the risk of thermal cell damage in microfluidic systems using nDEP-barriers to guide cells in flows can be kept minor. For systems designed to trap cells for sustained periods of time, flow speeds must be kept extremely low in order to minimise DEP forces and therefore the Joule heat dissipated by the dielectrophoretic fields. Under well-controlled conditions, Müller *et al.* observed consecutive cell divisions in dielectric field cages [Muller T 2003].

4.5 Concluding Remarks

Two experimental methods for *in situ* temperature measurements were presented and similar temperatures in the vicinity of active nDEP-barriers were obtained. The fluorescence method permits an optical assessment of 2D temperature distributions; its absolute precision depends on the preceding calibration procedure and illumination homogeneity. The thermoprecipitation method allows for 1D temperature detection. Its spatial precision depends on the optical contrast of the transition isotherm which decreases with increasing distance from the heat source. The method's thermal precision is intrinsic.

Both fluorescence and thermoprecipitation techniques allow visualising thermal patterns in microfluidic systems under working conditions. Their spatial and temporal resolutions are sound to good. They can both be recommended for temperature measurements in optically accessible systems, depending on the application: The fluorescence method is particularly suited for observing global temperature gradients at some distance from Joule heat sources, whereas the polymer method is ideal for detecting isotherms in steep temperature gradients close to heat sources.

From a biological point of view, Joule heating must be taken into account when nDEP-barriers are to deflect or trap mammalian cells in PBS or other saline buffers. Temperatures in the vicinity of active electrode pairs can rise above 45 °C, which represents hyperthermal stress for mammalian cells. Lowering voltages is the key to lowering temperature. Macroscopic cooling or using lower a conductivity buffer further reduces the risk of thermal cell damage.

Chapter 5

Biological Applications and Measurements

In the present chapter, direct applications of the previously described chips and setups are showcased. Experimental results encompass proofs of principle of cell deviation and trapping, membrane permeabilisation witnessed by optical means, exchanges of cell liquid environments, and combinations thereof. Common to all presented applications is the use of electric fields in microfluidic channels and external fluid control.

Several parts of this chapter are built on the results of semester (BSc) or diploma (MSc) student projects that I had the chance to coach.

5.1   Manipulation of Stationary Cells

In this section, we will focus on experiments with cells that are held in place. Electric field injection for dielectrophoresis or electroperforation does not rely on moving parts, which is a prerequisite when working

with stationary objects. Cells of interest can be chosen from a population and held in an area of microscope observation for a duration defined by an operator or a lab computer.

5.1.1 Multiple Erythrocytes Lysis - Haemoglobin Leak

Red blood cells (RBCs) are a simple model system for studying electropermeabilisation (EP) within microfluidic systems. The result of lysis can be optically assessed as haemoglobin leaks out of the cells [Zimmermann U 1974]. Because RBCs do not contain nuclei, only transparent sacks - so-called *ghosts* - are left over.

DEP trapping of particles in structures similar to ours had been demonstrated in the 1990s by the Fuhr group [Schnelle T 1993, Fuhr G 1994c, Muller T 1996], but no cell membrane permeabilisation had been shown for nDEP-caged cells in top-bottom electrodes devices.

Concept In a top-bottom horseshoe electrode arrangement such as shown in Fig. 3.1, a limited number of RBCs can be trapped by negative dielectrophoretic forces against flow. This horseshoe shape is chosen for two reasons: The field in the open slit is inhomogeneous, which is a prerequisite for DEP. At the same time, the opening permits observation of the cells exposed to the field, which is important for real-time EP characterisation.

The dielectrophoresis signal will not induce a transmembrane potential leading to permeabilisation if amplitude and frequency are chosen correctly. On top of this static nDEP signal, strong electric field pulses leading to membrane breakdown can be superimposed. In the case of RBCs, membrane permeabilisation can be optically detected as the cells turn into ghosts. The haemoglobin efflux kinetics can be studied *in situ*.
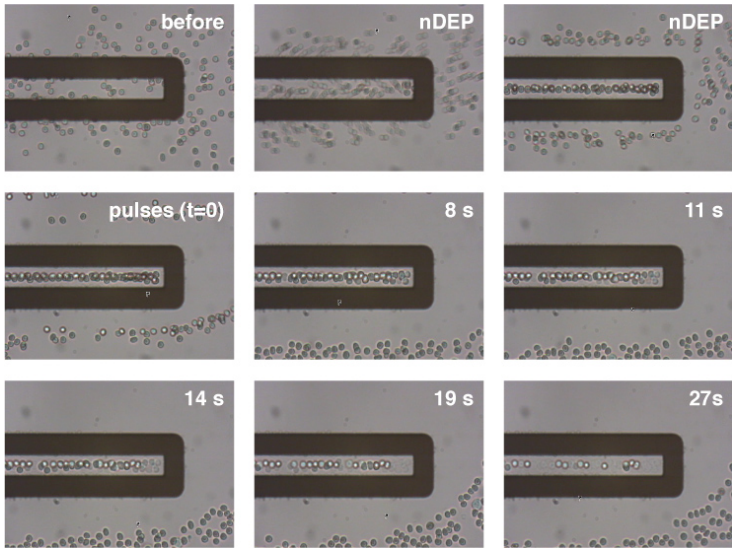
Figure 5.1: Video screenshot top-views of RBCs suspended in PBS flowing from left to right. Upon activation of an nDEP signal on the top-bottom electrodes trap, cells at the exterior of the trap are repulsed and cells in its interior are captured and lining up. Superimposed EP pulse trains lead to membrane permeabilisation and the creation of ghost cells. The process of haemoglobin diffusion out of the lysed cells is completed in less than 30 s.
(DEP: 2.65 kV/cm sinus at 1 MHz, EP: 34 V_{pp} saturated sinus at 50 kHz in trains of 10 cycles repeated at 3 Hz)

Experimental Results For this study, a special voltage amplifier permitting the superimposition of dielectrophoresis and electroperme-abilisation signals was conceived [Gfeller V 2002]. EP signals are trains of rectangular high-intensity pulses at low frequencies. The time of a half-period must be chosen such that the cell can entirely polarise and build up a maximum transmembrane voltage. Charge build-up in RBCs in PBS is typically a matter of one microsecond.

Fresh human RBCs from a healthy donor are suspended in PBS prior

to experiments. Injected into a 20 μm high and several 100 μm wide channel, erythrocytes flow near a semi-open top-bottom nDEP trap. Upon application of a sinusoidal nDEP signal of 2.65 kV/cm at 1 MHz, cells are repulsed from electrode edges. The cells inside de trap are collected and lined up, the ones outside are repelled. After collection, high intensity field pulses are superimposed to the continuous nDEP signal. Permeabilisation pulses are administered in trains of 10 saturated sini of 17 kV/cm at 50 kHz, repeated at 10 Hz. Erythrocytes in the trap are electropermeabilised, whereas the cells outside are unaffected. Electrical cell lysis can be appreciated by the vanishing of contrast due to haemoglobin efflux. A typical experimental result is shown in Fig. 5.1.

As stated in the concept, the opening slit in the electrodes is necessary for nDEP and advantageous for cell observation, but the field strength between the electrodes must be calculated as a function of geometry. This can be done using the conformal mapping method [Linderholm P 2005, 2006b] given in Appendix **??** [2006b]. For the case of a set of facing couples of coplanar electrode strips (width: 25 μm, gap: 15 μm), separated by a channel height of 20 μm, the effective field strength distribution for the applied 34 V_{pp} is shown in Fig. 5.2. Curves are taken along lines in the cross-sectional plane perpendicular to the electrodes, at different distances from the line at mid-height of the channel At the center of the trap, an absolute field strength of 9.5 kV/cm is present. This value is well above the strength of 4-5 kV/cm required to induce permeabilisation of mammalian cells [Chang DC 1989]. However, the maximum field strength achievable with this system will not suffice to permeabilise certain bacteria (for instance, *Escherichia Coli* require field strengths of 13-17 kV/cm [Sheng Y 1995]).

Conclusion In our microfluidic devices, cells can be captured against steady flow by negative dielectrophoresis. Contact-less lysis of stationary cells can be achieved, whereas cells outside the trap are unaltered. We have shown this in the example of nDEP-trapped
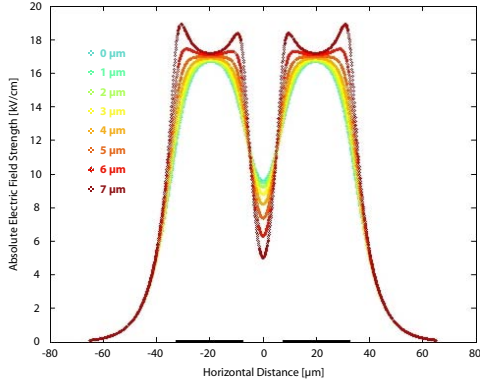
Figure 5.2: Numerical evaluation of the analytical expression of the total electric field strength between two top-bottom electrode pairs, indicated by the two black bars on the x-axis. The absolute field strength is evaluated in planes at different heights with respect to the centre plane. For a channel height of 20 μm and an electrode gap of 15 μm, the electric field strength at mid-height drops from 17 to 9.5 kV/cm for an applied voltage of 34 V$_{pp}$. At an off-center distance of 3 μm, the place at which the poles of centred 6 μm diameter particles pass, the field strength is about 9 kV/cm.

erythrocytes turning into ghosts in less than half a minute. The whole process of dielectrophoretic trapping and EP pulse application can be optically monitored.

The field strength at the centre of the trap achievable within the presented device is $9.5/17 = 55\%$ of the equivalent field of a parallel plate capacitor. Despite this field reduction due to the combination of DEP with EP, almost 10 kV/cm can be achieved using standard electronic components. Such field strengths are largely sufficient for the permeabilisation of mammalian cells, but might not suffice for a permeabilisation of bacteria.

5.1.2   Single-Cell Lysis - Nucleic Stain Uptake

The next logical steps in validating our technology for biological essays based on electric field cell manipulation are the passage from the multi- to the single-cell level and the extension from erythrocytes to eukaryotic cells. On individually captured cells, membrane breakdown threshold conditions may be assessed. One possible optical detection method is the use of non-permeat nucleic stains, increasing their fluorescence efficacy manifold when in contact with nucleic acids.

Concept   Downscaled cell traps reduce the probability of spontaneous cell capture, therefore single-cell trap chips feature a focalising nDEP funnel concentrating flowing cells into the flow line crossing the trap (see Fig. 5.3, left). Once a cell is held in place using an adequate nDEP signal, electropermeabilisation (EP) pulses can be superimposed to the static signal as described before.

In such single-cell traps, EP threshold experiments were carried out on *Saccharomyces Cerevisiae* (baker's yeast) [Tonteling M 2003/2004].

Experimental Results   Baker's yeast cells obtained from a grocery store were suspended in PBS. The buffer was enriched with Propidium Iodide (PI), a fluorescent dye that increases emission efficacy manifold when attached to DNA or RNA [Molecular Probes 1999].

The experimental procedure is shown in Fig. 5.3: Yeast cells are guided by flow and nDEP barriers into a circular single-cell trap that is activated when the cell is about the orifice. To the nDEP signal, an electropermeabilisation signal is superimposed. The amplitude of the EP signal is gradually increased and dark-field (fluorescence) pictures are acquired for each voltage step. The light intensity profile reveals increase of fluorescence of the cell, due to influx and DNA-binding of PI.

As EP signal frequency, again 50 kHz was chosen. This value is close

to the critical 100-200 kHz electrode-electrolyte double layer capacitance cutoff, but still well below the 500 kHz membrane polarisation charge relaxation time τ of Holzapfel's [C 1982] frequency-dependent expression for transmembrane voltage $\Delta\psi$, previously given in chapter 2:

$$\Delta\psi = \frac{1.5 \cdot r \cdot E_0 \cdot \cos\theta}{\sqrt{1 + (\omega\tau)^2}} \ , \ \text{with} \ \ \tau = r \cdot C_m \cdot (\rho_{int} + \rho_{ext}/2) \ , \quad (2.30)$$

where r is the spherical cell radius, E_0 is the external electric field of pulsation ω, θ is the angular location on the cell membrane in respect to the pole-pole axis aligned with E_0. C_m is the membrane capacitance, ρ_{int} and ρ_{ext} are the cell and the medium electric resistivity, respectively.

Note that for wall-less cells suspended in PBS and of the size of yeast cells, τ is about 0.1-1 μs.

Raw experimental EP threshold data for several cells is shown in table 5.1. Cell sizes were measured on video data by fitting a circle to the cell perimeter. EP thresholds were assessed by gradual voltage increase, and the corresponding field strengths E_0 were calculated by the relation V/h, where V is the applied voltage and h the electrode-electrode distance (*i.e.* channel height). The calculated transmembrane voltage $\Delta\psi$ is a function of the cell radius and the field strength:

$$\Delta\psi = 1.5 \cdot r \cdot E_0 \cdot \cos\theta \qquad (2.29)$$

Comparing our transmembrane threshold voltages (5-6.5 V) with values from literature (0.5-1.5 V) [Zimmermann U 1996] or our critical field strength (12-14 kV/cm) with the one found by Hojo *et al.* (3.5 kV/cm) [S 2003] reveals a strong discrepancy which is discussed below.
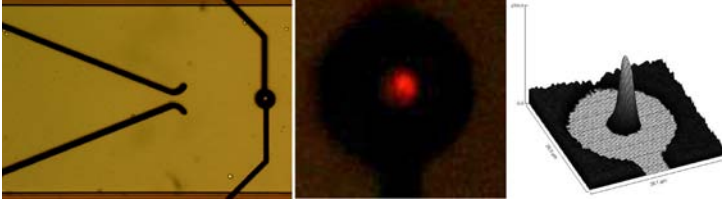
Figure 5.3: (left) Photographic top-view of the microfluidic device (channel width: 300 μm, channel height: 20 μm) used for the single yeast cell Propidium Iodide DNA staining assay. Cells suspended in PBS containing 15 μM PI are flowing from left to right and caught by the circular top-bottom nDEP trap. (centre) Dark-field zoom view of a yeast cell captured by the nDEP field between two ring electrodes (rim width: 10 μm, orifice diameter: 15 μm). The cell is fluorescing in red after the application of permeabilisation pulses above the transmembrane voltage threshold. Time delay between the administration of the pulses and the full development of fluorescence: about one minute. (right) 3D visualisation of the light intensity profile of the same cell. The height in this plot corresponds to the intensity in arbitrary units.

Conclusion We have shown contact-less single-cell trapping and electric field mediated permeabilisation of eukaryotes in microfluidic channels. Membrane breakdown threshold voltages were assessed by fluorescent nucleic staining using propidium iodide. However, the critical voltages applied at 50 kHz were 3-4 times higher than the values for DC voltages found in literature. Part of our overestimation is due to field reduction caused by the central electrode opening: Finite Element Modelling (FEM) of the electric field distribution of the double ring nDEP trap (see Fig. 5.4) showed that due to the open electrode configuration the fields strength in the volume of interest is lower, but only by 28 %. Compared to threshold values for bilipid membranes, our overestimation is also due to the additional chitin cell wall of the yeast fungus. The cell wall absorbs a part of the induced potential $\Delta\psi$. Most probably, however, is our overestimation due to an increased polarisation time τ, due to the cell wall. With τ increased, a lower

	R [μm]	t.h. [V]	[kV/cm]	$\Delta\psi$ [V]
cell 1	3.2	27.0	13.5	6.48
cell 2	2.6	26.7	13.4	5.21
cell 3	3.5	24.7	12.4	6.48
cell 4	2.4	28.0	14.0	5.04

Table 5.1: Electropermeabilisation thresholds (t.h.) experimentally assessed on individually captured and observed yeast cells in PI-loaded PBS. The applied external potential was increased in small steps until membrane permeability was witnessed by PI fluorescence staining of the nucleus.
(The field strength indicated in this table is the pure result of V/h, not taking field fringing into account. The effect of field fringing is illustrated separately in the simulation of Fig. 5.4: fields at the centre of the double ring trap are roughly one third lower.)

frequency should be applied in order to allow a complete charge build-up. As explained before, frequencies below 20 kHz cannot be used in our system due to insufficient current coupling across the electrode-electrolyte interface double layer capacitance. In chapter 6 the subject of poor current injection will be picked up and an elegant workaround will be presented.

In terms of response time, using the nucleic stain propidium iodide in our system was not satisfactory rapid. In high numerical aperture (NA) optical systems, fast but minute fluorescence increase due to PI binding to cytosol RNA can be observed [Marszalek P 1990, Sixou S 1993, Djuzenova CS 1996, Gabriel B 1999]. Our microfluidic system is based on 500-700 μm thick glass chips and thus on long working distance objectives. Therefore only important fluorescence increase due to PI binding to nucleic DNA can be recorded [Seger U 2002]. The subject of a faster fluorophore compatible with our requirements will be revisited in section 5.2.
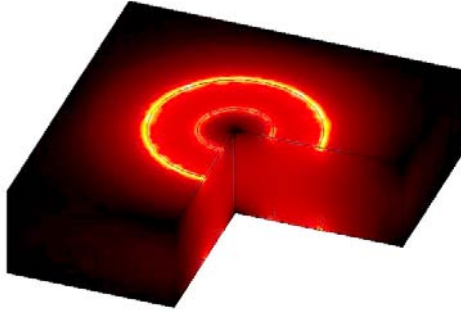
Figure 5.4: FEM simulation of the electric field in a double ring trap of 20 μm separation, 10 μm rim width and 15 μm orifice diameter (colour scale: arbitrary units). Extreme current densities appear at the outer metal electrode edges. Trapped cells do not get into these high-field zones due to nDEP repulsion.
At the centre of the volume, the field is homogeneous. Compared with a closed disks geometry, the field strength along the vertical axis of the open ring geometry is still 78 % at midheight, and 72 % at the points 3 μm above and below the centre.

5.1.3   Cell Immersion - Proof of Principle

In the previous paragraphs, dielectrophoresis and electropermeabilisation have been used in simple fluidic devices having one inlet and one outlet only. We now want to enhance the system's functionality by using more than two fluidic ports. This will add the new dimension of applications where the reaction of cells to fields *and/or* chemicals is important.

Concept   In a large number of biological assays, the reaction of cells exposed to a different chemical environment is tested [Chen CS 2005]. If a fast reaction is to be studied, macroscopic set-ups are not always adequate. Time-control of the addition of chemicals to the cell buffer in a macroscopic well plate might not be sufficiently precise due to

diffusion limitations. That's where microfluidics "come in handy": If one or several cells can be kept in place and if flow-patterns between two and more streams can be changed in a controlled manner, cells can be exposed to and washed from different liquids in arbitrary protocols. [Besselink GAJ 2004, Olofsson J 2004]

In the present paragraph, we present our contribution to this field: using semi-open negative dielectrophoretic traps, cells can be collected from an initial stream, and then exposed to a second. We termed this procedure cell immersion [Seger U 2004] by lateral shifting of flows.

Experimental Results A first proof of principle is shown in Fig. 5.5. In the global top-view, flow patterns for the collection and the immersion phase are given (Fig. 5.5, top row). Flows are oriented from left to right. Cells in PBS enter the system *via* the lower inlet, Rhodamine B dyed buffer *via* the upper. (Rhodamine B has a sufficient contrast under brightfield illumination. It is expected to stain cell membranes, and this would be assessable under darkfield conditions.) The black patterns are top-bottom electrodes that overlap in the channel section. In the zoom view, the collection (OFF) and immersion (ON) of human RBCs is visible (Fig. 5.5, bottom row). The freshly harvested human erythrocytes are suspended in PBS and the trapping electrodes are energised with a sinusoidal nDEP signal of 2.5 kV/cm theoretical peak. (The same field distribution as shown in Fig. 5.2 applies, the practical value is only $9/17 = 53$ % of the maximum value, thus 1.3 kV/cm.)

Fluids are controlled by overpressures applied onto liquid reservoirs, the lateral position of the interface between the fluids can be controlled to some micrometers. For long channels and slow flow speeds, lateral precision is blurred by diffusion.

Conclusion We have presented a successful implementation of the cell immersion concept. By precisely controlling laminar flows, dielectrophoretically trapped cells can be exposed to a second reagent by
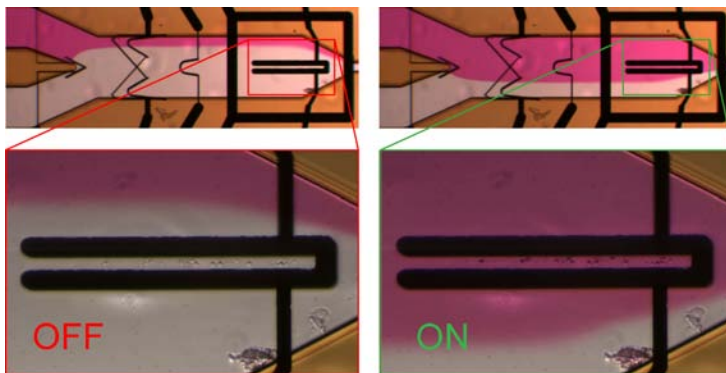
Figure 5.5: Global and zoomed top-views of a microfluidic device allowing cell immersion by lateral shifting of the interface between two adjacent liquid streams. RBCs suspended in PBS buffer are entering the system from the lower inlet. They are collected in the dielectrophoretic horseshoe trap, lining up along its symmetry axis (OFF). In a second step, flow patterns are changed and the trapped cells are immersed with Rhodamine B dye entering the system from the upper inlet (ON). The cells are exposed to the stream of dye before being washed by PBS again. Rhodamine B was expected to stain the immersed cells.
(Estimated flow speed in the main channel: 50 μm/s; nDEP signal: 1.3 kV/cm at 1 MHz.)

lateral shifting of laminar flows. Cell immersion was shown in our devices for human RBCs initially suspended in PBS and then immersed by Rhodamine B. In our experiments, no cell membrane staining was observed.

Immersion protocols can be arbitrarily chosen, the time delay between two states is in the range of seconds.

5.1.4 Single-Cell Immersion - Viability Assay

The device used for the original cell immersion proof of principle was not optimal in terms of electrode width and flow restriction, and there

were no cell-guiding nDEP barriers as they are required for single cell handling. These points were addressed with the second generation cell immersion design elaborated in the frame of this thesis.

Concept The present cell immersion device features a trap for a small number of cells, and it is asymmetric as the inlet for the second liquid/reagent is in the side-wall of the main channel, 400 μm upstream of the trap (see Fig. 5.6). Single cells in flow can be selected, collected and immersed.

Experimental Results Human Leukemia T Cells (Jurkat) are cultured suspended in RPMI-1640 medium with 10 % FCS and 1 % Pen-Strep at 37°C. Negative DEP is generated by sinusoidal signals of 2.5 kV/cm at 1 MHz. Bipolar, sinusoidal 100 kHz electric pulses with variable field strengths from 5 to 10 kV/cm are superimposed to the nDEP signal and delivered in trains of 10 pulses on demand. Fluid flows ranging from 50 to 150 μm/s are generated by overpressures in the order of 5 to 40 mbar.

In the lateral single cell immersion chip of Fig. 5.6, a Jurkat cell suspended in culture medium was guided into the trap and immersed by Trypan Blue dyed PBS from the lower inlet within less than 10 s. In the present experiment, the 13.9 μm diameter cell has not protruded into the 13.1 μm wide gap. This fact is illustrative for one of the general drawbacks of combined DEP immobilisation and electropermeabilisation: within a population cells of a vary in size, and no DEP/EP design can be optimal for a large variety of cell sizes. In section 5.2, flow-through permeabilisation concepts will be presented.

In Fig. 5.7 two live cells are held captured in the active nDEP-trap while being immersed by PBS containing Trypan Blue. Both cells do not turn blue, as they are intact. After the application of sinusoidal pulses of 8 kV/cm at 100 kHz, one of the cells is lysed and turns blue while the other one remains unstained.
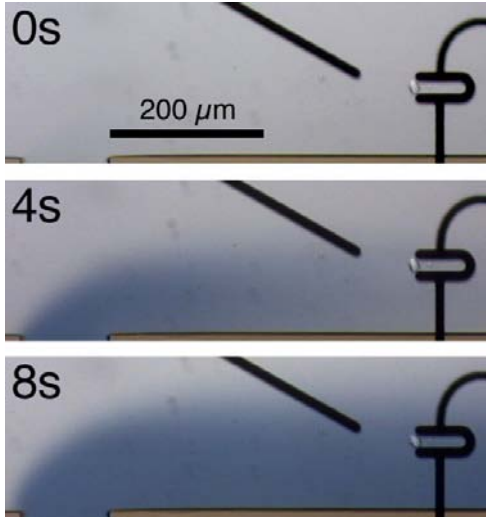
Figure 5.6: Photographic top-view of a microfluidic device designed for lateral single-cell immersion. Time sequence of the immersion of a Jurkat cell originally suspended in RPMI-1640 culture medium: Within less than 10 s, its chemical environment is changed to Trypan Blue stained PBS (entering the channel from below). By desactivating the inclined guiding electrode pair during immersion, the arrival of additional cells in the trap can be prevented.
(Trap design: 8 μm electrodes, 16 μm gap. Trap fabrication: 10.7 μm electrodes, 13.1 μm gap. DEP signal: 2.5 kV/cm at 1 MHz. Flow speed: 120 μm/s from left to right.)

Conclusion We have presented a microfluidic chip in which a small number of cells flowing in a channel can selectively be trapped, held and released. Collected cells can be immersed with and washed from a second liquid in user-defined sequences. Optionally, high electric field pulses can be applied to the captured cells. As an example, electrically induced cell death (cell lysis) was assessed optically by Trypan Blue staining [Seger U 2004b]. The present device is a precious tool for electropermeabilisation research studying the effect of changes in the
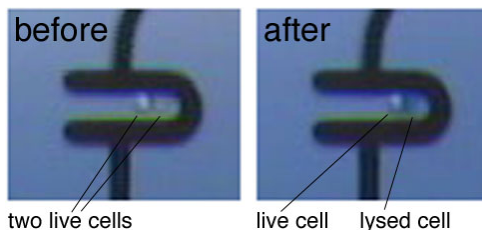
Figure 5.7: Close-up at two Jurkat cells captured in the nDEPtrap and immersed by Trypan Blue. The amplitude of the electric field used to generate the nDEP force is in the order of 2.5 kV/cm. Both cells are alive (left). 5 s after superimposition of additional, higher electric field pulses at lower frequency (8 kV/cm at 100 kHz), the cell situated at the zone of highest field density turns blue, indicating it has been lysed, i.e. its membrane has been disrupted (right).

chemical environment of single cells.

5.2 Manipulation of Moving Cells

In this section, we will concentrate on experiments with cells in flows. Working with moving cells has other objectives and requirements than manipulating stationary cells. Intrinsically, optical feedback and image acquisition must be faster as one individual cell cannot be observed for unlimited time.

The manipulation of cells in flow permits the study of a larger number of cells, thus the work on populations. Flow-through cell manipulation is therefore a research tool that can potentially be extended to industrial applications.

5. Biological Applications and Measurements

5.2.1 Cell Lysis in Flow - Ca^{2+} Uptake

The response time of propidium iodide (PI) as an optical tracer for membrane permeabilisation revealed to be slow on an optical system having relatively low fluorescence sensitivity. We had used PI for permeabilisation threshold studies (see paragraph 5.1.2). For flow-through systems, a faster tracer system compatible with our setup was proposed and implemented.

Concept The system chosen consists of a Ca^{2+} sensitive fluorophore, pre-loaded into cells and witnessing the Ca^{2+} influx from calcium-rich medium into the cytoplasm. Sub-second time resolution is expected from this tracer system because a) the diffusion rate of calcium ions is much higher than the one of PI molecules due to size, b) there is active transport due to the negative charge of the cell interior and c) the fluorescence enhancer needs only to reach the cytoplasm and interact with the pre-loaded fluorophore and does not need to diffuse into the cell nucleus and intercalate the DNA backbone [Gabriel B 1999].

Experimental Results As ion-sensitive fluorophore, Fluo3 (absorption: 506 nm, emission: 526 nm) was chosen [Molecular Probes 2005]. Fluo3 is a polar molecule that does not spontaneously penetrate the cell membrane. Incubation with Fluo3-AM however is possible. The AM (Acetoxymethyl) ester renders the Fluo3-AM complex apolar and cell-permeat. (Please refer to Appendix A for a detailed recipe of the used solutions.) Once Fluo3-AM molecules are in the cell, their AM tails are digested by esterases (hydolysing enzymes), and a part of the resulting Fluo3 molecules are occupied by the intracellular calcium. A living cell preloaded with Fluo3 is therefore slightly fluorescent, whereas Fluo3-AM in dead cells as well as in the surrounding medium, does not fluoresce.

Bright- and darkfield video screenshots of an experiment carried out

with a CHO (chinese hamster ovary) cell are shown in Fig. 5.8. The Fluo3-loaded cell flows between two pairs of top-bottom electrode lines (top) and is slightly fluorescent (centre). During the actual electropermeabilisation process, extracellular Ca^2+ ions diffuse into the cell, bind to the remaining Fluo3 molecules and increase the cell's total fluorescence (bottom).

Figure 5.8: Bright- and darkfield top-views of two 25 μm wide line pair electrodes of 20 μm height separation and 15 μm opening. A CHO (chinese hamster ovary) cell is slowly flowing from left to right. The cell is suspended in calcium-rich buffer and pre-loaded with the calcium-dependent fluorescent dye Fluo3 (top, brightfield BF). Initially, the cell is slightly fluorescent due to the intracellular calcium (centre, darkfield DF). Upon the application of 10 rectangular 2.5 kV/cm pulses at 100 kHz, the cell membrane becomes permeable to the extracellular calcium diffusing into the cell and increasing the fluorescence within a fraction of a second (bottom, DF).

Conclusion We have used the calcium-sensitive fluorescent dye Fluo3 as a fast electropermeabilsation tracer allowing the use of long working distance microscopes and standard camera equipment

[Hmamda A 2003]. Apart from the anticipated faster response time, the Fluo3/Fluo3-AM method has several other advantages over the propidium iodide method: a) dead cells do not fluoresce as no enzymatic activity can digest the AM ester, b) upon permeabilisation, fluorescence increases fastly (ion influx) and then decreases slowly (molecules efflux), a behaviour that permits a distinction between transiently and permanently permeable (*i.e.* lysed) cells, and c) Fluo3-AM is not as hasardous as mutagenic nucleic stains such as propidium iodide or ethidium bromide.

Chinese hamster ovary cells were cultured in suspension at the EPFL Laboratoire de Biotechnologie Cellulaire *(LBTC, Prof. F.M. Wurm). The cells were kindly provided by Dr. M. de Jesus and Dr. L. Baldi.*

5.2.2 Dielectrophoretic Deflection Filter

Researchers from the EPFL *Laboratoire de Chimie Physique des Polymères et Membranes* (LCPPM) are routinely producing attoliter vesicles from whole cells by a combination of exocytosis and shear force. These vesicles have the same membrane composition as their mother cells and are interesting model systems for cellular signalling reactions [Pick H 2005].

A purified population of vesicles is desired, but the traditional filter technique allows only for a coarse size separation of large cell residues from vesicles and small cell debris. For a finer discrimination between vesicles and small cell debris, techniques such as centrifugation in a density gradient do not have an optimal yield.

Inspired by the original work of Schnelle [T 1999] *et al.*, we wanted to implement a selective dielectrophoretic filter system aiming at separating small cell debris from membrane vesicles in flow.

Concept   The underlying principle of Schnelle's approach is the competition of hydrodynamic drag with dielectrophoresis. Size discrimination is possible because the Stokes drag force is proportional to the

radius R of a particle, whereas the dielectric force is proportional to its volume R^3.

In a pre-filtered suspension, membrane vesicles may be smaller than the cell residues. For that reason, our approach is based on the additional fact that dielectrophoresis does not only depend on the particle size, but also on each particle's overall capacity to become dipolar. Dead cells with membrane defects are less polarisable than intact ones, therefore a dead cell experiences a smaller DEP force than a live cell of same size. It remained to be shown whether intact, small vesicles (less than 3 μm in diameter) would experience larger DEP forces than cell residues of comparable size.

Schnelle used curved line electrode pairs in the flow of one liquid, we implemented straight line electrode pairs reaching from a first flowing liquid into a second, flowing side to side. The second liquid was clean buffer, ready to accommodate the selectively deviated vesicles (see Fig. 5.9 for an illustration).

With this dielectrophoretic deflection filter (DEPDEP) concept we aimed at a selective deviation of vesicles from the initial stream into the clean buffer stream and a non-altered trajectory for dead cell residues and debris remaining within the initial stream.
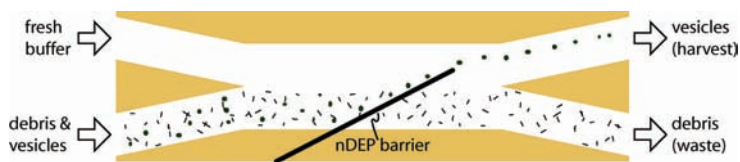
Figure 5.9: Top-view illustration of the DEPDEF concept: A suspension of vesicles and cell residues (debris) enters the microfluidic channel from the lower inlet. Fresh buffer enters the channel from the upper inlet. A flowpattern with two parallel streams is establised. An nDEP-barrier reaching from the lower stream into the upper selectively guides vesicles into the latter. Selection criteria are particle size *and* particle integrity. The two streams leave the mainchannel *via* two separate outlets, the lower one carrying away the waste, the upper one the freshly suspended harvest.

5. Biological Applications and Measurements

Experimental Results (A) Human embryonic kidney (HEK293) cells were cultivated in DMEM culture medium with 2.2 % FCS at 37 °C under 5 % CO_2 humid atmosphere. The HEK cells were modified and selected to express the fluorescent GFP-NK1 receptor on the membrane and the DsRed marker in the cytoplasm. Native vesicle production was provoked by incubation in DMEM with 25 μg/ml Cytochalasin B. (Cytochalasin B is a cell-permeable mycotoxin isolated from a fungus. It blocks the formation of contractile microfilaments and shortens actin filaments, which leads to exocytosis - the creation of membrane blobs at the cell surface.) Vesicles were torn off by shear stress during shaking for 5 minutes, followed by filtration through a 2 μm pores filter. Intact vesicles (fluorescent green on the membrane, red inside), membrane residues (green) and colourless cell debris were resuspended in PBS. This suspension was introduced into the lower inlet of the DEPDEF chip as schematically shown in Fig. 5.9. Clean PBS buffer was fed through the upper inlet. A laminar pattern with the two liquids flowing side-by-side at speeds below 50 μm/s was established. Upon activation of the DEP filter electrode pair at variable field strengths up to 5 kV/cm ($f = 100$ kHz - 15 MHz), neither vesicles ($\emptyset < 3\mu$m) nor other particles in the mixture got deflected. If the field strength was increased further, bubbles formed at the electrodes.

(B) A mixture of human RBCs and 5 μm latex beads suspended in PBS was introduced into both inlets of the DEPDEF device. Stable flow was established and the nDEP barrier energised with a 1.4 kV/cm sinus at 1 MHz. There is a range of flow speeds around 200 μm/s at which the erythrocytes were not held back by the barrier. Cells and beads have comparable volume, but different shapes, leading to a selective deflection of the latter.

Conclusion (A) Working with vesicles, pre-filtered membrane residues and cell debris did not reveal the desired behaviour: no sufficient field strength capable of deflecting these small particles could be generated in the 20 μm high channel without creating bubbles at

96
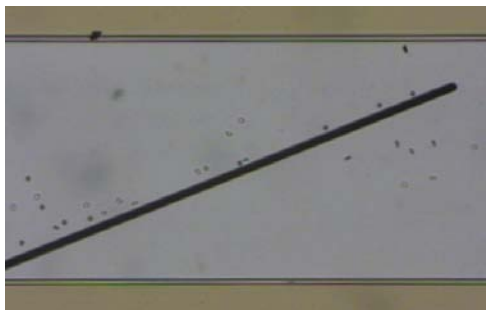
Figure 5.10: Photographic top-view of an inclined nDEP-barrier acting as a DEPDEF. The negative DEP signal is a 1.4 kV/cm sinus at 1 MHz. A mixture of human Erythrocytes and 5 μm diameter latex beads suspended in PBS flows at approximately 200 μm/s from left to right. The beads (spherical, homogeneously coloured) are selectively deflected whereas the RBCs (oblate, colour varying with orientation) break through the field barrier. Part of this behaviour is due to the asymmetric shape of the RBCs (disk diameter: 6.6 μm, disk height: 3.3 μm (mean values, from [Gimsa J 1996]).

the unpassivated electrodes. The only particles that were - although lacking an integral membrane - affected by the negative dielectrophoresis between the electrodes were large agglomerates. These collections of material must have formed posterior to filtration by sedimentation due to stagnant flow outside the microchannel. If vesicles are to be deflected, low conductivity buffer and/or channels of lower heights [Dürr M 2003] should be used.

(B) In the frame of the DEPDEF project, we managed to control the experimental conditions of flow (see e.g. Fig. 3.7) and dielectrophoresis signal sufficiently well to separate a mixture of human erythrocytes and 5 μm beads [Demierre N 2003]. This results is shown in Fig. 5.10. Erythrocytes are more likely than beads to pass through the nDEP barrier even though both types of particles have comparable volume. In suspension, and under iso-osmolar conditions, red blood cells are

oblate, disk-like particles of an average 6.6 μm diameter and 3.3 μm disk height [Gimsa J 1996]. Approaching an active nDEP barrier, RBCs orient themselves along the top-bottom electric field, *i.e.* they "stand up". For nDEP deflection, this is inefficient for two reasons: The dielectric repulsion force is aligned along the short semi-axis, *i.e.* an RBC appears like a small particle. At the same time, the Stokes drag force acts on a standing disk, *i.e.* the RBC behaves like a big particle. The critical flow speed for retaining RBCs by nDEP barriers is smaller than for spherical particles of same volume. This is a reason for the selective deviation of 5 μm beads over erythrocytes in our DEPDEF device.

(A+B) No outstanding findings could be proven with the DEP deflection filter. However, the concept of an nDEP barrier reaching from one flow into a second turned out to be a very promising tool. We will see this in the following sections.

Native vesicles from modified human embryonic kidney cells were produced and provided by P. Pascoal (EPFL, LCPPM).

5.2.3 Cell Dipping - Proof of Principle

In cell immersion, particles are kept in place and liquids are brought to them. One can also do this the other way around . . .

Concept In cell dipping, cells can be pushed from one liquid environment into another in a very short, defined time frame. This is useful for drug exposition and for cell washing during time-sensitive experiments, and when a large number of cells has to be processed.

Experimental Results Freshly harvested RBCs from a healthy donor are suspended in PBS. Fig. 5.11 shows an example of cell dipping in a microchannel, applied to a population of RBCs. The lower

part of the channel contains a PBS solution in which the cells, entering the channel from the left, are suspended. The upper part of the channel contains rhodamine coloured PBS. Flow speed in the main channel is 300 μm/s. With nDEP barriers (2.7 kV/cm at 1 MHz), the cells are guided from the buffer into the dye solution - where they are maintained for 2.5 s - and brought back to the buffer. Waste dye and washed cells leave this part of the microfluidic chip in separate channels, optical observation of the dipped cell population can take place further downstream. The stream of the dye is kept three times inferior to the one of the sample (1.6 nl/s), so dye consumption is reduced and contamination of the sample outlet with dye is prevented.
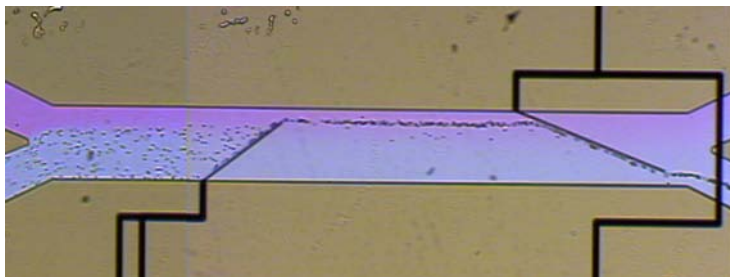
Figure 5.11: Photographic top-view of cell dipping in a microchannel, assembled from two video screenshots. A population of RBCs originally suspended in PBS buffer is deviated laterally into an adjacent stream of rhodamine-coloured PBS. After 3 s exposure to the dye, all cells are brought back into the initial PBS in which they leave this part of the microchannel. With this electrode configuration ($\phi_{dip} = 37°$, $\phi_{wash} = 22°$), the transit time from the buffer to the dye is about 0.3 s, whereas the passage from the dye to the buffer takes about 0.5 s. Considerable lateral diffusion of the dye can be noticed. Flow ratios at the inlets are set such that no dye contaminates the cell outlet.
(Flow speed: about 300 μm/s; nDEP: 2.7 kV/cm at 1 MHz.)

Conclusion To our knowledge, the here presented chip [Seger U 2004] is the first microfabricated nDEP device that allows the user to

swap a large number of cells between two liquid environments in a fast and controlled manner. No macroscopic system offers such fast and absolute protocols for drug exposition and cell washing.

As cell dipping is a flow-through concept, a large number of cells can be treated sequentially, but under identical conditions.

5.2.4   Improved Cell Dipping

In cell dipping, exposure times of individual cells to the reagent stream can be controlled by the change of flow speeds *ad hoc*, but only to some extent. The lower speed limit is given by diffusive mixing of the reagent and the initial cell-carrying liquid, the upper speed limit is given by the efficiency of the nDEP barrier. For exposure times below and above speed-modulable values, channel and electrode layout must be adapted. This issue is addressed by a second generation, improved cell dipping devices.

Concept   Diffusive mixing occurs along the interface between the two parallel streams. The length of this interface may be reduced by the introduction of a central separation wall (see Fig. 5.12). Flatter nDEP barrier angles for both the dipping and the washing steps ($\phi_{dip} = \phi_{wash} = 17°$) allow for the use of higher flow speeds at the same field strengths. Compared to the original cell dipping device, acceptable flow speeds are more than twice as high ($\sin(37°)/\sin(17°) \approx 2.06$).

Experimental Results   Baker's yeast cells (*Saccharomyces Cerevisiae*) are suspended in PBS. They enter the improved cell dipping device from the lower inlet. Trypan Blue dyed buffer enters the device from the upper inlet and flow patterns are stabilised. At flow speeds of 200 μm/s at the common channel section, the 5 μm cells are deviated from their initial buffer to the dye by nDEP signals of 4.2 kV/cm at 1 MHz. Between dipping and washing, the residence time in the

Figure 5.12: Top-view (assembled from video screen-shots) of an improved cell dipping device: Flatter nDEP barriers allow for higher flow speeds, the central separation limits lateral diffusion and additional nDEP traps allow for particle collection in either branch. The common channel is 300 μm wide, each branch is 200 μm wide, they are separated over a length of 1.4 mm. In the current experiment, 5 μm diameter yeast cells are deflected from PBS into Trypan Blue dyed buffer.
(Flow speed: 200 μm/s, nDEP signal at the barrier: 4.2 kV/cm at 1 MHz)

dye is about 10 s. (The length of the central channel separation is 1.4 mm, the lengths of the common channel sections are 0.8 mm. See Fig. 5.12.)

The multicell trap in the upper branch allows for cell retention in dipped state for prolonged exposure times, somewhat resulting in non-specific cell immersion. Fig. 5.13 is a close-up of such a trap. Yeast cells flowing at 150 μm/s are collected for several seconds (left) before the nDEP signal of the trap is switched off and the cells continue their path (right). One can clearly see that the device is operated below the maximum flow speed as the cells are repulsed more than 10 μm from the 8 μm thick top-bottom electrodes.

Conclusion The improved cell dipping device behaves as expected. There is less lateral diffusion due to shortened contact zones. The addition of cell retaining barriers in the dipping branch allow *e.g.* to make cell packets that are released periodically. The main application of the collecting traps however is to allow groups of cells to be exposed longer to the reagent of the upper branch. Using these traps gives rise to hybrid cell immersion and dipping. It is clear that the additional

exposure time varies for each cell of a retained group. This effect may be used to statistically determine threshold exposure times for given reactions on populations.
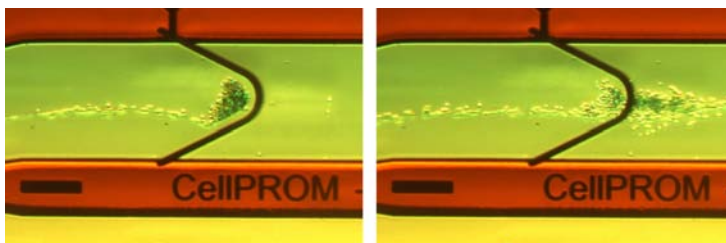
Figure 5.13: Close-up of the cell collecting trap in the upper branch of the improvec cell dipping device. The channel width is 200 μm, the electrode thickness 8 μm (Length of the black bar: 100 μm). Yeast cells are trapped and held in the second liquid (left) and released after several seconds of accumulation (right).
(Flow speed: 150 μm/s, nDEPsignal at the trap: 4.2 kV/cm at 1 MHz)

5.2.5   Dipped Electrical Lysis - Fluorophore Efflux

The integration of supplementary electrodes in the branches of improved cell dipping devices allows also to implement electropermeabilisation functionality.

Cells can be extracted from their initial buffer very shortly before electric alteration in a poration medium. If there are several pairs of electroporation electrodes at different distances along the path, experiments sensitive to exposure time to the poration medium can be carried out.

The use of two different liquid flows for cell supply and experiment allows for the use of optical assays not relying on fluorescence efficacy increase.

Concept   An improved cell dipping device with a heavily increased, serpentine dipping path is shown in Fig. 5.14. The total length of each 100 μm wide branch is 26 mm ($8 \cdot 3$ mm in the y-direction plus 2 mm in the x-direction). There are four locations at which electrodes penetrate the dipping branch: the first - indicated by a circle - about 0.5 mm after branching, the following ones at 6.9, 13.3 and 19.7 mm. The possibility to apply electropulses at different locations allows for varying pre-pulse incubation time, post-pulse observation time or inter-pulse delay time in the case of multiple administration.

Experimental Results   Human T-lymphocytes (Jurkat cells) are cultured in RPMI 1640 based complete growth medium (CGM) with 10 % FCS under 5 % CO_2 at 37 °C. Fluorescein Diacetate (FDA, $C_{24}H_{16}O_7$) 5 μg/ml acetone stock solution is prepared. As poration medium, a 1:3 mixture of PBS and non-conducting, iso-osmolar sugar solution is taken. Half an hour before experiments, 30 parts of cell suspension are incubated with 1 part of FDA stock solution (final FDA concentration: 0.16 μg/ml).

FDA is cell permeat and fluorescein (absorption: 494 nm, emission:
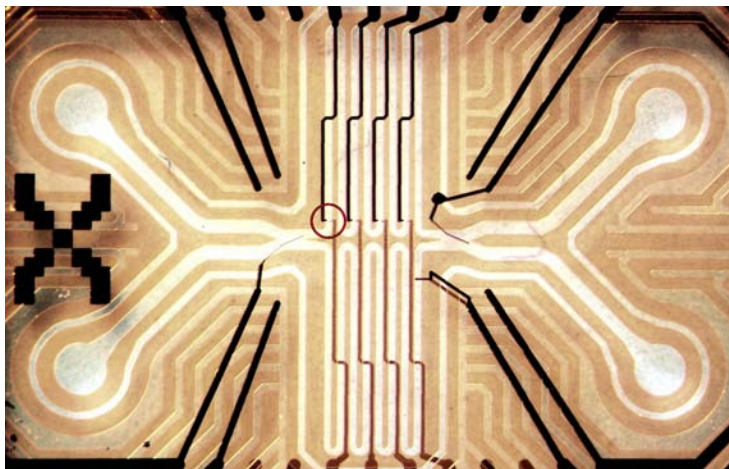
Figure 5.14: Global top-view of the improved cell dipping chip with extended, serpentine dipping and bypass branches featuring four locations for cell altering field injection (the first of which is marked by a circle).
The channel is 300 μm wide and 0.8 mm long at the common sections for dipping and washing, and each serpentine branch is 100 μm wide and 2.6 mm long. The four field injection zones in the upper branch are situated 0.5 mm after the branching and then three times every 6.4 mm.

518 nm) is formed by intracellular hydrolysis of the Diacetate tail. FDA in buffer is already fluorescent. In order to eliminate background signal, fluorescein-loaded cells are traditionally resuspended in clean buffer by centrifugation, supernatant removal and vortexing. Apart from time consumption, another disadvantage is FDA leakage: 2 h after resuspension, cells have typically lost 3 orders of magnitude of relative fluorescence [Molecular Probes 2006]. With our cell dipping device, both problems do not occur: cells removed from fluorescent background buffer as they are dipped into poration medium, only seconds before permeabilisation. This transfer is shown in Fig. 5.15.
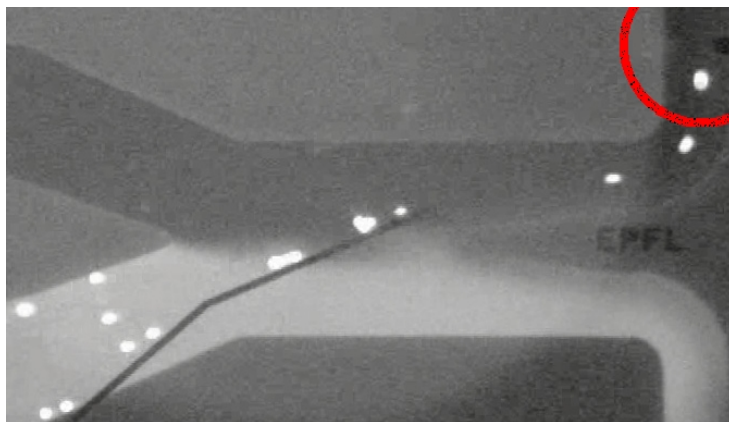
Figure 5.15: Darkfield top-view (zoom of Fig. 5.14) of the dipping step of the FDA efflux experiment: Cells in culture medium previously incubated with 0.16 μg/ml fluorescein diacetate (FDA) for half an hour enter the device from the lower inlet. Living cells are fluorescent as the FDA has been transformed into fluorescein by intracellular hydrolysis. The FDA not taken up by the cells makes the buffer to fluoresce, resulting in undesired background. Cells are guided by an nDEP barrier of a top-bottom electrode pair to the clean poration buffer which has entered the chip from the upper inlet and flows side-by-side to the coloured medium. After a curve to the left, the flowing cells in the dipping branch encounter a first zone where they can be exposed to a laterally oriented electric field between two top-bottom electrode stubs reaching into the channel (the darker and brighter shades visible in the circle in the top right corner of the image).

The nDEP dipping barrier was supplied with 2.1 kV/cm sini at 1 MHz. Rectangular pulses at 100 kHz with 25 % duty cycle (*i.e.* one 2.5 μs pulse each 10 μs) were generated with a commercial digital function generator (Agilent 33220A) and amplified with a custom electronic board to a final voltage of 20..26 V_{pp}. The pulses were applied to electrodes situated further downstream in the dipping branch. Pairs of electropermeabilisation electrode stubs reach into the 100 μm wide channel from each side - one on the top, one on the bottom of the 20 μm high channel. The maximal tip-to-tip field strength was thus 20..26 V_{pp} /$\sqrt{50^2 + 20^2} = 3.7..5.4$ kV$_{pp}$/cm.

When fluorescein-loaded Jurkat cells were exposed to repeated rectangular electropermeabilisation pulses of 4.7 kV$_{pp}$/cm of 2.5 μs duration, extra- and intracellular ions and molecules mixed by diffusion. The efflux of fluorescein resulted in a decrease of the cell fluorescence and an increase of the buffer fluorescence. In Fig. 5.16, four video screenshots illustrating the field-mediated membrane permeabilisation of a cell triplet are shown.

Conclusion The combination of cell dipping with electropermeabilisation allows for time-sensitive experiments in our microfluidic device. We have shown that with the *in situ* medium exchange, pre-experimental resuspension steps can be omitted and that altering field pulses can be administered at precise location/time lapses after dipping. Also, otherwise leaky products - such as fluorescein - may be used as optical tracers.

We believe that the combined dipping/pulsing chip is a helpful device for the characterisation of osmolarity-induced changes in electropermeabilisation threshold, for the evaluation of incubation times for membrane altering chemicals and for the study of efflux kinetics. Again, a large number of cells can be treated in that flow-through device, and cells can optionally be collected at either outlet. If cells are brought back into their original medium by the washing barrier, they are readily freed from by products that may have a toxic effect.

The experiment presented in this section has been carried out in Würzburg, at the Lehrstuhl für Biotechnologie *(Prof. U. Zimmermann), in the group* Electromanipulation of Cells *(Dr. V.L. Sukhorukov). The microfluidic device and its control hardware were fabricated at EPFL; videoequipment, cells and reagents were kindly provided by the University of Würzburg.*
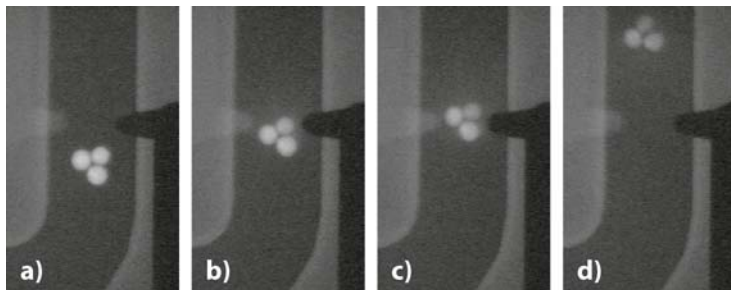
Figure 5.16: Top-view of laterally acting top-bottom electrode stubs placed in the 100 μm wide upper branch of a serpentine cell dipping device. The electrode stubs are 25 μm long. They are horizontally separated by 50 μm and vertically be 20 μm (channel height), resulting in some 54 μm tip-to-tip separation. A FDA-loaded Jurkat cells triplet is passing between the two electrode tips energised with 4.7 kV$_{pp}$/cm at 100 kHz. The cell membranes are permeabilised and the fluorophore is leaking out. The time for total FDA depletion is in the range of tens of seconds.

5.2.6 Dipped Electrodeformation

The characterisation of cell elasticity is important in the detection of diseases, and in cell membrane and cytoskeleton research. Cell deformation can be assessed using various methods (see paragraph 1.1.3). Electrodeformation is a very prominent one, particularly since the introduction of microfabricated planar line [Sukhorukov VL 1998] or concentric circles [Wong PK 2005] electrode structures.

At the *Lehrstuhl für Biotechnologie* of the University of Würzburg, research on electrodeformation on mammalian cells is carried out. The

group delivered evidence that electric cell deformation precedes electropermeabilisation [Sukhorukov VL 1998, Zimmermann U 2000] and that stiffer cells are more resistant to high intensity DC pulses [Mussauer H 1999, Müller KJ 2001].

A medically important fields is the measurement of red blood cell elasticity: Erythrocytes of 6-8 μm diameter have to be sufficiently flexible to squeeze through the smallest body vessels, capillaries of about 5 μm diameter. (Through that squeezing, the interaction surface between RBSs and capillary wall is greatly enhanced, which increases the exchange of oxygen and carbon-dioxide.) In a normal live cycle of RBCs, 120 days old, stiff cells are destroyed in liver and spleen. Pathologically stiff erythrocytes can cause serious circulatory troubles, and they can lead to death of unborn babies [Mannschreck BK 2005]. Blood-banks are have to test all cryoconserved blood samples for physiological values of RBC deformability before administration to patients (personal communication V.L. Sukhorukov).

In the context of erythrocyte disease diagnosis, a microfluidic chip combining cell dipping and electrodeformation (see Fig. 5.17) was conceived.

Concept Electrodeformation of cells occurs in media of lower conductivity than the cytosol. In an externally applied DC field, transient charge accumulation at the poles of the cell is due to the Maxwell-Wagner polarisation mechanism. This dipole builds up within some nanoseconds and stretches the cell before it relaxes again. In continuous AC fields, sustained cell stretching can be established. With microfabricated, planar electrodes designed to expose multiple cells to identical conditions, cells in suspension can be attracted to electrode edges by positive DEP prior to electrodeformation.

The use of planar microelectrode pairs on transparent substrates bears the advantages that the elongation of cells as a function of a predefined force can be observed optically, on a multitude of cells.
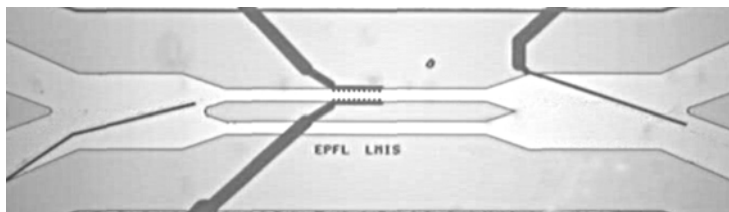
Figure 5.17: Top-view video screenshot of an operational device for dipped electrodeformation. In the 300 μm wide common channel section, human RBCs suspended in PBS are pushed into the parallel flow of low conductive, 300 mOsm sugar solution by a top-bottom pair of 1 MHz dielectrophoretic dipping electrodes. In the 50 μm wide (upper) dipping channel, an electric field perpendicular to the flow can be established between two planar sawtooth electrode, patterned on the bottom of the channel. In the present experiment, the RBCs are brought back into the PBS by the active washing barrier (in deformation-only experiments, this would not be becessary).

The remaining disadvantage of the microelectrode method was the preceding cell preparation: cells must be washed and resuspended in low conductivity sugar medium. This step takes between 5 and 10 minutes, during which cytosolic electrolyte constantly leaks from the cells into the buffer, leading to uncontrollable alterations of both the erythrocytes' and the suspension media electrical properties.

With the newly developed chip cells will be dipped into deformation medium only seconds before experiments, and this will minimise electrolyte leakage.

Experimental Results Fresh Blood was diluted in PBS (300 mOsm, 10 mS/cm). The deformation buffer usually taken is pure 300 mOsm sorbitol solution having a conductivity of 100 μS/cm. In the present device, this would have lead to a dysfunction of the dipping barrier tip reaching into a pDEP medium. Therefore the deformation buffer taken here was a 20:1 sorbitol:PBS dilution with a conductivity of about 0.6 mS/cm. The dipping barrier - operated at

109

1 MHz - would exhibit the desired nDEP, whereas the deformation electrodes - operated at 5 MHz - would exhibit pDEP.

The deformation electrodes have sawtooth shapes in order to enhance field inhomogeneity in the xy plane (*N.B.* the field is most inhomogeneous in the z direction). The facing tip-to-tip distance is 23 μm and the channel height is 20 μm.

An experimental result is shown in Fig. 5.18. RBCs in adjusted deformation medium gain almost a factor two in length when pulled by the electrodeforming force of a 4 kV/cm HF field. They get back to normal shape after field release.
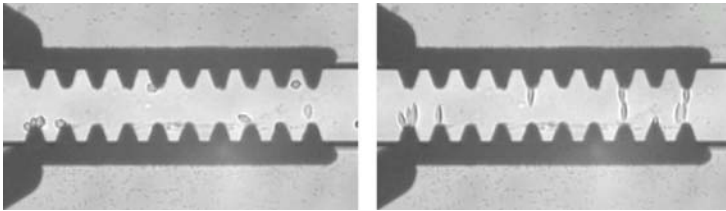
Figure 5.18: Close-up (zoom of Fig. 5.17) of the single-sided sawtooth electrode structure permitting electrical cell deformation due to field inhomogeneities and pDEP conditions. The electrodes have 10 tips, separated by 20 μm, the facing tip-to-tip distance is 23 μm. Human red blood cells have been brought from 10 mS/cm PBS into 0.6 mS/cm low conductivity buffer by cell dipping shortly before the experiment. Upon the application of a 4 kV/cm field at 5 MHz, cells get stretched by an average factor of 1.9x (right). After field release, they regain their initial shape (left).

Conclusion We have presented a microfluidic device combining the two concepts of electrodeformation and cell dipping. In this chip, RBCs were transferred into low conductivity buffer only seconds before being subjected to electrodeforming fields. This precedure reduces electrolyte efflux to a minimum. Cell elongation in defined AC fields

was observed using a microscope and cell deformability was characterised using simple image acquisition and analysis. Thanks to the microchannels and fluidic control, this procedure could be done in a repeated manner, allowing for the measurement of a statistically significant number of cells.

With the here presented enhancement by cell dipping, electrodeformation has evolved further into the direction of a valuable research and diagnosis tool.

5.3   Summary

In this chapter, tools for biological and biophysical experiments were presented; some of which have a potential for applied drug research.

The microfluidic devices for electric and fluidic cell manipulation first shown are capable of dielectrophoretic cell collection which can be superimposed by permeabilising pulses. Electric lysis of stationary groups or individual cells was optically monitored by influx/efflux of dyes and membrane permeabilisation threshold values were assessed.

The functionality of chips designed for long term observation of stationary cells can be enhanced with additional fluid flows immersing the cells with other substances. Multiple or single cells were submitted to different chemicals, in particular a single-cell immersion Trypan Blue staining assay was carried out.

The manipulation of moving cells allows to analyse individual cells of small to medium sized populations one-by-one. The rapid optical permeabilisation tracer system Fluo3/Ca^{2+} for two port chips was introduced and tested.

Dielectrophoretic barriers in flow can selectively deviate particles of

different sizes. In our system, a separation of beads from erythrocytes, but no separation of intact membrane vesicles from small cell debris could be shown.

Parallel laminar flows in a channel can accommodate laterally shifted particles. We have experimentally shown and then improved the concept of cell dipping and cell washing by nDEP deflection.

Cell dipping can be combined with electropermeabilisation and electrodeformation, both of which require buffer other than culture medium. We have shown that cells can be submitted to new chemical environments at precise moments just before *in situ* experiments with electric fields are carried out. We have observed fluorophore efflux in the case of flow-through electropermeabilisation and cell collection and elongation in the case of dipped electrodeformation.

The functional blocks of the chips tested with biological material can be combined to form more advanced devices, they could also be extended by other microfluidic techniques such as cell handling by pressure pulses or cell characterisation by impedance measurements. Potential improvements of the present devices include better electric current injection efficiency at low frequency, individual cell retrieval, on-chip cell culture and compatibility with short working distance microscopy.

Chapter 6

Cell Manipulation using Liquid Electrodes

6.1 The Liquid Electrode Concept

In this chapter, a novel engineering tool for field injection into microchannels is presented. At first, the concept itself is shown, then adaptations or replacements of existing cell manipulation schemes and simulations thereof, and finally experimental results: with so-called liquid electrodes cells can reliably be dipped and they can be electropermeabilised below the kilohertz.

6.1.1 Motivation

An important limitation of metal microelectrodes is that they exhibit very high impedances at low frequencies, as current has to pass the series "double-layer capacitance". The physical background to this phenomenon is the solid-liquid interface between electronic and ionic current conduction. Since the interface impedance is inversely proportional to the surface area of the electrode, microelectrodes in general have a very high impedance ($M\Omega$) at low frequencies (< 1 kHz).

Furthermore, metallic microelectrodes in direct contact with liquid have a limited life-time: the metal slowly corrodes, starting from edges where extreme current densities appear. The by-products of electrode degradation or other electro-chemical reactions may harm biological particles in proximity. Variations in flow speed above the electrodes result in changed electric behaviour due to thermal or ionic evacuation or supply.

The abovementioned limitations of metal electrodes can be overcome by an alternative approach of electric current injection into microchannels. In addition, with that approach, the fabrication and operation of devices for cell manipulation will both be cheaper and more simple.

6.1.2 Description of the Concept

The liquid electrode concept is a methodology where the solid-liquid interface of a traditional metal electrode patterned in a microchannel is replaced by a continuous liquid-liquid "interface" through which ionic current is exchanged. Practically, it consists of an aperture to a channel that is fluidically linked to a supplementary chamber equipped with a large metal patch which has an ohmic connection to external instrumentation. The so-called liquid electrode (LE) is defined as the *equipotential surface spanning across the aperture* (Fig. 6.1, left).

The electric field at the liquid electrode surface not only depends on the shape of the aperture, but also on its orientation in respect to the microfluidic channel, insulating channel walls and neighbouring electrodes. The chemical and electrical properties of the liquid electrode can be tailored shape and height of the recessed LE chamber, the shape of the metal patch, and chemical and electrical properties of the fluid). Even though the LE chamber has a dead end, it must be entirely filled with the same conducting liquid that is present in the channel. Using PDMS, this can be achieved by gas evacuation through the lid (Fig. 6.1, right).
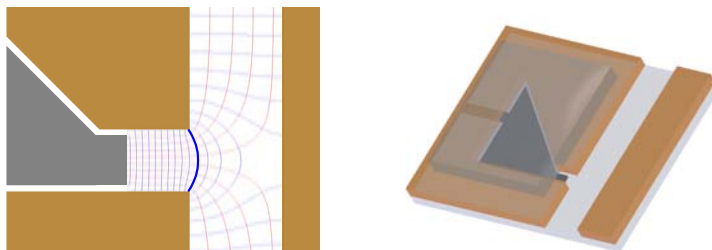
Figure 6.1: Conceptual view of a liquid electrode, defined as the equipotential surface spanning an opening in the wall of a channel. The properties of the liquid electrode, such as shape, current-density, potential and frequency dependent characteristics are determined by the shapes of the aperture and the chamber behind it, the latter of which is equipped with a metal patch and filled with a conductive liquid. (left)
Top view of a typical embodiment of a liquid electrode. On the bottom (and possibly the top and/or side walls) of a liquid-filled microchamber a solid state metal patch is patterned. It has an ohmic connection to a voltage supply. The LE chamber is connected to a microchannel by an aperture in the side wall. Again, it is the equipotential surface at this opening that represents the actual liquid electrode. (right)

Liquid Electrodes Advantages   The expected advantages with the liquid electrodes as described here include a low frequency bandwidth extension for current injection and pick-up, a more homogeneous field at the aperture as compared to the electric field at a solid-state electrode, easier cleaning and longer metal life-time.

Further advantages are that (biological) particles do not get in direct contact with surfaces others than the channel walls, and - as the electrode patches in the liquid electrode chamber are more stable - less electrochemical by-products are released into the working area.

6.1.3   Design Rules

The simplest way to fabricate liquid electrodes is to use planar electrodes on a glass wafer, channels of photosensitive polymer and a lid of PDMS. As a consequence, the LEs are placed laterally, on the channel side walls. Therefore, concepts of electric cell manipulation must be readopted and proven for lateral electrode configurations. In particular, electrokinetic (dielectrophoretic) particle handling schemes that rely on field fringing must be substituted by schemes that rely on controlled lateral electric field patterns given by the position of LE pairs. We will see later that these requirements can be met and that lateral DEP is particularly suited for particle positioning in the xy plane.

Vertical Field Development   If the field distribution at each liquid electrode is homogeneous in the z direction, calculations and simulations can be reduced to two dimensions. Vertical homogeneity is also required to rule out unwanted particle lifting by DEP. For these reasons the metal patch must be placed a certain distance from the aperture so that the field is fully developed in the z direction. It is obvious that full development is the case for a configuration where the LE chamber is far away from the liquid electrode. Practically, this solution is not ideal for the waste of "real estate" on the chip, and for the reason of unnecessary ohmic loss in this "access resistance". In order to find

an optimal distance, the field development from a bottom electrode patch to the liquid electrode was solved analytically using the set of conformal mappings proposed by Linderholm [P 2005].

We found, that this distance should be equal to, or greater than the aperture height in order to obtain a vertically homogeneous field at the liquid electrode surface.

Current Injection and Frequency Behaviour   The liquid electrode chamber can be of arbitrary shape, but should become wider with the distance to the channel (see Fig. 6.1). Such a triangular shape limits the impedance of the liquid electrode at both high and low frequencies. At high frequencies, the majority of the current is emitted from zones close to the tip of the patch; at low frequencies current from the whole surface of the patch is directed through the LE. The chamber and the working zone cavity (channel) are connected by a short conduit.

The shapes of the corners between the channel and the conduit influence the local field distribution. The electrical field is concentrated by pointed shapes, soft fringing occurs at round shapes. Electric field geometry cannot be totally decoupled from fluidic properties as the dimension of the LE opening and the shapes of the corners affect the fluid flow in the microchannel (Fig. 6.2).

Temperature Considerations   High temperatures may result in irreparable damage on cells and biological sample. Electric current passing through a conducting medium results in Joule heating. Several methods of in-situ temperature measurements are available, many of them yield results averaged over the channel height when temperature patterns near electrodes on top and/or bottom are to be characterised (see chapter 4). Using liquid electrodes, more precise temperature distribution maps can be acquired because no part of the working zone is optically hidden by the metal patches. Various techniques of

117
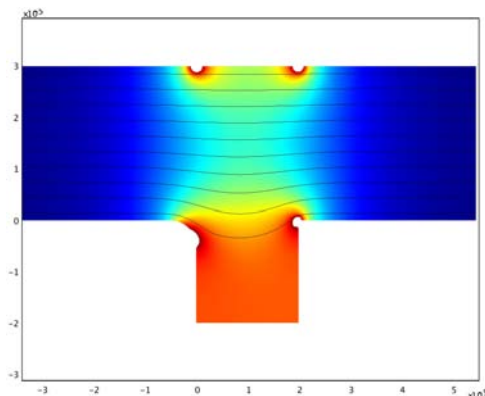
Figure 6.2: 2D FEM simulation of the electric field strength at a solid-state electrode (top) and a liquid electrode (bottom). Electric field intensity is given in an arbitrary colour scale, high fields above a threshold value are white. Extreme fields occur at the metal electrode edges as well as at the sharp corner of the LE aperture. A flatter intensity gradient (so-called *soft fringing*) occurs at the rounded corner.
Fluidic streamlines are indicated in black. The laminar flow is deviated into the aperture.

temperature determination can be used, such as fluorescence quenching [Ross D 2001], temperature-sensitive liquid crystals [Müller T 2003] or thermal precipitation of suitable polymers [Seger U 2005].

In practice, the use of LEs instead of metal electrodes lowers the risk of having zones of damaging temperatures, appearing where the current densities are very high. With metal electrodes, current densities are unavoidably highest at electrode edges and tips; with liquid electrodes, the homogeneity of electric filed distributions can be engineered, and therefore, a much smoother current distribution can be obtained (soft fringing).

6.1.4   Device Microfabrication and Connectivity

Electrodes were structured on 500 μm thick float glass using photolithography (Shipley S-1813 positive photoresist on MicroChem LOR5A lift-off resist), metal deposition (20/200 nm Ti/Pt sputtered in a Pfeiffer Vacuum Spider-600) and lift-off (Microposit 1165 remover). Titanium was used as an adhesion layer between the glass and the platinum. During lift-off, the sacrificial resist layers were removed using ultrasonic agitation.

The channels and liquid handling structures were then patterned using a 20 μm layer of high-aspect ratio SU-8 (MicroChem SU8-2015 photosensitive epoxy). The SU-8 was prebaked at 60º for three minutes to improve adhesion and then exposed in a mask aligner (Süss MicroTec MA-6) to UV radiation. Unexposed SU-8 was selectively removed during development and the remaining structures were final cured in an oven at 150 °C under inert N_2 atmosphere.

The cover lid of the chip was moulded in PDMS (Dow Corning Sylgard DC 184 silicone). The cover lid is several mm thick and features vertical liquid reservoirs directly moulded in it. Before operation, in order to ensure a good seal between the silicone and the glass surface, an oxygen plasma can be used to alter the surface of the PDMS. As a positive side-effect, the modified silicone is hydrophilic, which facilitates the priming of the system. The channels are then filled with medium, which will slowly cover the metal surfaces as the trapped gases evaporate through the PDMS lid. (Alternatively to the oxygen plasma procedure prior to chip sealing, assembled chip-silicone sandwiches can be degassed in a desiccator.)

The liquid electrodes chips have their macroscopic contact pads oriented upwards. They are simply connected to external electric circuitry by spring-loaded contacts (Samtec SEI-115-02 surface mount terminal). From the top, a PMMA (plexiglass) pressure routing head is added, connecting the on-chip reservoirs to the external pressure

bridging circuits (see section 3.4.2). A schematic of the liquid electrode setup is shown in Fig. 6.3.

Prior to operation, the needed liquids are pipetted into the corresponding reservoirs and levelled. For some experiments a slight hydrostatic backpressure is desired; in that case the waste/outlet reservoirs are filled some mm higher than the inlets.
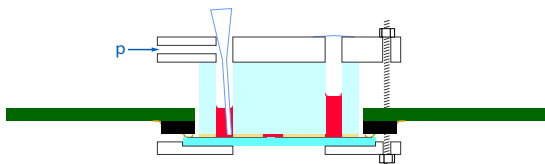
Figure 6.3: Schematic side-view of a setup using liquid electrodes chips. The SU-8 channels on glass are sealed by a silicone lid featuring reservoirs. Liquids are controlled by the application of gas pressures through a routing head. The chip is electrically connected to a PCB via spring-loaded connectors. The setup is held together by screws from the head to the bottom counter piece, it is mounted onto an inverted microscope for observation.

6.1.5 Electric Chip Characterisation

The impedance spectrum of a liquid electrode pair used for electropermeabilisation was measured with an Agilent 4294A impedance analyser. Four liquids of different conductivity were used. The Bode plot shows plateaux of widths of 3 orders of magnitude. The bottom-end interface capacitance cut-off frequency is below 100 Hz (Fig. 6.4). The impedance behaviour of this LE pair should be compared to Fig. 3.11 covering the same frequency range with the same four electrolytes for a pair of solid state electrodes.

Figure 6.4: Magnitude and phase impedance plots for a pair of liquid electrodes with varying electrolyte conductivity.

6.2 Concepts adopted for Liquid Electrodes

Dielectrophoretic elements such as top-bottom nDEP barriers rely on the field fringing between two narrow, opposite current injection strips (see numerous works by the Fuhr group, *e.g.* [Schnelle T 1999]). In principle, the corresponding electrode pair might be placed vertically or laterally. To our knowledge, there are no reports on microfluidic structures using lateral electrodes for DEP generation.

6.2.1 Cell Trapping

In Fig. 6.5, lateral nDEP barriers are created with liquid electrodes. The fringing field repels a particle flowing in a channel from left to

right. The nDEP wall is effective as long as the dielectrophoretic repulsion is superior to the Stokes drag. The amount of field fringing can be controlled be the sizes and the distances of the LEs. Analytical calculations of the field between facing electrode pairs were presented in the 2006 Linderholm, Seger and Renaud paper which is reprinted in Appendix B.
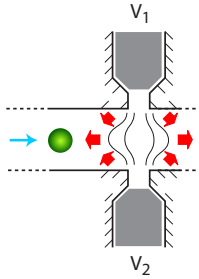
Figure 6.5: nDEP barrier using liquid electrodes and liquid flow. Under nDEP conditions, the cell is repulsed by the fringing electrical field. Using the balance between viscous drag and nDEP force, the cell can be stably maintained in front of the nDEP barrier. If a second such structure is used simultaneously, the cell can be stably captured between two nDEP barriers.

6.2.2 Cell Deviation

Lateral negative dielectrophoresis (nDEP) in field between two coplanar lateral electrodes is a novel manner of handling particles in microchannels (Fig. 6.6). Arrangements of liquid electrodes can be used to repulse and thus to sort suspended particles laterally in flow, to focus them onto one streamline or to push them into auxiliary channel outlets.

An important advantage of lateral DEP structures is that the force acts in a direction parallel to the substrate instead of acting along the

height axis. This fundamental difference makes the sorting of parti-
cles much easier since the force can deviate them along a direction
parallel to the bottom of the channel. A dielectrophoretic force is
generated by the inhomogeneous electric field between the two elec-
trodes. If the electrical properties (permittivity and conductivity) of
the medium and the particles in suspension and the applied frequency
impose negative dielectrophoresis, the configuration in Fig. 6.6 leads
to lateral nDEP forces that tend to deflect dielectric particles towards
the opposite side of the main channel. If the main channel separates
in several channels afterwards, the perpendicular force can select the
output that each particle will take by controllable deviation.
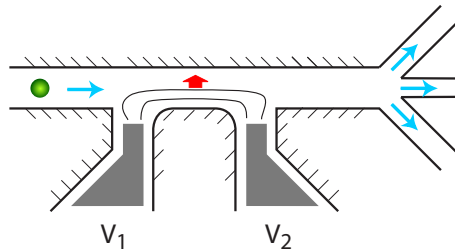
Figure 6.6: Sorting device using nDEP and liquid electrodes. The
inhomogeneous field imposed by the two lateral liquid electrodes im-
poses a nDEP force towards the opposite channel wall. This lateral
displacement can *e.g.* be used for particle focusing or sorting into
different outlets.

The relative position and orientation between lateral electrodes and
the main channel can enhance inhomogeneities of the electric field in
some places while making it uniform in other regions. If two LEs are
placed on the same side wall, the shape of the isolating wall situated
between the two is a geometrical factor to be considered: Its length
and its protrusion into the channel modulate the lateral nDEP force
field.

6. Cell Manipulation using Liquid Electrodes

Particle Tracking Simulation   There is a major difference between particle deflection using facing electrodes field barriers at an angle to the flow [*e.g.* Dürr M 2003] and lateral nDEP: In field barrier deflection, the particle is guided upstream of the electrode pair at an equilibrium position between electric and friction forces. Above a certain critical flow speed, a field barrier fails. This is not the case for lateral nDEP deflection: particles are crossing a distributed force field over some length, during some time. With increasing speed, lateral deviation efficacy will decrease, but not cease.

To evaluate the influence of channel and electrode geometry on lateral nDEP deflection efficiency, particle tracking was simulated using MATLAB. The electric field distribution was calculated as a function of channel width, electrode width and inter-electrode gap using the method described by Linderholm [P 2005]. The dielectrophoretic force was mapped as a function of particle and buffer characteristics. Using the iterative algorithm given in Appendix C, the sum of forces was translated into instantaneous speed. According to Morgan and Green [H 2003, § 5.4], Newton's second law $F = m \cdot a$ can be written as

$$m\frac{d\vec{v}}{dt} = \vec{F}_{DEP} + \mathfrak{f}(\vec{u} - \vec{v}) \;,\tag{6.1}$$

where m is the mass of the particle, $\vec{v}$ is its velocity, $\vec{F}_{DEP}$ the dielectrophoretic force acting on it and $\vec{u}$ is the velocity of the flowing buffer. The friction factor for a sphere $\mathfrak{f} = 6\pi\eta r$ links the expression with Stokes law $\vec{F}_{Stokes} = \mathfrak{f}(\vec{u} - \vec{v})$.

This differential equation yields the following solution:

$$\vec{v} = (\frac{\vec{F}_{DEP}}{\mathfrak{f}} + \vec{u})(1 - e^{-\frac{\mathfrak{f}}{m}t}) + \vec{v}_0 \cdot e^{-\frac{\mathfrak{f}}{m}t} \;,\tag{6.2}$$

where v_0 is the initial velocity.

The acceleration/inertia term $e^{-(\mathfrak{f}/m)\,t}$ has a time constant $m/\mathfrak{f}$ of

about 100 μs for 15 μm diameter particles in water, therefore the expression of terminal velocity

$$\vec{v} = (\frac{\vec{F}_{DEP}}{\mathfrak{f}} + \vec{u}) \tag{6.3}$$

only was taken into account in our particle tracking simulation.

In the simulation algorithm the particle velocity v_n is calculated at a given position p_n at a given time t_n, and the new position at time $t_{n+1} = t_n + \Delta t$ is determined as $p_{n+1} = p_n + v_n \cdot \Delta t$.

The lateral force field is mainly active over the first half of the structure; once particles have travelled to the position of the second electrode, they are out of reach of the lateral DEP (Fig. 6.7). In a 80 μm wide channel, at a flow speed of 100 μm/s and for an applied voltage of 10 V between two LE patches, particles of 3.8 μm radius are deflected well beyond the channel mid-width; this is important for applications like cell sorting or cell dipping.
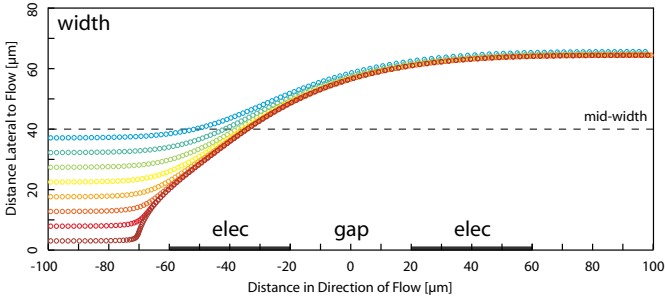
Figure 6.7: Particle tracking simulation for lateral nDEP deflection. This graph was calculated using an iterative algorithm in discrete time adding drag forces and DEP forces. The used geometrical parameters are the following: electrodes widths: 40 μm, interelectrode gap: 40 μm, channel width: 80 μm.

Parameters Influencing Particle Deviation   The lateral deflec-
tion efficiency depends on a great number of "soft" parameters, such
as field strength, frequency/buffer, particle size and flow speed. The
effect of all of these parameters can be emulated by sweeping one pa-
rameter - *e.g.* flow speed - only. The inflence of "hard", geometrical
parameters however must be evaluated individually. In the present
study we looked at the factors electrode width (*elec*), interelectrode
distance (*gap*) and channel width (*width*).

Fig. 6.8 a) shows the relationship of speed on deflection efficiency. As
anticipated, there is no speed at which deflection ceases completely.
However, above four-fold nominal speed (400 μm/s), particles don't
get deflected any further than the mid-width of the channel.

The influence of the interelectrode gap on deflection efficiency is de-
picted in Fig. 6.8 b). For very small gaps, the electric field will not
develop into the full width of the channel, small gaps are inefficient for
lateral nDEP deflection. Very big gaps are not ideal either, because
over the majority of the distance, the field will be fully developped,
thus homogeneous. There will therefore be no DEP force in that zone:
power is dissipated for nothing, so efficiency is low. In the case de-
picted here, the optimum gap size lies between 40 and 80 μm, it is
inferior to the channel width.

In the plots c) and d) of Fig. 6.8, the influence of channel width on
deflection efficienccy is shown, once in absolute values, once relatively.

6.2.3   Permeabilisation

Electric fields can induce membrane breakdown of cells in flow, if the
static or pulsed electric fields attain strengths typically above 1 kV
/ cm. Homogenous fields are generally preferred, for the lack of di-
electrophoretic components and for the more accurate modelling of
the influence of the field on the particle. The wider the electrodes,
the more homogeneous the field becomes. Liquid electrodes for lateral
electropermeabilisation are shown in (Fig. 6.9).
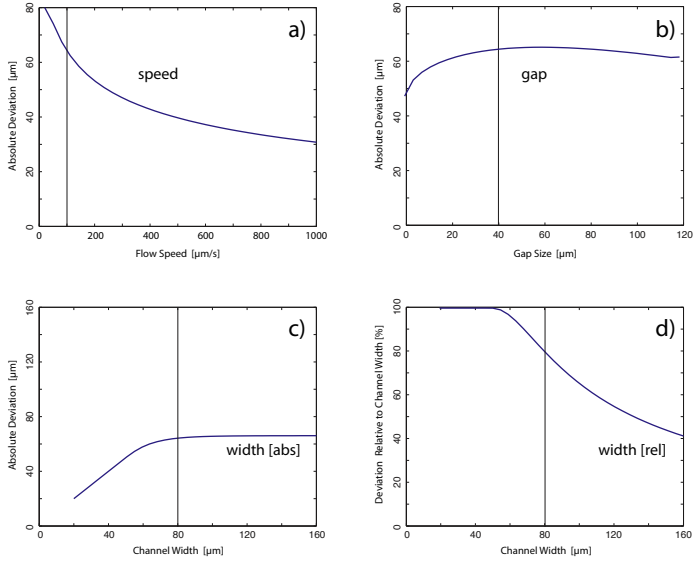
Figure 6.8: Simulated lateral nDEP deflection efficiencies (minimum deflections) as functions of flow speed and design parameters variations. With increasing flow, particles get less deflected, but they will not "tunnel" the force field a). Too small and too large gaps result in non-optimal deflection yields b). The reach of the nDEP force field is limited c), increasing the channel width results in lower relative lateral displacement d).
The fixed parameters are the same as the ones for Fig. 6.7. The thin grey lines indicate the reference value of the swept parameter.
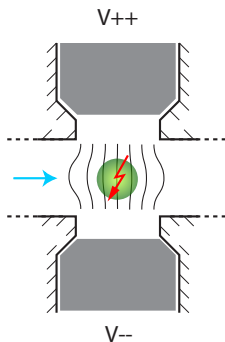
Figure 6.9: Cell electroporation and cell lysis. The electrical field from two liquid electrodes is used to electropermeabilise a cell reversibly, or to lyse it irreversibly depending on the applied field.

6.3 Applications of Liquid Electrodes

6.3.1 Cell Dipping using Liquid Electrodes

The previously discussed cell dipping concept can also be implemented using liquid electrodes (Fig. 6.10). One pair of LEs is used to deviate the cells from liquid 1 to liquid 2. For washing, a second pair of LEs brings the cells back in the original buffer. Again, the exposure time can be controlled by varying flow speeds and channel geometries.

Experimental Human RBCs are suspended in low conductivity, 300 mOsm sorbitol solution (one drop of blood is diluted in 1 ml medium). The liquid electrodes setup is primed with pure sorbitol solution. Cells are introduced into the microchannel and parallel flow-patterns are established (see Fig. 6.11, top row). At an estimated flowspeed of 150 μm/s at the intersection, the RBCs are laterally deflected and dipped into the clean solution flowing in the upper branch

Figure 6.10: Liquid electrode cell dipping. Cells coming from the lower inlet are pushed into a reagent liquid stream coming from the upper inlet by the nDEP force generated by a liquid electrode pair. In the upper dipping branch incubation takes place, with the possibility to apply liquid electrode electropermeabilisation pulses. After the washing nDEP deviation, cells and reagent leave the chip through different outlets.

(see Fig. 6.11, bottom row). This is the first proof of principle for cell dipping using LE lateral nDEP deflection.

In terms of fluidics, the present design can be characterised using videography: channel width variations lead to irregular particle movements and the position of the channel separation is not optimal. In terms of electrical field strengths, one can consult the estimates of paragraph 6.2.2, where a liquid electrode geometry similar to the present structure was used: using LE metal patches recessed by 20 μm (the height of the channel), 49 % of the injected power is dissipated in the access resistances. For the applied voltage of 34 V_{pp} (*i.e.* 12 V_{rms}), this leaves some 6 V to drop over the channel between the two liquid electrodes that are separated by 40 μm). The maximum experienced field strength is thus in the order of 0.7 kV/cm. This is 3-5 times weaker than the field strengths occurring in devices using top-bottom

nDEP barriers for RBC deviation.
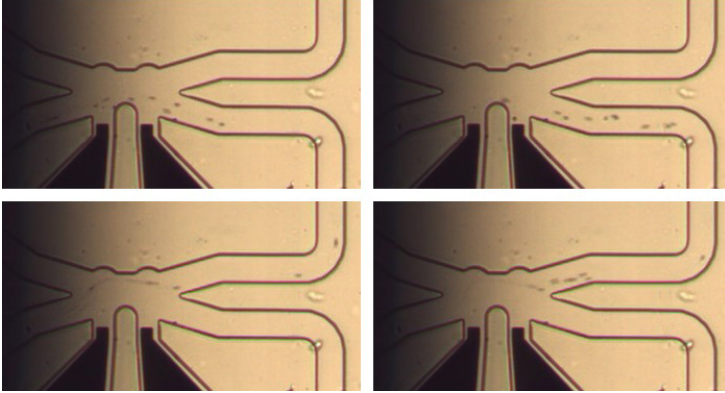
Figure 6.11: Experimental proof of liquid electrode cell dipping. Human Erythrocytes suspended in low conductivity medium from the bottom inlet to the bottom branch past a pair of inactive lateral nDEP liquid electrodes. Clean solution is flowing from the upper inlet into the upper branch (top row pictures).
Upon activation of the dipping LE pair, the RBCs are deviated laterally into the upper branch. The nDEP signal is a 34 V_{pp} sinus at 110 kHz. The estimated flow speed is 150 μm/s (bottom row pictures).

6.3.2 Frequency Dependency of the Electropermeabilisation Threshold

Fresh human erythrocytes were suspended in low conductivity poration buffer (300 mOsm sorbitol, 10 μS/cm). Using a pair of liquid electrodes situated in a turn of a LE cell dipping device (Fig. 6.10), electropermeabilisation fields were applied to cells in flow. With increasing voltage, haemoglobin efflux was observed, first rarely, then on all passing cells. These ranges, measured at different frequencies are plotted in Fig. 6.12. As the field distribution in the channel was inhomogeneous, no field strengths but the applied voltages are indicated.

This threshold-frequency relationship is definitely not an artefact due to the chip's impedance spectrum (Fig. 6.4) nor is it a heating effect (low conductivity buffer was used). Comparing the raw data with the transmembrane voltage induction plot of Fig. 2.11 we believe this is experimental evidence of the Jeltsch and Holzapfel AC transmembrane voltage formula - acquired on a microfluidic device.
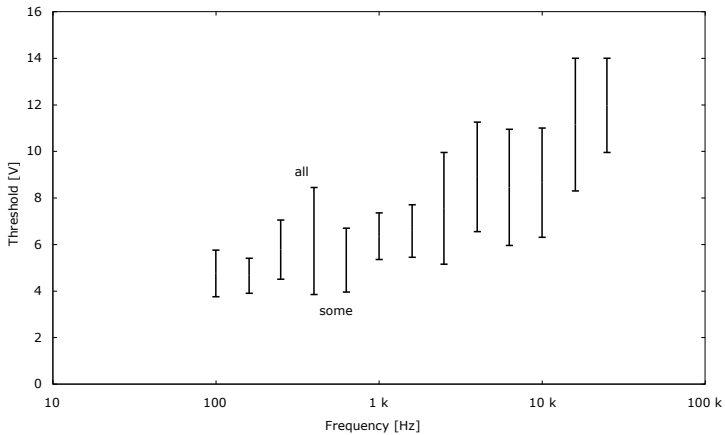
Figure 6.12: Frequency dependency of the electropermeabilisation threshold assessed in a microchip using liquid electrodes. Red blood cells suspended in 300 mOsm sorbitol buffer of conductivity 10 μS/cm were passed between in an AC field. For each frequency, the voltage was increased until rare hemolysis was observed ("some") and then further until the complete population of erythrocytes ("all") was lysed.
The vertical bars indicate these ranges in arbitrary units.

6.4   Summary

The major drawback of microfluidic devices featuring solid-state electrodes is that they are limited in low frequency bandwidth by the

electrode-electrolyte capacitance. Other disadvantages are extreme current densities at the electrode edges (leading to heat, chemical reactions and metal erosion), sensitivity to flow speed variations and altered interface due to debris deposition.

The above issues were addressed by the introduction of the liquid electrode concept: A liquid electrode ensemble consists of an aperture and a recessed chamber equipped with a metal patch. The liquid electrode itself is the equipotential surface spanning across the aperture, through which ionic current is exchanged.

A number of other currently existing microelectrode devices can benefit from a substitution of the metal electrode to a liquid electrode. In many cases, the measurement and manipulation concepts can be kept unchanged, and only the channel geometry adapted. Three adapted concepts were presented: field barriers using LEs, lateral nDEP deflection and electropermeabilisation in flow. Deflection efficacy was simulated using a particle tracking algorithm based on vectorial force addition of Stokes drag and analytically calculated nDEP force.

We have experimentally shown lateral deflection in a LE cell dipping device: even though the device geometry was not optimised, RBCs flowing at 150 μm/s were deviated well beyond half the width of the channel. Therefore, local field strengths below 0.7 kV/m were required. This is significantly less than what we have priorly used for top-bottom metal electrodes nDEP barrier devices of comparable performance.

In an electropermeabilisation device using liquid electrodes, we have also assessed a frequency-dependent membrane breakdown spectrum of RBCs in low conductivity medium. Frequencies down to 100 Hz were used, this is 2 orders of magnitude below the cut-off frequency of metal electrodes.

In summary, the liquid electrode concept was successfully introduced and first experiments related to the subject of the present thesis have been carried out. Liquid electrodes are very promising tools to replace solid electrodes wherever soft field fringing, lower frequencies, simpler fabrication of lateral electrodes and more rugged operation

are required. Further research and development on liquid electrodes is currently being carried out at LMIS4.

The Liquid Electrode Concept has been initiated, pursued and refined by Pontus Linderholm, Thomas Braschler, Nicolas Demierre and myself, and an international patent application has been filed [Renaud P 2006]. Only aspects in direct relationship with this thesis were presented and further developed in this chapter.

Chapter 7

Conclusions

This is a dissertation about small channels, small electrodes and biological cells in suspension. It focuses on the developments of research instruments for electromanipulation of cells in flow.

Concepts, Tools and Theory   A common characteristic of all devices presented is the use of dielectrophoresis (DEP) as a tool for *cell handling*. The DEP phenomenon must be understood in order to predict forces as a function of particle and medium characteristics and of electric field geometry. The effective dipole moment principle leading to the protoplast model of Kaler & Jones provides sufficient insight, assuming that cells are spheres of homogeneous membrane and interior.

The second, important concept is *cell modification* by electropermeabilisation. There is a wealth of research papers treating theories of electropermeabilisation giving rise to electroporation, *i.e.* pore precursoring, establishment and disappearance. There are also many reports on transport of genetic material through those pores, leading to electrotransfection. These theories were *not* the scope of this thesis. For the present work only the understanding of Jeltsch's and Holzapfel's

AC transmembrane voltage induction relation is required.

All devices are microfluidic chips. Flow is largely used for particle handling in counterforce with nDEP, therefore Stokes' drag force relation is used. Pressure driven flow is also used for the introduction of additional chemical environments, their behaviour is governed by laminar flows and diffusion.

The electric field development is analytically solved using Linderholm's conformal mappings where possible. For more complex electrode and channel configurations, finite element modeling (Comsol Multiphysics) is used. Iterative simulation algorithms are programmed in MATLAB.

7.1   Summary

Chip Fabrication and Operation Microfluidic chips were designed and fabricated for specific tasks. Clean room microfabrication using planar technologies for electrode and channel patterning on glass, followed by flip-chip assembly, dicing and hole drilling gave rise to transparent, chemically inert devices. They were mounted in custom-made chip holders ensuring both electrical and fluidic micro-macro interfacing.

Electric signals were generated using standard function generators and custom-made bi-amplification circuits and voltages of 34 V_{pp} over 20 μm distance (channel height) allowed for theoretical electric peak-to-peak field strengths of 17 kV$_{pp}$/cm up to 5 MHz.

Flows were controlled using gas overpressures onto fluid reservoirs, the pressures were defined by external pressure bridging. Pressure control was well below the tenth of a millibar (*i.e.* the hydrostatic pressure of 1 mm of water), resulting in minimal flow speeds in the order of some μm/s. This flow control allowed for the establishment of parallel laminar flows and for the positioning of cells at the intersection of two perpendicular channels.

Experiments were observed on an inverted long working distance microscope under bright- or darkfield conditions and recorded to video.

Cell Handling   Cells were captured individually and held against flow in negative dielectrophoretic (nDEP) traps. For cells suspended in highly conductive solutions, such as PBS or cell culture media, *rms* fields in the order of 2.5 kV/cm were sufficient to withstand flows speeds above 100 μm/s. Cell trapping was mainly used prior to electropermeablisation or cell immersion.

Multiple cells in flow were deviated using top-bottom nDEP barriers. Lateral shifting was used in the DEP deflection filter experiment, where 5 μm diameter polystyrene beads could be selectively removed from a mixture of RBCs with beads. The most important concept/application in terms of cell handling is cell dipping: cells could be guided from an initial liquid stream into a second. This corresponds to the microfluidic on-chip version of "cell re-suspension in no time": cells can now be exposed to or washed from chemical environments in a fraction of a second!

Cell Modification   Cell membranes were modified using electropermeabilisation pulses. In systems with volumes between electrodes comparable to cell size, each lone cell in that volume experiences the same external electric field. This is a powerful method to rule out cell-cell interactions during exposition. If a flow is applied, a statistically significant number of events can be recorded.

Single and multiple cell electropermeabilisation was shown either on immobile or on flowing cells. Membrane breakdown was optically witnessed using nucleic stains or a faster, ion-sensitive fluorophore.

Direct Applications of Cell Dipping   The cell dipping concept was combined with flow-through electropermeablisation. Fluorescein-loaded Jurkat cell suspended in background fluorescing culture medium were transferred into low-conductive poration medium only seconds before permeabiliation. In this way, re-suspension was prevented and fluorophore leakage was minimised.

7. Conclusions

In a second experiment, erythrocytes were dipped into low ionic buffer prior to electrodeformation. As only little electrolyte leakage occured, the experimental conditions were clearly defined. Erythrocytes were stretched by a factor 2 in a 4 kV/cm field at 5 MHz.

Temperature Measurements   Temperature distributions near active nDEP barriers were visualised within chips by the use of temperature sensitive Rhodamine B. This data was fitted to a cylindrical heat propagation model and temperatures above 45 °C were reached for fields from 3.9 kV/cm (valid for PBS with a conductivity of 1.2 S/m). Temperature threshold values in vicinity of barriers were also visualised using the original method of thermoprecipiation of modified isopropylacrylamides suspended in PBS having tailored LCSTs (lower critical solution temperatures) of 29 and 40 °C. Isotherms as a function of applied voltage were assessed and the data was in good agreement with the fluorescence method.

Liquid Electrodes   The liquid electrode concept elaborated in the research team at LMIS4 was shown to be a simple, yet rugged, approach for electromanipulation of cells. The promise of simpler fabrication and operation paired with lower cut-off frequency at the bottom end was held.
Lateral electrodes nDEP deflection was simulated using artificial particle tracking and experimentally shown in the case of RBCs being deviated across a 60 μm wide channel by a field of 0.7 kV/cm. Also, a membrane breakdown spectrum as a function of frequency was assessed using liquid electrodes for electropermeabilisation: the result was in good agreement with Holzapfel's expression of transmebrane voltage.

7.2 Outlook

Future Research   The combined cell dipping devices presented in this thesis are ideal tools for research on secondary factors influencing membrane breakdown: because buffer exchange is fast, time-sensitive experiments of conditions that would be lethal to macroscopically (=slowly) handled cells can be carried out on chip. This includes *e.g.* osmotic swelling in DI water, permeabilisation and resuspension in physiological solution.

Another possibility of combined cell-dipping would be electrodeformation in flow, using facing liquid electrodes producing a homogeneous field.

A lateral DEP electrode configuration such as used for lateral nDEP deflection could also be used to produce a cell-size-selective field for electropermeabilisation, ruling out size distribution in a cell population.

Superimposed nDEP and EP signals could also be used to define a field barrier that retains cells as long as their membrane is intact.

Also, low-frequency electrorotation experiments could benefit from an implementation of liquid electrodes.

Potential Device Improvements   The main limitation of the presented devices is that they are restricted to assays with low resolution optical feedback. The use of thinner glass wafers / thinned chips would permit the use of short working distance microscopy.

The device fabrication process is compatible with a straightforward implementation of on-chip impedance measurements, a μDACS assessment of the membrane state after electropermeabilisation or dipping into a reagent such as an membrane perforator would allow to characterise opening and resealing kinetics.

The versatility of the present devices could be enhanced with low volume cell suspension exchange ports, through which a user could retrieve (or inject) small samples for further treatment.

7. Conclusions

The possibility of on-chip cell culture would equally make these devices more attractive to the biologist community.

References

A-Hassan E, Heinz WF, Antonik MD, D'Costa NP, Nageswaran S, Schoenenberger CA and Hoh JH, 1998: *Relative microelastic mapping of living cells by atomic force microscopy.* Biophysical Journal, *vol. 74*: 1564–1578. 5

Arnold WM, 1998: *Dielectric measurements using novel three-electrode technique.* In *1998 Annual Report Conference on Electrical Insulation and Dielectric Phenomena, Vols 1 and 2*, pp. 356–359 (I E E E, New York). 12

Arnold WM and Zimmermann U, 1982: *Rotating-Field-Induced Rotation and Measurement of the Membrane Capacitance of Single Mesophyll-Cells of Avena-Sativa.* Zeitschrift Fur Naturforschung C-a Journal of Biosciences, *vol. 37.* 12

Asami K, Yonezawa T, Wakamatsu H and Koyanagi N, 1996: *Dielectric spectroscopy of biological cells.* Bioelectrochemistry and Bioenergetics, *vol. 40*(2): 141–145. 13

Ashkin A, 2000: *History of optical trapping and manipulation of small-neutral particle, atoms, and molecules.* Ieee Journal of Selected Topics in Quantum Electronics, *vol. 6*(6): 841–856. 9

Ashkin A, Dziedzic JM, Bjorkholm JE and Chu S, 1986: *Observation of a Single-Beam Gradient Force Optical Trap for Dielectric Particles.* Optics Letters, *vol. 11*(5): 288–290. 9

Auroux PA, Iossifidis D, Reyes DR and Manz A, 2002: *Micro total analysis systems. 2. Analytical standard operations and applications.* Analytical Chemistry, *vol. 74*(12): 2637–2652. 1

Barrau C, Teissie J and Gabriel B, 2004: *Osmotically induced membrane tension facilitates the triggering of living cell electropermeabilization.* Bioelectrochemistry, *vol. 63*: 327–332. 36

REFERENCES

Barrett LM, Skulan AJ, Singh AK, Cummings EB and Fiechtner GJ, 2005: *Dielectrophoretic manipulation of particles and cells using insulating ridges in faceted prism microchannels.* Analytical Chemistry, *vol. 77*(21): 6798–6804. 9

Becker FF, Wang XB, Huang Y, Pethig R, Vykoukal J and Gascoyne PRC, 1995: *Separation of Human Breast-Cancer Cells from Blood by Differential Dielectric Affinity.* Proceedings of the National Academy of Sciences of the United States of America, *vol. 92*(3): 860–864. 11

Beebe DJ, Mensing GA and Walker GM, 2002: *Physics and applications of microfluidics in biology.* Annual Review of Biomedical Engineering, *vol. 4*. 2

Benz R, Beckers F and Zimmermann U, 1979: *Reversible electrical breakdown of lipid bilayer membranes: A charge-pulse relaxation study.* Journal of Membrane Biology, *vol. 48*: 181–204. 35

Besselink GAJ, Vulto P, Lammertink RGH, Schlautmann S, van den Berg A, Olthuis W, Engbers GHM and Schasfoort RBM, 2004: *Electroosmotic guiding of sample flows in a laminar flow chamber.* Electrophoresis, *vol. 25*: 3705–3711. 87

Braschler T, Johann R, Heule M, Metref L and Renaud P, 2005: *Gentle cell trapping and release on a microfluidic chip by in situ alginate hydrogel formation.* Lab on a Chip - Miniaturisation for Chemistry and Biology, *vol. 5*: 553–559. 11, 53

Brody JP, Han Y, Austin RH and Bitensky M, 1995: *Deformation and flow of red blood cells in a synthetic lattice: Evidence for an active cytoskeleton.* Biophysical Journal, *vol. 68*: 2224–2232. 4

Brody JP, Yager P, Goldstein RE and Austin RH, 1996: *Biotechnology at low Reynolds numbers.* Biophysical Journal, *vol. 71*: 3430–3441. 2, 44

Bronkhorst PJH, Streekstra GJ, Grimbergen J, Nijhof EJ, Sixma JJ and Brakenhoff GJ, 1995: *A new method to study shape recovery of red blood cells using multiple optical trapping.* Biophysical Journal, *vol. 69*: 1666–1673. 5

Bryant G and Wolfe J, 1987: *Electromechanical stresses produced in the plasma membranes of suspended cells by applied electric fields.* Journal of Membrane Biology, *vol. 96*: 129–139. 5

Cepko CL, Roberts BE and Mulligan RC, 1984: *Construction and Applications of a Highly Transmissible Murine Retrovirus Shuttle Vector.* Cell, *vol. 37*(3): 1053–1062. 3

Chan HY and Li WJ, 2002: *A polymer-based micro thermal actuator for micromanipulations in aqueous environment.* International Journal of Nonlinear Sciences and Numerical Simulation, *vol. 3*(3-4): 775–778. 10

Chang DC, 1989: *Cell Poration and Cell Fusion Using an Oscillating Electric Field.* Biophysical Journal, *vol. 56*(4): 641–652. 80

Chang DC, 1992c: *Structure and Dynamics of Electric Field-Induced Membrane Pores as Revealed by Rapid-Freezing Electron Microscopy.* In Chang DC, Chassy BM, Saunders JA and Sowers AE (eds.) *Guide to Electroporation and Electrofusion*, pp. 9–27 (Academic Press, San Diego, California). 34

Chang DC and Reese TS, 1990: *Changes in Membrane-Structure Induced by Electroporation as Revealed by Rapid-Freezing Electron-Microscopy.* Biophysical Journal, *vol. 58*(1): 1–12. 34

Chang DC, Saunders JA, Chassy BM and Sowers AE, 1992b: *Overview of Electroporation and Electrofusion.* In Chang DC, Chassy BM, Saunders JA and Sowers AE (eds.) *Guide to Electroporation and Electrofusion*, pp. 1–6 (Academic Press, San Diego, California). 15

Chen CS, Jiang X and Whitesides GM, 2005: *Microengineering the environment of mammalian cells in culture.* MRS Bulletin, *vol. 30*: 194–201. 86

Cheung K, Gawad S and Renaud P, 2005: *Impedance spectroscopy flow cytometry: On-chip label-free cell differentiation.* Cytometry Part A, *vol. 65A*(2): 124–132. 14

Chiou PY, Ohta AT and Wu MC, 2005: *Massively parallel manipulation of single cells and microparticles using optical images.* Nature, *vol. 436*(7049): 370–372. 3

Chiu DT, Jeon NL, Huang S, Kane RS, Wargo CJ, Choi IS, Ingber DE and Whitesides GM, 2000: *Patterned deposition of cells and proteins onto surfaces by using three-dimensional microfluidic systems.* Proceedings of the National Academy of Sciences of the United States of America, *vol. 97*(6): 2408–2413. 11

Chou CF, Tegenfeldt JO, Bakajin O, Chan SS, Cox EC, Darnton N, Duke T and Austin RH, 2002: *Electrodeless dielectrophoresis of single- and double-stranded DNA.* Biophysical Journal, *vol. 83*(4): 2170–2179. 8

Coakley WT, Bardsley DW, Grundy MA, Zamani F and Clarke DJ, 1989: *Cell Manipulation in Ultrasonic Standing Wave Fields.* Journal of Chemical Technology and Biotechnology, *vol. 44*(1): 43–62. 9

Coppeta J and Rogers C, 1998: *Dual emission laser induced fluorescence for direct planar scalar behavior measurements.* Experiments in Fluids, *vol. 25*(1): 1–15. 63

Coulter WH, 1953: *Means for Counting Particles Suspended in a Fluid.* 13

REFERENCES

Crowley JM, 1973: *Electrical Breakdown of Biomolecular Lipid-Membranes as an Electromechanical Instability*. Biophysical Journal, *vol. 13*. 14

Curtis A and Wilkinson C, 1997: *Topographical control of cells*. Biomaterials, *vol. 18*. 11

Daridon A, Throndset W, Liau I, Farell K, Tseng F, Javadi S and Manger I, 2002: *A Programmable Cell Assay Platform for Kinetic Studies of a Single Cell*. In *Micro Total Analysis Systems*, vol. 1 of *Mesa Monographs*, pp. 31–33 (Kluwer Academic Publishers, Nara). 10

de Gennes PG, 1999: *Problems of DNA entry into a cell*. Physica A, *vol. 274*(1-2): 1–7. 37

Declercq F, 2003/2004: *nDEP-Based Electronic Detection of Cells Captured in Microfluidic Devices*. Semester Project, Microsystems Laboratory, EPFL. 52

Demierre N, 2003: *DEPDEF: A Dielectrophoretic Deflection Filter for Biological Matter*. Semester Project, Microsystems Laboratory (Collaboration with LCPPM, Prof. H. Vogel), EPFL. 97

Dev SB, Rabussay DP, Widera G and Hofmann GA, 2000: *Medical applications of electroporation*. Ieee Transactions on Plasma Science, *vol. 28*. 15

Di Carlo D and Lee LP, 2002: *Enhanced Velocity Gradients within Microfluidics for Cellular Manipulation*. In *Micro Total Analysis Systems*, vol. 2 of *Mesa Monographs*, pp. 799–801 (Kluwer Academic Publishers, Nara). 14

Djuzenova CS, Zimmermann U, Frank H, Sukhorukov VL, Richter E and Fuhr G, 1996: *Effect of medium conductivity and composition on the uptake of propidium iodide into electropermeabilized myeloma cells*. Biochimica Et Biophysica Acta-Biomembranes, *vol. 1284*(2): 143–152. 36, 85

Dobbe JGG, Streekstra GJ, Hardeman MR, Ince C and Grimbergen CA, 2002: *Measurement of the Distribution of Red Blood Cell Deformability Using an Automated Rheoscope*. Clinical Cytometry, *vol. 50*: 313–325. 5

Docoslis A, Kalogerakis N, Behie LA and Kaler KVIS, 1997: *A novel dielectrophoresis-based device for the selective retention of viable cells in cell culture media*. Biotechnology and Bioengineering, *vol. 54*(3): 239–250. 8

Duffy DC, Schueller OJA, Brittain ST and Whitesides GM, 1999: *Rapid prototyping of microfluidic switches in poly(dimethyl siloxane) and their actuation by electro-osmotic flow*. Journal of Micromechanics and Microengineering, *vol. 9*(3): 211–217. 6

Durr M, Kentsch J, Muller T, Schnelle T and Stelzle M, 2003: *Microdevices for manipulation and accumulation of micro- and nanoparticles by dielectrophoresis.* Electrophoresis, *vol. 24* (4): 722–731. 60, 97, 124

Elson EL, 1988: *Cellular mechanics as an indicator of cytoskeletal structure and function.* Annual review of biophysics and biophysical chemistry, *vol. 17*: 397–430. 4

Engel J, Donath E and Gimsa J, 1988: *Electrorotation of Red-Cells after Electroporation.* Studia Biophysica, *vol. 125.* 12

Engelhardt H and Sackmann E, 1988: *On the measurement of shear elastic moduli and viscosities of erythrocyte plasma membranes by transient deformation in high frequency electric fields.* Biophysical Journal, *vol. 54* (3): 495–508. 5

Erickson D, Sinton D and Li DQ, 2003: *Joule heating and heat transfer in poly(dimethylsiloxane) microfluidic systems.* Lab on a Chip, *vol. 3* (3): 141–149. 60

Fertig N, Meyer C, Blick RH, Trautmann C and Behrends JC, 2001: *Microstructured glass chip for ion-channel electrophysiology.* Physical Review E, *vol. 6404.* 10

Fiedler S, Shirley SG, Schnelle T and Fuhr G, 1998: *Dielectrophoretic sorting of particles and cells in a microsystem.* Analytical Chemistry, *vol. 70* (9): 1909–1915. 8

Fox MB, Esveld DC, Valero A, Luttge R, Mastwijk HC, Bartels PV, van den Berg A and Boom RM, 2006: *Electroporation of cells in microfluidic devices: a review.* Analytical and Bioanalytical Chemistry, *vol. 385.* 17

Friend AW, Finch E and Schwan HP, 1975: *Low Frequency Electric Field Induced Changes in the Shape and Motility of Amoebas.* Science, *vol. 187* (4174): 357–359. 5

Fu AY, Spence C, Scherer A, Arnold FH and Quake SR, 1999: *A microfabricated fluorescence-activated cell sorter.* Nature Biotechnology, *vol. 17.* 6

Fuchs A, Freida D, Chartier I, Sarrut N, Villiers C, Medoro G, Manaresi N, Romani A, Altomare L, Guerrieri R and Tartagni M, 2002: *MeDICS: A Lab-on-a-Chip for Cell Separation Based on Dielectrophoresis.* In Donzel Ao (ed.) *NanoTech.* 8

Fuhr G, Hagedorn R, Muller T, Wagner B and Benecke W, 1991: *Linear Motion of Dielectric Particles and Living Cells in Microfabricated Structures Induced by Traveling Electric-Fields.* In *Ieee Micro Electro Mechanical Systems - an Investigation of Micro Structures, Sensors, Actuators, Machines and Robots*, pp. 259–264 (I E E E, New York). 8

REFERENCES

Fuhr G, Glasser H, Muller T and Schnelle T, 1994: *Cell Manipulation and Cultivation under Ac Electric-Field Influence in Highly Conductive Culture Media.* Biochimica Et Biophysica Acta-General Subjects, *vol. 1201*(3): 353–360. 7

Fuhr G, Muller T, Schnelle T, Hagedorn R, Voigt A, Fiedler S, Arnold WM, Zimmermann U, Wagner B and Heuberger A, 1994c: *Radiofrequency Microtools for Particle and Live Cell Manipulation.* Naturwissenschaften, *vol. 81*(12): 528–535. 78

Fuhr G, Schnelle T, Muller T, Hitzler H, Monajembashi S and Greulich KO, 1998: *Force measurements of optical tweezers in electro-optical cages.* Applied Physics a-Materials Science and Processing, *vol. 67*(4): 385–390. 9

Gabriel B and Teissie J, 1999: *Time courses of mammalian cell electroperme-abilization observed by millisecond imaging of membrane property changes during the pulse.* Biophysical Journal, *vol. 76*: 2158–2165. 85, 92

Galaev I and Mattiasson B, 1993: *Thermoreactive water-soluble polymers, nonionic surfactants, and hydrogels as reagents in biotechnology.* Enzyme and Microbial Technology, *vol. 15*(5): 354–366. 64

Galaev I and Mattiasson B, 1999: *'Smart' polymers and what they could do in biotechnology and medicine.* Trends in Biotechnology, *vol. 17*(8): 335–340. 65

Gan L, Roshan Deen G, Loh X and Gan Y, 2001: *New stimuli-responsive copolymers of N-acryloyl-N'-alkyl piperazine and methyl methacrylate and their hydrogels.* Polymer, *vol. 42*(1): 65–69. 66

Garret-Flaudy F, 2000: *Thermoresponsive oligomers solubility and application for affinity precipitation* (EPFL, Lausanne). 64

Gascoyne PRC and Vykoukal J, 2002: *Particle separation by dielectrophoresis.* Electrophoresis, *vol. 23*(13): 1973–1983. 11

Gawad S, Schild L and Renaud P, 2001: *Micromachined impedance spectroscopy flow cytometer for cell analysis and particle sizing.* Lab on a Chip, *vol. 1*(1): 76–82. 14, 59

Gawad S, Batard P, Seger U, Metz S and Renaud P, 2002: *Leukocytes Discrimination by Impedance Spectroscopy Flow Cytometry.* In *Micro Total Analysis Systems*, vol. 2 of *Mesa Monographs*, pp. 649–651 (Kluwer Academic Publishers, Nara). 8

Gawad S, Cheung K, Seger U, Bertsch A and Renaud P, 2004: *Dielectric spectroscopy in a micromachined flow cytometer: Theoretical and practical considerations.* Lab on a Chip, *vol. 4*(3): 241–251. 14, 62

Gfeller V, 2002: *Design and Fabrication of a Pulse Generator for Electroporation of Individual Cells in Microchannels.* Semester Project, Microsystems Laboratory, EPFL. 79

Giddings JC, 1989: *Field-Flow Fractionation of Macromolecules.* Journal of Chromatography, *vol. 470.* 5, 11

Gimsa J, Muller T, Schnelle T and Fuhr G, 1996: *Dielectric spectroscopy of single human erythrocytes at physiological ionic strength: Dispersion of the cytoplasm.* Biophysical Journal, *vol. 71*(1): 495–506. 97, 98

Glaser RW, Leikin SL, Chernomordik LV, Pastushenko VF and Sokirko AI, 1988: *Reversible electrical breakdown of lipid bilayers: formation and evolution of pores.* Biochimica et biophysica acta, *vol. 940*: 275–287. 36

Glasser H and Fuhr G, 1998: *Cultivation of cells under strong ac-electric field - Differentiation between heating and trans-membrane potential effects.* Bioelectrochemistry and Bioenergetics, *vol. 47*(2): 301–310. 7, 59

Glasser H, Schnelle T, Muller T and Fuhr G, 1999: *Electric field calibration in micro-electrode chambers by temperature measurements.* Thermochimica Acta, *vol. 333*(2): 183–190. 59

Golzio M, Teissie J and Rols MP, 2002: *Direct visualization at the single-cell level of electrically mediated gene delivery.* Proceedings of the National Academy of Sciences of the United States of America, *vol. 99*: 1292–1297. 36

Graessmann M and Graessmann A, 1983: *Microinjection of Tissue-Culture Cells.* Methods in Enzymology, *vol. 101.* 3

Graham FL and van der Eb AJ, 1973: *Transformation of Rat Cells by DNA of Human Adenovirus-5.* Virology, *vol. 54.* 3

Grier DG, 2003: *A Revolution in Optical Manipulation.* Nature, *vol. 424*: 810–816. 9

Groner W, Mohandas N and Bessis M, 1980: *New optical technique for measuring erythrocyte deformability with the ektacytometer.* Clinical Chemistry, *vol. 26*: 1435–1442. 5

Gross D, Loew LM and Webb WW, 1986: *Optical imaging of cell membrane potential changes induced by applied electric fields.* Biophysical journal, *vol. 50*: 339–348. 34

Guck J, Ananthakrishnan R, Mahmood H, Moon TJ, Cunningham CC and Kas J, 2001: *The optical stretcher: A novel laser tool to micromanipulate cells.* Biophysical Journal, *vol. 81*(2): 767–784. 5

REFERENCES

Guck J, Schinkinger S, Lincoln B, Wottawah F, Ebert S, Romeyke M, Lenz D, Erickson HM, Ananthakrishnan R, Mitchell D, Kas J, Ulvick S and Bilby C, 2005: *Optical deformability as an inherent cell marker for testing malignant transformation and metastatic competence.* Biophysical Journal, *vol. 88*(5): 3689–3698. 4

Haas K, Sin WC, Javaherian A, Li Z and Cline HT, 2001: *Single-cell electroporation for gene transfer in vivo.* Neuron, *vol. 29*(3): 583–591. 16

Hapala I, 1997: *Breaking the barrier: Methods for reversible permeabilization of cellular membranes.* Critical Reviews in Biotechnology, *vol. 17*(2): 105–122. 4

He H, Chang DC and Lee YK, 2006: *Micro pulsed radio-frequency electroporation chips.* Bioelectrochemistry, *vol. 68*: 89–97. 16

Hibino M, Itoh H and Kinosita K, 1993: *Time Courses of Cell Electroporation as Revealed by Submicrosecond Imaging of Transmembrane Potential.* Biophysical Journal, *vol. 64*(6): 1789–1800. 34

Higaki S, Gebhardt BM, Lukiw WJ, Thompson HW and Hill JM, 2003: *Gene expression profiling in the HSV-1 latently infected mouse trigeminal ganglia following hyperthermic stress.* Current Eye Research, *vol. 26*(3-4): 231–238. 59

Hmamda A, 2003: *Optical Real-Time Detection of Electropermeabilisation.* Master's thesis, Microsystems Laboratory, EPFL. 94

Ho SY and Mittal GS, 1996: *Electroporation of cell membranes: A review.* Critical Reviews in Biotechnology, *vol. 16*(4): 349–362. 34, 35

Hochmuth RM, 2000: *Micropipette aspiration of living cells.* Journal of Biomechanics, *vol. 33*: 15–22. 4

Hojo S, Shimizu K, Yositake H, Muraji M, Tsujimoto H and Tatebe W, 2003: *The relationship between electropermeabilization and cell cycle and cell size of Saccharomyces cerevisiae.* IEEE Transactions on Nanobioscience, *vol. 2*(1): 35–39. 36, 83

Holmes D and Morgan H, 2002: *Dielectrophoretic Chromatography of Cells.* In *Micro Total Analysis Systems*, vol. 2 of *Mesa Monographs*, pp. 829–831 (Kluwer Academic Publishers, Nara). 11

Holz RW and Senter RA, 1985: *Plasma-Membrane and Chromaffin Granule Characteristics in Digitonin-Treated Chromaffin Cells.* Journal of Neurochemistry, *vol. 45*(5): 1548–1557. Times Cited: 26. 3

Holzapfel C, Vienken J and Zimmermann U, 1982: *Rotation of Cells in an Alternating Electric-Field - Theory and Experimental Proof.* Journal of Membrane Biology, *vol. 67*(1): 13–26. 12, 37, 83

Holzel R, 1997: *Electrorotation of single yeast cells at frequencies between 100 Hz and 1.6 GHz.* Biophysical Journal, *vol. 73*(2): 1103–1109. 12

Huang LR, Tegenfeldt JO, Kraeft JJ, Sturm JC, Austin RH and Cox EC, 2002: *A DNA prism for high-speed continuous fractionation of large DNA molecules.* Nature Biotechnology, *vol. 20*(10): 1048–1051. 7

Huang Y and Pethig R, 1991: *Electrode Design for Negative Dielectrophoresis.* Measurement Science and Technology, *vol. 2*(12): 1142–1146. 7, 12

Huang Y and Rubinsky B, 1999: *Micro-Electroporation: Improving the Efficiency and Understanding of Electrical Permeabilization of Cells.* Biomedical Microdevices, *vol. 2*(2): 145–150. 16

Huang Y and Rubinsky B, 2001: *Microfabricated electroporation chip for single cell membrane permeabilization.* Sensors and Actuators a-Physical, *vol. 89*(3): 242–249. 16

Huang Y, Holzel R, Pethig R and Wang XB, 1992: *Differences in the Ac Electrodynamics of Viable and Nonviable Yeast-Cells Determined through Combined Dielectrophoresis and Electrorotation Studies.* Physics in Medicine and Biology, *vol. 37*(7): 1499–1517. 12

Huang Y, Wang XB, Becker FF and Gascoyne PRC, 1997: *Introducing dielectrophoresis as a new force field for field-flow fractionation.* Biophysical Journal, *vol. 73.* 11

Hughes MP, 1998: *Computer-aided analysis of conditions for optimizing practical electrorotation.* Physics in Medicine and Biology, *vol. 43*(12): 3639–3648. 12

Idziak I, Avoce D, Lessard D, Gravel D, Zhu X and Idziak I, 1999: *Thermosensitivity of Aqueous Solutions of Poly(N,N-diethylacrylamide).* Macromolecules, *vol. 32*(4): 1260–1263. 66

Ito Y, 1999: *Surface micropatterning to regulate cell functions.* Biomaterials, *vol. 20.* 11

Jacob H, Amsden T and White J, 1972: *Membrane microfilaments of erythrocytes: alteration in intact cells reproduces the hereditary spherocytosis syndrome (vinblastine-colchicine-strychnine-electron microscopy-cell rigidity).* Proceedings of the National Academy of Sciences of the United States of America, *vol. 69*: 471–474. 4

Jager EWH, Inganas O and Lundstrom I, 2000: *Microrobots for micrometer-size objects in aqueous media: Potential tools for single-cell manipulation.* Science, *vol. 288*(5475): 2335–2338. 10

REFERENCES

Jaroszeski MJ, Heller R and Gilbert R, 2000: *Electrochemotherapy, Electrogenetherapy, and Transdermal Drug Delivery*, vol. 37 of *Methods in Molecular Medicine* (Humana Press, Totowa, New Jersey). 15

Jeltsch E and Zimmermann U, 1979: *Particles in a homogeneous electrical field: A model for the electrical breakdown of living cells in a Coulter counter.* Bioelectrochemistry and Bioenergetics, *vol. 6*: 349–384. 37

Johnson DA and Feke DL, 1995: *Methodology for fractionating suspended particles using ultrasonic standing wave and divided flow fields.* Separations Technology, *vol. 5*(4): 251–258. 9

Jones TB, 1995: *Electromechanics of Particles* (Cambridge University Press, Cambridge). 12, 19, 58

Jordan M, Schallhorn A and Wurm FM, 1996: *Transfecting mammalian cells: Optimization of critical parameters affecting calcium-phosphate precipitate formation.* Nucleic Acids Research, *vol. 24*: 596–601. 4

Kaler KVIS and Jones TB, 1990: *Dielectrophoretic Spectra of Single Cells Determined by Feedback-Controlled Levitation.* Biophysical Journal, *vol. 57*(2): 173–182. 12

Kane RS, Takayama S, Ostuni E, Ingber DE and Whitesides GM, 1999: *Patterning proteins and cells using soft lithography.* Biomaterials, *vol. 20*(23-24): 2363–2376. 11

Khine M, Lau A, Ionescu-Zanetti C, Seo J and Lee LP, 2005: *A single cell electroporation chip.* Lab on a Chip, *vol. 5*(1): 38–43. 17

Kiesel M, Reuss R, Endter J, Zimmermann D, Zimmermann H, Shirakashi R, Bamberg E, Zimmermann U and Sukhorukov VL, 2006: *Swelling-Activated Pathways in Human T-Lymphocytes Studied by Cell Volumetry and Electrorotation.* Biophysical Journal, *vol. 90*: 4720–4729. 12

Klein TM, Wolf ED, Wu R and Sanford JC, 1987: *High-Velocity Microprojectiles for Delivering Nucleic-Acids into Living Cells.* Nature, *vol. 327*(6117): 70–73. 3

Klenchin VA, Sukharev SI, Serov SM, Chernomordik LV and Chizmadzhev YA, 1991: *Electrically induced DNA uptake by cells is a fast process involving DNA electrophoresis.* Biophysical Journal, *vol. 60*: 804–811. 38

Koch M, Evans AGR and Brunnschweiler A, 1999: *Design and fabrication of a micromachined Coulter counter.* Journal of Micromechanics and Microengineering, *vol. 9*(2): 159–161. 13

Koutsouris D, Guillet R, Lelievre JC, Guillemin MT, Bertholom P, Beuzard Y and Boynard M, 1988: *Determination of erythrocyte transit times through micropores. I. Basic operational principles.* Biorheology, *vol. 25*: 763–772. 4

Kundu T, Bereiter-Hahn J and Karl I, 2000: *Cell property determination from the acoustic microscope generated voltage versus frequency curves.* Biophysical Journal, *vol. 78*: 2270–2279. 5

Kurschner M, Nielsen K, Andersen C, Sukhorukov VL, Schenk WA, Benz R and Zimmermann U, 1998: *Interaction of lipophilic ions with the plasma membrane of mammalian cells studied by electrorotation.* Biophysical Journal, *vol. 74*: 3031–3043. 12

Kurschner M, Nielsen K, Von Langen JRG, Schenk WA, Zimmermann U and Sukhorukov VL, 2000: *Effect of fluorine substitution on the interaction of lipophilic ions with the plasma membrane of mammalian cells.* Biophysical Journal, *vol. 79*: 1490–1497. 12

Lee SW and Tai YC, 1999: *A micro cell lysis device.* Sensors and Actuators a-Physical, *vol. 73*(1-2): 74–79. 14

Lettieri GL, de Rooij NF and Verpoorte E, 2002: *Microfluidic Device for Bioanalysis using Freely Moving Beads trappped in a Recirculating Flow.* In *Micro Total Analysis Systems*, vol. 2 of *Mesa Monographs*, pp. 630–632 (Kluwer Academic Publishers, Nara). 6

Li PCH and Harrison DJ, 1997: *Transport, manipulation, and reaction of biological cells on-chip using electrokinetic effects.* Analytical Chemistry, *vol. 69*. 14

Lin YC and Huang MY, 2001b: *Electroporation microchips for in vitro gene transfection.* Journal of Micromechanics and Microengineering, *vol. 11*(5): 542–547. 16

Lin YC, Jen CM, Huang MY, Wu CY and Lin XZ, 2001: *Electroporation microchips for continuous gene transfection.* Sensors and Actuators B-Chemical, *vol. 79*(2-3): 137–143. 16

Lin YC, Li M and Wu CC, 2004: *Simulation and experimental demonstration of the electric field assisted electroporation microchip for in vitro gene delivery enhancement.* Lab on a Chip - Miniaturisation for Chemistry and Biology, *vol. 4*: 104–108. 16, 38

Linderholm P, 2006b: *2-Dimensional Microimpedance Imaging for Cell Culture Monitoring.* Ph.D. thesis, Ecole Polytechnique Fédérale de Lausanne (EPFL). 80

151

REFERENCES

Linderholm P and Renaud P, 2005: *Comment on "AC frequency characteristics of coplanar impedance sensors as design parameters" by Jongin Hong, Dae Sung Yoon, Sung Kwan Kim, Tae Song Kim, Sanghyo Kim, Eugene Y. Pak and Kwangsoo No, Lab Chip, 2005, 5, 270.* Lab on a Chip, *vol. 5*(12): 1416–1417. 80, 117, 124

Linderholm P, Seger U and Renaud P, 2006: *Analytical Expression for Electric Field between two Facing Strip Electrodes in Microchannel.* Electronics Letters, *vol. 42*: 25–26. 122

Lou J, Finegan TM, Mohsen P, Hatton TA and Laibinis PE, 1999: *Fluorescence-based thermometry: Principles and applications.* Reviews in Analytical Chemistry, *vol. 18*(4): 235–284. 63

Lurquin PF, 1997: *Gene transfer by electroporation.* Molecular Biotechnology, *vol. 7*(1): 5–35. 15

Mannschreck BK, 2005: *Uteriner Blutfluss und maternale Erythrozytenverformkeut bei Schwangeren mit reduziertem uterinem Blutfluss und intravenöser Magnesium-Applikation.* Ph.D. thesis, Universitäts-Frauenklinik mit Poliklinik Tübingen. 108

Manz A, Harrison DJ, Verpoorte EMJ, Fettinger JC, Paulus A, Ludi H and Widmer HM, 1992: *Planar Chips Technology for Miniaturization and Integration of Separation Techniques into Monitoring Systems - Capillary Electrophoresis on a Chip.* Journal of Chromatography, *vol. 593*(1-2): 253–258. 6

Manz A, Effenhauser CS, Burggraf N, Harrison DJ, Seiler K and Fluri K, 1994: *Electroosmotic Pumping and Electrophoretic Separations for Miniaturized Chemical-Analysis Systems.* Journal of Micromechanics and Microengineering, *vol. 4*(4): 257–265. 6

Marszalek P, Liu DS and Tsong TY, 1990: *Schwan Equation and Transmembrane Potential Induced by Alternating Electric-Field.* Biophysical Journal, *vol. 58*(4): 1053–1058. 85

McConnaughey WB and Petersen NO, 1980: *Cell poker: An apparatus for stress-strain measurements on living cells.* Review of Scientific Instruments, *vol. 51*: 575–580. 4

McCutchan J and Pagano JS, 1968: *Enhancement of Infectivity of Simian Virus 40 Deoxyribonucleic Acid with Diethylaminoethyl-Dextran.* Journal of the National Cancer Institute, *vol. 41*(2): 351–. 3

McNeil PL, 1989: *Incorporation of Macromolecules into Living Cells.* Methods in Cell Biology, *vol. 29.* 3

Metz S, Holzer R and Renaud P, 2001: *Polyimide-based microfluidic devices.* Lab on a Chip, *vol. 1*(1): 29–34. 60

Micka B, Trojaneck B, Niemitz S, Lefterova P, Kruopis S, Huhn D, Wittig B, Schadendorf D and Schmidt-Wolf IGH, 2000: *Comparison of non-viral transfection methods in melanoma cell primary cultures.* Cytokine, *vol. 12*(6): 828–833. 4

Mitchison JM and Swann MM, 1954: *The Mechanical Properties of the Cell Surface: I. The Cell Elastimeter.* Journal of Experimental Biology, *vol. 31*: 443–460. 4

Mohandas N, Winardi R, Knowles D, Leung A, Parra M, George E, Conboy J and Chasis J, 1992: *Molecular basis for membrane rigidity of hereditary ovalocytosis: A novel mechanism involving the cytoplasmic domain of band 3.* Journal of Clinical Investigation, *vol. 89*: 686–692. 4

Molecular-Probes, 1999: *Propidium Iodide Nucleic Acid Stain P-3566 Product Information.* 82

Molecular-Probes, 2005: *Fluo Calcium Indicators F-1242 Product Information.* 92

Molecular-Probes, 2006: *Loading and retention characteristics of intracellular marker dyes, Figure 15.3, The Handbook - A Guide to Fluorescent Probes and Labeling Technologies (10th Edition).* 104

Morgan H and Green NG, 2003: *AC Electrokinetics - Colloids and Nanoparticles.* Microtechnologies and Microsystems Series (Research Studies Press, Hertfordshire). 58, 124

Muller KJ, Sukhorukov VL and Zimmermann U, 2001: *Reversible electropermeabilization of mammalian cells by high- intensity, ultra-short pulses of submicrosecond duration.* Journal of Membrane Biology, *vol. 184*(2): 161–170. 16, 108

Muller T, Gerardino A, Schnelle T, Shirley SG, Bordoni F, DeGasperis G, Leoni R and Fuhr G, 1996: *Trapping of micrometre and sub-micrometre particles by high- frequency electric fields and hydrodynamic forces.* Journal of Physics D-Applied Physics, *vol. 29*(2): 340–349. 8, 78

Muller T, Schnelle T and Fuhr G, 1998: *Dielectric single cell spectra in snow algae.* Polar Biology, *vol. 20*(5): 303–310. 12

Muller T, Pfennig A, Klein P, Gradl G, Jager M and Schnelle T, 2003: *The potential of dielectrophoresis for single-cell experiments.* IEEE Engineering in Medicine and Biology Magazine, *vol. 22*(6): 51–61. 7, 59, 74, 118

REFERENCES

Mussauer H, Sukhorukov VL, Haase A and Zimmermann U, 1999: *Resistivity of red blood cells against high-intensity, short-duration electric field pulses induced by chelating agents.* Journal of Membrane Biology, *vol. 170*: 121–133. 108

Neumann E, Schaeferridder M, Wang Y and Hofschneider PH, 1982: *Gene-Transfer into Mouse Lyoma Cells by Electroporation in High Electric-Fields.* Embo Journal, *vol. 1*(7): 841–845. 3, 15

Neumann E, Sowers AE and Jordan CA, 1989: *Electroporation and Electrofusion in Cell Biology* (Plenum Press, New York). 58

Neumann E, Kakorin S and Toensing K, 1999: *Fundamentals of electroporative delivery of drugs and genes.* Bioelectrochemistry and Bioenergetics, *vol. 48*(1): 3–16. 40

Nieuwenhuis JH, Bastemeijer J, Sarro PM and Vellekoop MJ, 2003: *Integrated flow-cells for novel adjustable sheath flows.* Lab on a Chip, *vol. 3*(2): 56–61. 13

Nilsson A, Petersson F, Persson HW, Jönsson H and Laurell T, 2002: *Autologous Blood Recovery and Wash in Microfluidic Channel Arrays utilizing Ultrasonic Standing Waves.* In *Micro Total Analysis Systems*, vol. 2 of *Mesa Monographs*, pp. 625–626 (Kluwer Academic Publishers, Nara). 9

Nolkrantz K, Farre C, Brederlau A, Karlsson RID, Brennan C, Eriksson PS, Weber SG, Sandberg M and Orwar O, 2001: *Electroporation of single cells and tissues with an electrolyte-filled capillary.* Analytical Chemistry, *vol. 73*(18): 4469–4477. 16

Olofsson J, Nolkrantz K, Ryttsen F, Lambie BA, Weber SG and Orwar O, 2003: *Single-Cell Electroporation.* Current Opinion in Biotechnology, *vol. 14*: 1–6. 16

Olofsson J, Pihl J, Sinclair J, Sahlin E, Karlsson M and Orwar O, 2004: *A microfluidics approach to the problem of creating separate solution environments accessible from macroscopic volumes.* Analytical Chemistry, *vol. 76*: 4968–4976. 87

Panayiotou M, Garret-Flaudy F and Freitag R, 2004: *Co-nonsolvency effects in the thermoprecipitation of oligomeric polyacrylamides from hydro-organic solutions.* Polymer, *vol. 45*(9): 3055–3061. 64, 72

Pavlin M, Pavselj N and Miklavcic D, 2002: *Dependence of induced transmembrane potential on cell density, arrangement, and cell position inside a cell system.* IEEE Transactions on Biomedical Engineering, *vol. 49*: 605–612. 36

Pethig R, Huang Y, Wang XB and Burt JPH, 1992: *Positive and Negative Dielectrophoretic Collection of Colloidal Particles Using Interdigitated Castellated Microelectrodes.* Journal of Physics D-Applied Physics, *vol. 25*(5): 881–888. 7, 8

Pick H, Schmidt EL, Tairi AP, Ilegems E, Hovius R and Vogel H, 2005: *Investigating cellular signaling reactions in single attoliter vesicles.* Journal of the American Chemical Society, *vol. 127*(9): 2908–2912. 94

Pohl HA, 1978: *Dielectrophoresis: The Behavior of Neutral Matter in Nonuniform Electric Fields* (Cambridge University Press, Cambridge). 7, 58

Prinz C, Tegenfeldt JO, Austin RH, Cox EC and Sturm JC, 2002: *Bacterial chromosome extraction and isolation.* Lab on a Chip, *vol. 2.* 7, 14

Purcell EM, 1977: *Life at Low Reynolds Number.* American Journal of Physics, *vol. 45*: 3–11. 2

Rae JL and Levis RA, 2002: *Single-cell electroporation.* Pflugers Archiv-European Journal of Physiology, *vol. 443*(4): 664–670. 16

Ramadan Q, Samper V, Poenar D, Liang Z, Yu C and Lim TM, 2006: *Simultaneous cell lysis and bead trapping in a continuous flow microfluidic device.* Sensors and Actuators, B: Chemical, *vol. 113*: 944–955. 14

Rand RP and Burton AC, 1964: *Mechanical Properties of the Red Cell Membrane - I. Membrane Stiffness and Intracellular Pressure.* Biophysical Journal, *vol. 4*: 115–135. 4

Reichle C, Schnelle T, Muller T, Leya T and Fuhr G, 2000: *A new microsystem for automated electrorotation measurements using laser tweezers.* Biochimica Et Biophysica Acta-Bioenergetics, *vol. 1459.* 9

Reid HL, Barnes AF and Lock PJ, 1976: *Technical methods: A simple method for measuring erythrocyte deformability.* Journal of Clinical Pathology, *vol. 29*: 855–858. 4

Renaud P, Linderholm P, Braschler T, Demierre N and Seger U, 2006: *Apparatus for Manipulating, Modifying and Characterising Particles in a Microchannel.* International Patent Application PCT/IB 2006/050345. 133

Reyes DR, Iossifidis D, Auroux PA and Manz A, 2002: *Micro total analysis systems. 1. Introduction, theory, and technology.* Analytical Chemistry, *vol. 74*(12): 2623–2636. 1

REFERENCES

Ross D and Locascio LE, 2002: *Fluorescence Thermometry in Microfluidics.* In *Eighth Temperature Symposium*, TEMPERATURE: Its Measurement and Control in Science and Industry, pp. 1051–1055 (AIP Conference Proceedings, Chicago). 63

Ross D, Gaitan M and Locascio LE, 2001: *Temperature measurement in microfluidic systems using a temperature-dependent fluorescent dye.* Analytical Chemistry, *vol. 73*(17): 4117–4123. 60, 118

Ryttsen F, Farre C, Brennan C, Weber SG, Nolkrantz K, Jardemark K, Chiu DT and Orwar O, 2000: *Characterization of single-cell electroporation by using patch- clamp and fluorescence microscopy.* Biophysical Journal, *vol. 79*(4): 1993–2001. 16, 35

Saleh OA and Sohn LL, 2001: *Quantitative sensing of nanoscale colloids using a microchip Coulter counter.* Review of Scientific Instruments, *vol. 72*(12): 4449–4451. 13

Sarkar A, Mitra B, Shastry A, Wadia S, Mulherkar R and Lal R, 2004: *A low voltage single cell electroporator with a microfabricated sense-porate aperture.* Proceedings of the IEEE International Conference on Micro Electro Mechanical Systems (MEMS), pp. 375–378. 16

Saulis G, 1993c: *Cell Electroporation .3. Theoretical Investigation of the Appearance of Asymmetric Distribution of Pores on the Cell and Their Further Evolution.* Bioelectrochemistry and Bioenergetics, *vol. 32*(3): 249–265. 36

Saulis G, 1997: *Pore disappearance in a cell after electroporation: Theoretical simulation and comparison with experiments.* Biophysical Journal, *vol. 73*(3): 1299–1309. 35

Schmid-Schönbein H, Weiss J and Ludwig H, 1973: *A simple method for measuring red cell deformability in models of the microcirculation.* Annals of Hematology, *vol. 26*: 369–379. 4

Schmidt C, Mayer M and Vogel H, 2000: *A chip-based biosensor for the functional analysis of single ion channels.* Angewandte Chemie-International Edition, *vol. 39*(17): 3137–3140. 7

Schneider H, Lemasters JJ, Hochli M and Hackenbrock CR, 1980: *Fusion of Liposomes with Mitochondrial Inner Membranes.* Proceedings of the National Academy of Sciences of the United States of America-Biological Sciences, *vol. 77*(1): 442–446. 3

Schnelle T, Hagedorn R, Fuhr G, Fiedler S and Muller T, 1993: *Three-Dimensional Electric-Field Traps for Manipulation of Cells - Calculation and Experimental-Verification.* Biochimica Et Biophysica Acta, *vol. 1157*(2): 127–140. 7, 8, 78

Schnelle T, Muller T, Gradl G, Shirley SG and Fuhr G, 1999: *Paired micro-electrode system: dielectrophoretic particle sorting and force calibration.* Journal of Electrostatics, *vol. 47*(3): 121–132. 8, 46, 60, 94, 121

Schnelle T, Muller T and Fuhr G, 2000: *Trapping in AC octode field cages.* Journal of Electrostatics, *vol. 50*(1): 17–29. 8

Schoenbach KH, Beebe SJ and Buescher ES, 2001: *Intracellular effect of ultrashort electrical pulses.* Bioelectromagnetics, *vol. 22*(6): 440–448. 16

Seger U, Gawad S, Scheer A and Renaud P, 2002: *Towards Single-Cell Controlled Electroporation in a Microfluidic Device.* In *Micro Total Analysis Systems*, pp. 796–798 (Kluwer Academic Publishers, Nara). 85

Seger U, Gawad S, Johann R, Bertsch A and Renaud P, 2004: *Cell Immersion and Cell Dipping in Microfluidic Devices.* Lab on a Chip, *vol. 4*(2): 148–151. 59, 74, 87, 99

Seger U, Gawad S, Tonteling M, Johann R and Vogel P Hand Renaud, 2004b: *Microfluidic Cell Immersion On-Chip Cell Viability Test.* In *Micro Total Analysis Systems*, vol. 2/2, pp. 270–272 (The Royal Society of Chemistry, Malmö). 90

Seger U, Panayiotou M, Schnydrig S, Jordan M and Renaud P, 2005: *Temperature measurements in microfluidic systems: Heat dissipation of negative dielectrophoresis barriers.* Electrophoresis, *vol. 26*: 2239–2246. 7, 118

Sheng Y, Mancino C and Birren B, 1995: *Transformation of Escherichia coli with large DNA molecules by electroporation.* Nucleic Acids Research, *vol. 23*: 1990–1996. 80

Shin YS, Cho K, Kim JK, Lim SH, Park CH, Lee BL, Park Y, Chung C, Han DC and Chang JK, 2004: *Electrotransfection of mammalian cells using microchannel-type electroporation chip.* Analytical Chemistry, *vol. 76*: 7045–7052. 16

Shoji M, Ikuta K and Korogi H, 2002: *Direct Nanomanipulation Tool for Biological Samples.* In *Micro Total Analysis Systems*, vol. 2 of *Mesa Monographs*, pp. 937–939 (Kluwer Academic Publishers, Nara). 10

Sixou S and Teissie J, 1993: *Exogenous Uptake and Release of Molecules by Electroloaded Cells - a Digitized Videomicroscopy Study.* Bioelectrochemistry and Bioenergetics, *vol. 31*(3): 237–257. 85

Sleep J, Wilson D, Simmons R and Gratzer W, 1999: *Elasticity of the red cell membrane and its relation to hemolytic disorders: An optical tweezers study.* Biophysical Journal, *vol. 77*: 3085–3095. 5

REFERENCES

Smith KC, Neu JC and Krassowska W, 2004: *Model of Creation and Evolution of Stable Electropores for DNA Delivery*. Biophysical Journal, *vol. 86*: 2813–2826. 35

Sowers AE and Lieber MR, 1986: *Electropore Diameters, Lifetimes, Numbers, and Locations in Individual Erythrocyte-Ghosts*. Febs Letters, *vol. 205*(2): 179–184. 35

Sugden B, Detroy B, Roberts RJ and Sambrook J, 1975: *Agarose Slab-Gel Electrophoresis Equipment*. Analytical Biochemistry, *vol. 68*(1): 36–46. 7

Sukhorukov VL, Mussauer H and Zimmermann U, 1998: *The effect of electrical deformation forces on the electropermeabilization of erythrocyte membranes in low- and high- conductivity media*. Journal of Membrane Biology, *vol. 163*(3): 235–245. 33, 107, 108

Sukhorukov VL, Reuss R, Zimmermann D, Held C, Muller KJ, Kiesel M, Gessner P, Steinbach A, Schenk WA, Bamberg E and Zimmermann U, 2005: *Surviving High-Intensity Field Pulses: Strategies for Improving Robustness and Performance of Electrotransfection and Electrofusion*. Journal of Membrane Biology, *vol. 206*: 187–201. 16

Takayama S, McDonald JC, Ostuni E, Liang MN, Kenis PJA, Ismagilov RF and Whitesides GM, 1999: *Patterning cells and their environments using multiple laminar fluid flows in capillary networks*. Proceedings of the National Academy of Sciences of the United States of America, *vol. 96*. 11

Taketo A, 1996: *Electrotransformation of Bacteria*. In Zimmermann U and Neil GA (eds.) *Electromanipulation of Cells*, pp. 107–135 (CRC Press, Boca Raton, Florida). 15

Tarek M, 2005: *Membrane electroporation: A molecular dynamics simulation*. Biophysical Journal, *vol. 88*: 4045–4053. 36

Teissie J, Golzio M and Rols MP, 2005: *Mechanisms of cell membrane electropermeabilization: A minireview of our present (lack of ?) knowledge*. Biochimica et Biophysica Acta - General Subjects, *vol. 1724*: 270–280. 34

Teruel MN, Blanpied TA, Shen K, Augustine GJ and Meyer T, 1999: *A versatile microporation technique for the transfection of cultured CNS neurons*. Journal of Neuroscience Methods, *vol. 93*(1): 37–48. 16

Thoumine O and Ott A, 1997: *Time scale dependent viscoelastic and contractile regimes in fibroblasts probed by microplate manipulation*. Journal of Cell Science, *vol. 110*: 2109–2116. 5

Tonteling M, 2003/2004: *Capture, Immersion and Electropermeabilisation of Single Cells*. Semester Project, Microsystems Laboratory, EPFL. 82

Tornay R, 2004/2005: *Software-Controlled Real-Time Sorting of Individual Cells in Flow.* Master's thesis, Microsystems Laboratory, EPFL. 39, 40

Tsukakoshi M, Kurata S, Nomiya Y, Ikawa Y and Kasuya T, 1984: *A Novel Method of DNA Transfection by Laser Microbeam Cell Surgery.* Applied Physics B-Photophysics and Laser Chemistry, *vol. 35*(3): 135–140. 3

van Rijn J, Van Den Berg J, Souren J, Van Wijk R and Joenje H, 1995: *Hepatoma cells adapted to proliferate under normally lethal hyperthermic stress conditions show rapid decay of thermoresistance and heat shock protein synthesis when returned to 37° C.* International Journal of Hyperthermia, *vol. 11*(5): 697–708. 59

Voldman J, Gray ML and Schmidt MA, 1999: *Microfabrication in biology and medicine.* Annual Review of Biomedical Engineering, *vol. 1*: 401–425. 2

von Böckh P, 2004: *Wärmeübertragung Grundlagen und Praxis* (Springer, Berlin). 61

Wang N, Butler JP and Ingber DE, 1993: *Mechanotransduction across the cell surface and through the cytoskeleton.* Science, *vol. 260*: 1124–1127. 5

Weaver JC and Barnett A, 1992: *Progress toward a Theoretical Model for Electroporation Mechanism: Membrane Electrical Behavior and Molecular Transport.* In Chang DC, Chassy BM, Saunders JA and Sowers AE (eds.) *Guide to Electroporation and Electrofusion*, pp. 91–117 (Academic Press, San Diego, California). 47

Weaver JC and Chizmadzhev YA, 1996: *Theory of electroporation: A review.* Bioelectrochemistry and Bioenergetics, *vol. 41*(2): 135–160. 36

Wong PK, Tan W and Ho CM, 2005: *Cell relaxation after electrodeformation: Effect of latrunculin A on cytoskeletal actin.* Journal of Biomechanics, *vol. 38*(3): 529–535. 107

Yang J, Huang Y, Wang XJ, Wang XB, Becker FF and Gascoyne PRC, 1999: *Dielectric properties of human leukocyte subpopulations determined by electrorotation as a cell separation criterion.* Biophysical Journal, *vol. 76.* 12

Yang MS, Li CW and Yang J, 2002: *Cell docking and on-chip monitoring of cellular reactions with a controlled concentration gradient on a microfluidic device.* Analytical Chemistry, *vol. 74*(16): 3991–4001. 10

Yasuda K, 2000: *Non-destructive, non-contact handling method for biomaterials in micro-chamber by ultrasound.* Sensors and Actuators B-Chemical, *vol. 64*(1-3): 128–135. 9

REFERENCES

Yun KS, Lee SI, Lee GM and Yoon E, 2002: *Design and Fabrication of a Micro/Nano-Fluidic Chip performing Single-Cell Positioning and Nano-liter Drug Injection for Single-Cell Analysis.* In *Micro Total Analysis Systems*, vol. 2 of *Mesa Monographs*, pp. 652–654 (Kluwer Academic Publishers, Nara). 10

Zimmermann U and Neil GA, 1996: *Electromanipulation of Cells* (CRC Press, Boca Raton, Florida). 15, 58, 83

Zimmermann U and Vienken J, 1982: *Electric Field-Induced Cell-to-Cell Fusion.* Journal of Membrane Biology, *vol. 67*(3): 165–182. 35

Zimmermann U, Pilwat G and Riemann F, 1974: *Dielectric breakdown of cell membranes.* Biophysical Journal, *vol. 14*: 881–899. 78

Zimmermann U, Friedrich U, Mussauer H, Gessner P, Hamel K and Sukhoruhov VL, 2000: *Electromanipulation of mammalian cells: Fundamentals and application.* Ieee Transactions on Plasma Science, *vol. 28*(1): 72–82. 108

Appendix A

Fluo3-AM Preparation

Stock Solutions and Pre-Experimental Incubation

- **Fluo3-AM stock solution**

  Fluo3-Acetoxymethyl (AM) is dissolved in DMSO (Dimethyl Sulfoxide, C_2H_6OS) to a 1 mM stock solution (F 14218, Molecular Probes).

- **CaCl$_2$ stock solution**

  Calcium chloride is dissolved in DI water to a 100 mM stock solution.

  (In order to prevent precipitation, it is important to use *phosphate-free* solutions in conjunction with $CaCl_2$.)

- **TRIS-buffered saline (TBS)**

  1.5 g TRIS, 7 g NaCl, and 0.2 g KCl are dissolved in 1 l DI water to an isotonic solution.

  (TRIS (Trishydroxymethylaminomethane) is an organic polyamine widely used as a buffer in biochemistry to control the pH in range between 6.5 and 9.7.)

- **Mix and incubate for 30 min @ 37°C**

  - 50 μl Fluo3-AM solution
  - 200 μl CaCl$_2$ solution
  - 250 μl TBS
  - 500 μl CHO cells in RPMI culture medium

A. Fluo3-AM Preparation

Appendix B

Transformations used for Conformal Mapping

Analytical expression for electric field between two facing strip electrodes in microchannel   P. Linderholm, U. Seger and P. Renaud

This reprint from the IEE Electronics Letters (Vol. 42, No. 3) describes the detailed coordinate transformations for one possible conformal mapping of the electric field between two facing electrodes, such as top-bottom nDEP barriers.

Analytical expression for electric field between two facing strip electrodes in microchannel

P. Linderholm, U. Seger and P. Renaud

An analytical solution is presented for the electric field between two facing strip electrodes situated in a microchannel, as frequently used in impedance cytometry applications. The measured change in resistance as induced by a 5 μm bead moving through the microchannel is in good agreement with the model. It is also demonstrated that the centre sensitivity is maximal for an electrode width equal to ~56% of the channel height.

Introduction: Microelectrodes are commonly used in bioMEMS devices for high-throughput screening, tissue characterisation and particle manipulation using dielectrophoresis [1–3]. Cellular properties such as cell size and intracellular conductivity can be extracted from the impedance variation due to a cell passing through the volume between two opposing electrodes [4]. However, very few analytical models have yet been published for impedimetric bioMEMS, and there is a great need for more accurate modelling tools.

Jacobs *et al.* presented an expression for the resistance through the medium between two strip electrodes in 1995 [5]. Their solution was for coplanar strip electrodes in a medium of infinite height compared to the electrode widths. In this Letter, we start with a different set of transformations due to the different geometry. First, the resistance between the two facing strip electrodes is derived, and then the electric field in the channel is solved. Finally, an expression for the sensitivity distribution in the microchannel is developed and verified using measurements in a microchannel as well as in a macroscopic channel.

Formulation: Let the physical geometry be defined in the Z-plane ($z = x + iy$). Exploiting symmetry, we will transform the right half of the microchannel into a rectangle, where the resistance can easily be calculated. The right half of the top electrode is defined by $z_1 = w/2 + ih/2$ and $z_2 = ih/2$, and the right half of the bottom electrode is defined by $z_3 = -ih/2$ and $z_4 = w/2 - ih/2$, where w is the electrode width and h is the height of the channel (Fig. 1b). We first bring the microchannel walls to the real axis of the T-plane by using a sine transformation of the Z-plane (Fig. 1c).
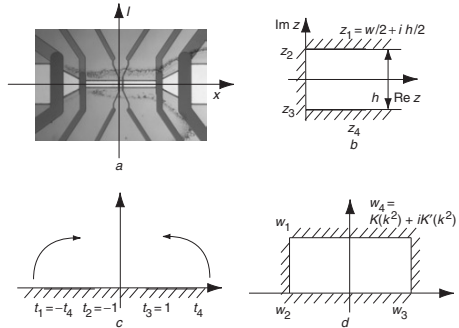
$$t = \sin\left(\pi \frac{iz}{h}\right) \quad (1)$$

Fig. 1 *Microdevice, microchannel, T-plane and representation of electrodes*

a Photographic top view of microdevice used for measurement. Dark stripes are strip electrodes on top and bottom of channel
b Cross-section of microchannel modelled in Z-plane
c Physical Z-plane transformed to T-plane by sine-mapping, from which Schwarz-Christoffel mapping can be carried out
d Rectangle, resulting from *c*, with two sidewalls representing electrodes (W-plane)

In geometric terms, the channel is first rotated 90°, and the electrodes are folded 'outwards' at $y = 0$. The left part of the channel

in Fig. 1b is mapped onto the bottom half in the T-plane (Fig. 1c). The midpoints of the electrodes are placed at ± 1 on the real axis in the T-plane. We can then introduce the Schwarz-Christoffel conformal mapping as

$$w = \int_0^t \frac{k}{\sqrt{(1 - u^2)(1 - k^2 u^2)}} \, du \quad (2)$$

where k is given by

$$k = \frac{1}{t_4} = \frac{1}{\sin(\pi(iz_4/h))} \quad (3)$$

Since only the upper half of the T-plane is mapped onto the rectangle in the W-plane, the total resistance is half of the resistance between the left and the right side of the rectangle (Fig. 1d). We can state the total resistance between the two electrodes as:

$$R(w, h) = \rho \frac{K(k^2)}{K(1 - k^2)} \quad (4)$$

where K is an elliptic integral of the first kind and ρ is the resistivity of the solution in the channel. We have used the fact that $K'(k^2) = K(1 - k^2)$ to derive (4). In the W-plane, the electric field is given by

$$E_W = \frac{U_{applied}}{2kK(k^2)} \quad (5)$$

where k is the modulus from (3), $U_{applied}$ is the voltage applied between the two electrodes, and K is an elliptic integral of the first kind. The gradient of the potential field in the W-plane is given by [6]:

$$E_T = E_W \overline{\frac{dw}{dt}} \quad (6)$$

where $\overline{dw}/dt$ is the conjugate of the derivative of w with regards to t. The current density in the physical Z-plane can then be found by multiplying E_W by the conjugates of the two derivatives of the transformation functions, which yields:

$$E_Z = E_W k[(1 - t^2)(1 - k^2 t^2)]^{-1/2} \overline{[(i\pi/h)\cos(i\pi z/h)]} \quad (7)$$

Equation (6) is one of the two main results of this Letter, since it gives the electric field inside the channel. However, we can also use it to quantify the perturbation induced by a non-conducting object in the detection volume. Following the development by Lehr [7], we define the sensitivity as the local power dissipation normalised to the total power dissipated in the medium, which gives:

$$S = \frac{\rho |j|^2}{\iint_{microchannel} \rho |j|^2} = \frac{R\rho |E_Z|^2}{U_{applied}^2} \quad (8)$$

where j is the current density. The sensitivity then gives the relative contribution per unit area (in the case of a 2D problem) to the total resistance. Substituting the expressions in (1), (3), (4), (5) and (7) into (8) gives the final expression for the sensitivity as:

$$S(x, y) = \frac{\left| \overline{ \begin{array}{c} \left[\left(1 - \sin(\pi(iz/h))^2\right)\left(1 - \sin(\pi(iz_4/h))^{-2}\sin(\pi(iz/h))^2\right)\right]^{-1/2} \\ \times \overline{[(i\pi/h)\cos(i\pi z/h)]} \end{array} } \right|^2}{4K\left(\sin(\pi(iz_4/h))^{-2}\right)K\left(1 - \sin(\pi(iz/h))^{-2}\right)} \quad (9)$$

The sensitivity distribution obtained from the above equation is plotted for two different ratios of electrode width and channel height in Fig. 2.

Experiment: To test the theoretical predictions, a microchannel ($l = 40$, $h = 20 \, \mu m$) with platinum electrodes ($w = 10 \, \mu m$) on top and bottom was fabricated using standard microfabrication technologies [8]. The change in resistance as an insulating 5.1 μm polystyrene bead passed through the channel was measured with an impedance analyser (Agilent 4294A). For the sensitivity optimisation, a 20 mm-wide channel was filled with PBS, and the change in resistance was recorded as an insulating PMMA 1 mm rod was moved between pairs of electrodes of different widths.
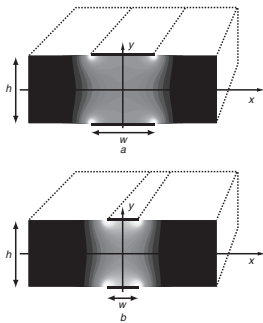
Fig. 2 *Sensitivity maps for $w/h = 1$ and 0.5*

a 2D sensitivity map computed from (9) using Matlab for $w/h = 1$ (8). Dotted lines indicate *l*-dimension of channel. White areas indicate high sensitivity
b Sensitivity map for $w/h = 0.5$

Results: Integrating (9) over the desired area, we can predict the resistance variation as a particle passes through the microchannel. Fig. 3*a* shows the theoretical and measured signal for a 5.1 μm bead. The signal was normalised with the maximum value along the centre axis.
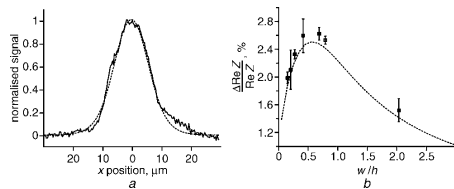

Fig. 3 *Resistance at 2 MHz, and relative change at 700 kHz*

a Theoretical (dotted line) and measured resistance at 2 MHz (solid line) from 5.1 μm bead, passing through centre of microchannel. Curves are normalised with maximum values
b Relative change in resistance at 700 kHz as insulating cylinder is placed between two facing electrodes in macrochannel. Dotted lines represent theoretical impedance variations

Fig. 3*b* shows the theoretical and measured sensitivity at the centre of the channel for different w/h ratios. From (9), it can be found that there is a

maximum in the signal for $w/h \simeq 0.561$. The sensitivity optimisation design rule suggested here is given for well-centred particles, but using (9) the geometry could also be optimised for maximal bandwidth, minimal sensitivity to uncertainty along the *h*-axis, etc. Using dielectrophoretic centring, we routinely achieve a precision of $\pm 5\%$ of the channel height.

Conclusions: We have derived an expression for the electric field between two facing strip electrodes in a microchannel. The model is valid for frequencies at which electrode interface impedances and parasitic capacitances are negligible. From this expression, we have shown how to calculate the sensitivity distribution and impedance changes for flow cytometry applications. We have also found that, to maximise the relative change in resistance as a particle flows between the electrodes, the electrode widths should be 56% of the channel height.

P. Linderholm, U. Seger and P. Renaud (*Microsystems Laboratory, Ecole Polytechnique Fédérale Lausanne, 1015 Lausanne, Switzerland*)

E-mail: pontus.linderholm@epfl.ch

References

1 Ayliffe, H.E., Frazier, A.B., and Rabbitt, R.D.: 'Electric impedance spectroscopy using microchannels with integrated metal electrodes', *J. Microelectromech. Syst.*, 1999, **8**, (1), pp. 50–57
2 Linderholm, P., Bertsch, A., and Renaud, P.: 'Resistivity probing of multi-layered tissue phantoms using microelectrodes', *Physiol. Meas.*, 2004, **25**, (3), pp. 645–658
3 Schnelle, T., *et al.*: 'Paired microelectrode system: dielectrophoretic particle sorting and force calibration', *J. Electrost.*, 1999, **47**, (3), pp. 121–132
4 Gawad, S., *et al.*: 'Dielectric spectroscopy in a micromachined flow cytometer: theoretical and practical considerations', *Lab Chip*, 2004, **4**, (3), pp. 241–251
5 Jacobs, P., Varlan, A., and Sansen, W.: 'Design optimization of planar electrolytic conductivity sensors', *Med. Biol. Eng. Comput.*, 1995, **33**, (6), pp. 802–810
6 Henrici, P.: 'Applied and computational complex analysis' (John Wiley & Sons, New York, 1974)
7 Lehr, J.: 'Vector derivation useful in impedance plethysmographic field calculations', *IEEE Trans. Biomed. Eng.*, 1972, **BME-19**, (2), p. 156
8 Seger, U., *et al.*: 'Cell immersion and cell dipping in microfluidic devices', *Lab Chip*, 2004, **4**, (2), p. 148

Appendix C

Artificial Particle Tracking

Script and Functions used in MATLAB

- **trackAndPlotParticlesSS.m**
  Main script for parameter sweeping and plotting

- **cellconstants_no_backplane.m**
  Calculates both access resistances

- **calculateCellConstant.m**
  Calculates the channel resistance

- **calculateRealCM.m**
  Calculates the Clausius-Mossotti factor of a protoplast

- **track1Particle.m**
  Core script that outputs a particle trajectory
  (uses calculateEfield.m and calculateForces.m)

```matlab
fTOP= logspace(log10(fTOPstart),log10(fTOPstop),n) +0.1;

%%
% trackAndPlotParticlesSS (SS stands for single side)
%
% /Volumes/hundredtwenty/epflwork/calculations - simulations/the M-files/06_depforceNEWgen

%%%
% fixed parameters given by the liquid electrode technology

technothickness= 20e-6;
recessdepth= technothickness;

%%%
% number of VARIANTS/PLOTS, max= 39 (3* all different markertypes)

n= 3;

%%%
% number of TRACKS per plot PLOTS, max= 13

t= 2;

%%%
% CHANNEL geometries

heightstart= 80e-6; heightstop= 160e-6; heightdelta= (heightstop-heightstart)/max((n-1),1); % i.e.
channel width
    height= heightstart:heightdelta:heightstop;
elecstart= 40e-6; elecstop= 50e-6; elecdelta= (elecstop-elecstart)/max((n-1),1);
    elec= elecstart:elecdelta:elecstop;
gapstart= 3e-6; gapstop= 120e-6; gapdelta= (gapstop-gapstart)/max((n-1),1);
    gap= gapstart:gapdelta:gapstop;

%%%
% GRAPH dimensions

graph_width= 200e-6;
graph_height= 150e-6;

%%%
% static properties of the MEDIUM (real values of epsilon only, cf. jones)

eta= 1e-3; visco= eta; % Nsm-2, viscosity of the medium
epsilon= 78; eps0= 8.854e-12; permitt= epsilon*eps0; % Fm-1, permittivity of the medium

%%%
% VOLTAGES (adding 0.0001 is a trick to provoke sufficient digits for the legend)

vBOTstart= 10.0 +0.0001; vBOTstop= 15.0 +0.0001; vBOTdelta= (vBOTstop-vBOTstart)/max((n-1),1);
    vBOT= vBOTstart:vBOTdelta:vBOTstop;
vTOPstart= 3.2 +0.0001; vTOPstop= 5.0 +0.0001; vTOPdelta= (vTOPstop-vTOPstart)/max((n-1),1);
    vTOP= vTOPstart:vTOPdelta:vTOPstop; % vTOP will be overwritten with 0 at line +/- 190

%%%
% FREQUENCIES

fBOTstart= 1e4 +0.1; fBOTstop= 1e7 +0.1;
    fBOT= logspace(log10(fBOTstart),log10(fBOTstop),n) +0.1;
fTOPstart= 1e4 +0.1; fTOPstop= 1e7 +0.1;
```

```matlab
fTOP= logspace(log10(fTOPstart),log10(fTOPstop),n) +0.1;

%%%
% MEDIUM and PARTICLES dielectric properties

permM= permitt;
condM= 0.14; % Sm-1 PBS: 1.4
permP= 2.4 * eps0; % epsilon polystyrene: 2.4
condP= 7e-6; % Sm-1 polystyrene 7e-6
protoplastmodel= true; % if flag set true, then use protoplast model, else homogeneous bead
permC= permitt; % cytoplasm properties
condC= 0.5; % Sm-1
cMemb= 1e-2; % Fm-2 membrane capacitance: 1 microF/cm2
gMemb= 0; % membrane conductance supposed nil

%%%
% CLAUSIUS-MOSSOTTI factors, will be overwritten

% [except if calculateRealCM in the main loop is "commented out"]
ReCMBOTstart= -0.5 +0.0001; ReCMBOTstop= 1 +0.0001; ReCMBOTdelta=
(ReCMBOTstop-ReCMBOTstart)/max((n-1),1);
    ReCMBOT= ReCMBOTstart:ReCMBOTdelta:ReCMBOTstop;
ReCMTOPstart= -0.5 +0.0001; ReCMTOPstop= 1 +0.0001; ReCMTOPdelta=
(ReCMTOPstop-ReCMTOPstart)/max((n-1),1);
    ReCMTOP= ReCMTOPstart:ReCMTOPdelta:ReCMTOPstop;

%%%
% PARTICLE size and start positions

particleRstart= 3.8e-6; particleRstop= 4.0e-6; particleRdelta=
(particleRstop-particleRstart)/max((n-1),1);
    particleR= particleRstart:particleRdelta:particleRstop;
initialX= -graph_width/2;
initialYstart= 27e-6; initialYstop= 3e-6; initialYdelta= (initialYstop-initialYstart)/max((t-1),1);
    initialY= initialYstart:initialYdelta:initialYstop;

%%%
% FLUID flow speed

flowXstart= 100e-6; flowXstop= 10000e-6; flowXdelta= (flowXstop-flowXstart)/max((n-1),1);
    flowX= flowXstart:flowXdelta:flowXstop;

%%%
% PRECISION in space and time

precision_dx= 1e-6; %default 1e-6
% dt is calculated dynamically as a function of the flow speed
% dt= 0.01; %default 0.01

%%%
% FIGURE handling

fignumstart= 1; fignumstop= fignumstart+n;
    fignum= fignumstart:1:fignumstop;

%%%
% COLOR handling

jetmap= jet;
nr_of_gridlines= t; % fan out the colors to the number of tracks
colorvector= jetmap(round((1:nr_of_gridlines)/nr_of_gridlines*40)+20,:);
```

```
colorvector(nr_of_gridlines+1,:)=  [0 0 0];
colorvector(nr_of_gridlines+2,:)=  [0 0 0];
%markervector= '+o*.xsd^v>ph<o*.xsd^v>ph';
markervector= 'oooooooooooooooooooooooooo';
markersizevector= [3,3,3,3,3,3,3,3,3,3,3,3,3,3,3,3,3,3,3,3,3,3,3,3,3,3];

%%%%%%%%%%%%%%%%%%%%%%%%%%
%%% the code starts here

px= [];
py= [];
p_vx= [];
p_vy= [];

spreading= [];
position= [];

for var= 1:n

%figure(fignum(var));
hold off

legendstring=[];
digits(3)
highest= 0;
lowest= heightstop;
finalpos= [];

for fan= 1:t

%%%%%%%%%%%%%%%%%%%%%%%%
%%% set the value(s) of the param to be swept to "var" instead of "1"
%%% (SW/sw stands for SWitch)

heightSW= 1;
elecSW= 1;
gapSW= var;
vBOTsw= 1;
vTOPsw= 1;
fBOTsw= 1;  computeReCMBOT= false; % on top of 'var': set flag to 'true' instead of 'false'
fTOPsw= 1;  computeReCMTOP= false; % (the script will then calculate and overwrite static CM

factor)  protoplastmodel= true; % true: protoplastmodel, false: homogeneous sphere
ReCMBOTsw= 1;
ReCMTOPsw= 1;
particleRsw= 1;
initialYsw= fan;
flowXsw= 1;
fignumsw= 1;
dt= 2*precision_dx/flowX(flowXsw);

kappaAccess= cellconstants_no_backplane(1e-3,2*recessdepth,technothickness);
[B, D, k, kappaChannel]= calculateCellconstant(elec(elecSW), gap(gapSW), height(heightSW));
Raccess= real(kappaAccess)/condM/elec(elecSW);
Rchannel= real(kappaChannel)/condM/technothickness;
Rtot= Rchannel+Raccess; % only 1x Raccess because Raccess is intrinsically doubled (mapping)
efficiency(var)= Rchannel/Rtot;
vol-tBOT= vBOT(vBOTsw)*efficiency(var);
vol-tTOP= 0; %vTOP(vTOPsw)*efficiency(var);
P(var)=voltBOT/2/Rtot+voltTOP^2/Rtot;

if computeReCMBOT
RealCauMosBOT= calculateReaICM(permP, condP, permM, condM, fBOT(fBOTsw), ...
protoplastmodel, permC, condC, cMemb, gMemb, particleR(particleRsw));
else
```

```
RealCauMosBOT= ReCMBOT(ReCMBOTsw);
end % if computeReCMBOT
if computeReCMTOP
RealCauMosTOP= calculateReaICM(permP, condP, permM, condM, FTOP(FTOPsw), ...
protoplastmodel, permC, condC, cMemb, gMemb, particleR(particleRsw));
else
RealCauMosTOP= ReCMTOP(ReCMTOPsw)
end %if computeReCMTOP

[px,py,p_vx,p_vy]= track1Particle(height(heightSW), elec(elecSW), gap(gapSW),
particleR(particleRsw), RealCauMosBOT, RealCauMosTOP, ...
initialX, initialY(initialYsw), flowX(flowXsw), voltBOT, voltTOP, ...
graph_width, precision_dx, dt, permitt, visco);
finalpos(fan)= py(length(py));
highest= max(highest, finalpos(fan));
lowest= min(lowest, finalpos(fan));

legendstring= [legendstring; '' num2str(finalpos(fan), '%02.2u') , ' m'];

%plot(px,py, 'LineStyle','none', 'Color',colorvector(fan,:), 'Marker',markervector(fan),
'MarkerSize',markersizevector(fan));
hold on;
end %for fan

%position(var)= mean(finalpos);
position(var)= min(finalpos);
spreading(var)= highest-lowest;

line ([-elec(elecSW)-gap(gapSW)/2 -gap(gapSW)/2], [0 0], 'Color', 'k', 'LineWidth',4);
line ([gap(gapSW)/2 elec(elecSW)+gap(gapSW)/2], [0 0], 'Color', 'k', 'LineWidth',4);
line ([-graph_width/2 graph_width/2], [0 0], 'Color', 'k');
%line ([-elec(elecSW)-gap(gapSW)/2 -gap(gapSW)/2],[height(heightSW) height(heightSW)],'Color','k',
'LineWidth',4);
%line ([gap(gapSW)/2 elec(elecSW)+gap(gapSW)/2],[height(heightSW) height(heightSW)] ,'Color','k',
'LineWidth',4);

axis([-graph_width/2 graph_width/2 0 graph_height])

%leg= legend(cellstr(legendstring), 'Location','NorthWest');
%legend(leg, 'boxoff');

electrostring=[];
electrostring= [electrostring; 'Voltage BOT: ',num2str(vBOT(vBOTsw),'%2.1f'),' V ', VoltageTOP:
',num2str(vTOP(vTOPsw),'%2.1f'),' V ', fBOT: ',num2str(fBOT(fBOTsw),'%02.2u'),' Hz ', FTOP:
',num2str(fTOP(fTOPsw),'%02.2u'),' Hz'];

efficiencystring=[];
efficiencystring= [efficiencystring; 'eff. vBOT: ',num2str(voltBOT,'%2.2f'),' V ', vTOP:
',num2str(voltTOP,'%2.2f'),' V ', efficiency: ',num2str(efficiency(var)*100,'%02.1f'),' % ', Power:
',num2str(P(var),'%02.2u'),' W'];

particlestring=[];
particlestring= [particlestring; 'Particle Radius: ',num2str(particleR(particleRsw)*1e6,'%2.2u'),'
μm ', Flow Speed: ',num2str(flowX(flowXsw)*1e6,'%4.02.2u'),' μm/s ', CM-Factor:
',num2str(RealCauMosBOT,'%2.3f'),' (@ BOT)'];

geometrystring=[];
geometrystring= [geometrystring; 'Electrodes: ',num2str(elec(elecSW)*1e6,'%4.02.2u'),' μm ', Gap:
',num2str(gap(gapSW)*1e6,'%02.2u'),' μm ', Height: ',num2str(height(heightSW)*1e6,'%4.02.2u'),'
μm ', Spreading: ',num2str((highest-lowest)*1e6,'%2.2f'),' μm'];

titlelines(1)= {electrostring};
titlelines(2)= {efficiencystring};
titlelines(3)= {particlestring};
titlelines(4)= {geometrystring};
```

```
%
%    Author: Pontus Linderholm, June 2005
%
% Calculates the cell constant between two coplanar electrodes (of width
% elec) separated by a gap (gap) in a microchannel of thickness (thickness)

function R=cellconstants_no_backplane (elec,gap,thickness);

digits (300); % for the variable precision, this value should be between 20-1000, the higher it is the :
pi_long = vpa ( 3.141592653589793238462643383279502884197169399375105820974944592307816406286); %from tl
%+++++++++++++++++++++++++++++++++++++++++++++
%      Z-plane geometry
%+++++++++++++++++++++++++++++++++++++++++++++
za = -thickness/2 + i * (gap/2 + eleC);
zb = -thickness/2 + i * gap/2;
zc = -thickness/2;
zd = thickness/2;
%+++++++++++++++++++++++++++++++++++++++++++++
%    sin-mapping of the electrode coordinates (U-plane if you wish)
%+++++++++++++++++++++++++++++++++++++++++++++
p=vpa(real(sin (pi*za/thickness)));
q=vpa(real(sin (pi*zb/thickness)));
r=vpa(real(sin (pi*zc/thickness)));
s=vpa(real(sin (pi*zd/thickness)));
%+++++++++++++++++++++++++++++++++++++++++++++
%      the bilinear coordinates are not needed, we just need the value of
%      the modulus k (which is equal to 1/u4)
%+++++++++++++++++++++++++++++++++++++++++++++
k=vpa((p*(q+r-2*s)-2*s*sqrt( (q-p)*(r-p))*sqrt(q-s) +r*s+q*(s-2*r)));
k1=vpa((q-r)*(p-s));

k=k/k1;
%+++++++++++++++++++++++++++++++++++++++++++++
%      The elliptic functions are calculated using the
%      Hilberg-approximations, because the ellipke function
%      is not defined in vpa (Variable Precision Arithmetics).
%+++++++++++++++++++++++++++++++++++++++++++++
k1=vpa(sqrt(1-k*k));
bigk=double(k)>sqrt(1/2);

if (-bigk) % The formula used depends on the value of the modulus k.
    KK_Hilberg = 2 * pi_long / log (2*(sqrt(1+k1)+(4*k1)^0.25)/(sqrt(1+k1)-(4*k1)^0.25));
end;

if (bigk)
    KK_Hilberg = log (2*(sqrt(1+k)+(4*k)^0.25)/(sqrt(1+k)-(4*k)^0.25))/(2 * pi_long);
end;
% The resistance is twice the normal half-plane, since only half the
% geometry was mapped in the sin-mapping
R=double(4*KK_Hilberg);
```

```
    title(titlelines, 'FontWeight','bold')

end %for var

%%% RAPPEL: list of parameters
% heightSW
% elecSW
% gapSW
% vBOTsw
% vTOPsw
% fBOTsw
% fTOPsw
% ReCMBOTsw
% ReCMTOPsw
% particleRsw
% flowXsw

figure(98)
%%      v---- sweep param
plot(gap, position)
title('Lowest Position')
%%      v----   v----   sweep params
axis([0 gap(gapSW) 0 height(heightSW)])

height
position

%{
figure(99)
plot(particleR, spreading)
title('Spreading')
axis([0 particleR(particleRsw) 0 height(heightSW)])
axis 'autoy'
%}
```

```
function [ReCM]= calculateRealCM(permP, condP, permM, condM, freq, ...
    protoplastmodel, permC, condC, cMemb, gMemb, particle_radius);

if protoplastmodel
    om= 2*pi*freq;
    tauC= permC/condC;
    tauMemb= cMemb*particle_radius/condC;
    tauMembPrim= cMemb*particle_radius/condM;
    tauM= permM/condM;
    A= om*om*(tauC*tauMemb-tauC*tauMembPrim) - 1 + i* om*(tauMembPrim-tauM-tauMemb);
    B= om*om*(tauC*tauMembPrim-2*tauM*tauMemb) - 2 - i* om*(tauMembPrim+2*tauM+tauMemb);
    CM= -A/B;
    ReCM= real(CM);
else
    Ep= permP - i* condP/(2*pi*freq);
    Em= permM - i* condM/(2*pi*freq);
    CM= (Ep-Em)/(Ep+2*Em);
    ReCM= real(CM);
end %if
```

```
function [B, C, D, k, kappa]= calculateCellConstant(elec, gap, height);

z1= i*height;
z2= 0;
z3= gap/2;
z4= gap/2 + elec;

u1= sinh( pi/height*( z1-i*height/2 ));
u2= sinh( pi/height*( z2-i*height/2 ));
u3= sinh( pi/height*( z3-i*height/2 ));
u4= sinh( pi/height*( z4-i*height/2 ));

Ctop= -u2*u2 +u1*(u2+u3-u4-u4) +2*sqrt((u1-u2)*(u1-u3)*(u2-u4)*(u3-u4)) +u2*u4 +u3*(u4-u3);
Cbot= (u2-u3)*(-u1+u2+u3-u4);

C= Ctop/Cbot;
C= real(C); % est purement réel, enlever tout résidu imaginaire

D= (u3*(1-C)-u2*(1+C))/2;
D= i*imag(D); % est purement imaginaire, enlever tout résidu réel

B= -u2*(1+C)-D; % est également purement imaginaire

v4= (u4+B)/(C*u4+D);

% the modulus is k^2
k= 1/v4;
k= real(k);

% the cell constant kappa
kappa= 4 * ellipke (k^2) / ellipke (1-k^2);
```

```
function [Ez]= calculateEfield(height, B, C, D, k, voltage, particle_x, particle_y, dx, dy);

k= real(k); % opération nécessaire car ellipke demande ça

Ew= voltage / (4 * ellipke (k^2));

x= particle_x-dx:dx:particle_x+dx;
y= particle_y-dy:dy:particle_y+dy;

[X, Y] = meshgrid(x,y);

Z= complex(X, Y);
dudz= pi/height * cosh(pi*Z/height - i*pi/2);

U= sinh( pi/height*( Z - i*height/2 ));
dvdu= (D-B*C)./(D+C*U);

V= (U+B)./(C*U+D);
dwdv= 1./sqrt((1-k*k.*V.*V).*(1-V.*V));

Ez= Ew.*conj(dwdv).*conj(dvdu).*conj(dudz);
```

```
function [px,py,p_vx, p_vy] = track1Particle(height, elec, gap, particle_radius, ReCMBOT, ReCMTOP, ...
    particle_start_x, particle_start_y, fluid_velocity_x, voltageBOT, voltageTOP, ...
    graph_width, precision_dx, dt, permitt, visco)

[B, C, D, k]= calculateCellConstant(elec, gap, height);

particle_x= particle_start_x;
particle_y= particle_start_y;

particle_vx= 0;
particle_vy= 0;

% time precision dt given external
time_ctr= 0;

dx= precision_dx;
dy= dx;

px= [];
py= [];

p_vx= [];
p_vy= [];

stopcondition= false;

while (~stopcondition)
    time_ctr= time_ctr+1;

    px(time_ctr)= particle_x;
    py(time_ctr)= particle_y;

    p_vx(time_ctr)= particle_vx;
    p_vy(time_ctr)= particle_vy;

    [EzBOT]= calculateEfield(height, B, C, D, k, voltageBOT, particle_x, particle_x, dx, dy);
    [EzTOP]= calculateEfield(height, B, C, D, k, voltageTOP, particle_x, height-particle_y, dx, -dy);

    [fx, fy] = calculateForces(EzBOT, EzTOP, particle_radius, ReCMBOT, ReCMTOP, precision_dx, permitt, \

    particle_vx= fx + fluid_velocity_x; % ignoring the velocity at t0
    particle_vy= fy + fluid_velocity_y;

    particle_x= particle_x + dt*particle_vx;
    particle_y= particle_y + dt*particle_vy;

    stopcondition= (particle_x > graph_width/2);
    stopcondition= stopcondition | (particle_y > height);
    stopcondition= stopcondition | (particle_y < 0);
    stopcondition= stopcondition | time_ctr>1000;

end;%while

% final location of each track
particle_x;
particle_y;
```

```
function [fx, fy] = calculateForces(EzBOT, EzTOP, particle_radius, ReCMBOT, ReCMTOP, precision_dx, permi

%%% corrected version: see footer: factor 2


dx= precision_dx;
dy= dx;

%%% scalar products of complex matrices, thomas' trick: scalarproduct= Re{Z * conj(Z)}

EzTOP= conj(EzTOP); %%% very important: flip the y-axis of the TOP field before continuing

Ezz2BOT= real(EzBOT.*conj(EzBOT));
Ezz2TOP= real(EzTOP.*conj(EzTOP));

[gradvect_xBOT, gradvect_yBOT]= gradient(Ezz2BOT,dx,dy);
[gradvect_xTOP, gradvect_yTOP]= gradient(Ezz2TOP,dx,dy);

gradient_xBOT= gradvect_xBOT(2:2);
gradient_yBOT= gradvect_yBOT(2:2);
gradient_xTOP= gradvect_xTOP(2:2);
gradient_yTOP= gradvect_yTOP(2:2);

fxBOT= permitt / 6 / visco * ReCMBOT * particle_radius^2 * gradient_xBOT *2 ;  %%% see at footer
fyBOT= permitt / 6 / visco * ReCMBOT * particle_radius^2 * gradient_yBOT *2 ;
fxTOP= permitt / 6 / visco * ReCMTOP * particle_radius^2 * gradient_xTOP *2 ;
fyTOP= permitt / 6 / visco * ReCMTOP * particle_radius^2 * gradient_yTOP *2 ;

fx= fxBOT+fxTOP;
fy= fyBOT+fyTOP; %%% the + sign is correct as the system has already been flipped once

%{
dielectrophoresisX= pi * permitt * ReCM * particle_radius^3 * gradient; !!!FALSE: factor 2 was missing
stokes= 6 * pi * eta * particle_radius;
f= dielectrophoresisX/stokes;
%}

% difference between jones (eq. 2.46) and morgan (4.9): factor 2 between expressions for DEP
```

Urban Seger-Sauli

Date of Birth	January 26th 1974
Nationality	Swiss
Marital Status	Married
Languages	German
	French
	English

Educational Background

2001-2006	Swiss Federal Institute of Technology Lausanne (EPFL)
	Grade expected: PhD in microtechnology Area of specialisation: Electrical cell manipulation
2001	University of Lausanne / University of Geneva / EPFL
	Grade obtained: Postgraduate diploma in biomedical engineering Area of specialisation: Cell deflection by dielectrophoresis
1994-2000	University of Neuchâtel
	Grade obtained: Diploma in physical electronics Area of specialisation: Microfluidic droplet dispensing
1989-1994	Kantonsschule Romanshorn
	Grade obtained: Matura (High school degree) Area of specialisation: Sciences

Employment History

2001-2006	Swiss Federal Institute of Technology Lausanne (EPFL)
	PhD studies in cell handling and modification by electric fields in microfabricated fluidic devices
2000-2001	Disetronic Medical Systems AG, Burgdorf: Innovation Group
	Development of methods to identify thermo-related differences between syringe pumps using polymer or glass cylinders [3 months appointment]
2000	Sercalo Microtechnology Ltd., Neuchâtel: Device Packaging Team
	Process ramp-up from prototype to small-series packaging of 8-channel MEMS optical attenuators [3 months appointment]
2000	Microchemical Systems SA, Corcelles: Electronics Laboratory
	Participation in the conception and fabrication of a self-calibrating digital module interfacing resistive gas sensors [3 months appointment]

Summary of Experience

Microtechnology	Design and fabrication of microfluidic bioinstruments in a clean room
Biotechnology	Assays related to biological cells suspended in media, cell culturing
Engineering	Discrete electronic circuits, data acquisition and analysis, FE modelling
Leadership	Supervision of students, collaboration with internal and external partners

Publications

P. Linderholm, U. Seger, P. Renaud. *Analytical expression for the electric field between two facing strip electrodes in a microchannel*, accepted for publication, IEE Electronics Letters.

U. Seger, M. Panayiotou, S. Schnydrig, M. Jordan, P. Renaud. *Temperature measurements in microfluidic systems: Heat dissipation of negative dielectrophoresis barriers*, Electrophoresis, 26, pp.2239-2246, 2005.

S. Gawad K. Cheung, U. Seger, A. Bertsch, P. Renaud. *Dielectric spectroscopy in a micro-machined* flow *cytometer: theoretical and practical considerations*, Lab on a Chip, 4(3), pp.241-251, 2004.

U. Seger, S. Gawad, R. Johann, A. Bertsch, P. Renaud. *Cell immersion and cell dipping in microfluidic devices*, Lab on a Chip, 4(2), pp.148-151, 2004.

Abstracts in Conference Proceedings

U. Seger, T. Braschler, N. Demierre, P. Linderholm, V.L. Sukhorukov, U. Zimmermann, P. Renaud. *Pressure-balanced 2-dimensional positioning of single cells in microchannels*, European Conference on Micro & Nanoscale Technologies for the Biosciences (NanoTech), Montreux, Switzerland, 2 pages, 2005.

U. Seger, S. Schnydrig, S. Gawad, P. Renaud. *Temperature distribution and risk of thermal cell damage near active nDEP-barriers in microfluidic channels*, NanoTech, Montreux, Switzerland, 2 pages, 2004.

U. Seger, S. Gawad, M. Tonteling, R. Johann, H. Vogel, P. Renaud. *Microfluidic cell immersion on-chip cell viability test*, Micro Total Analysis Systems Conference (µTAS), Malmö, Sweden, pp.270-272, 2004.

U. Seger, S. Gawad, P. Renaud. *In situ microfluidic cell dipping*, NanoTech, Montreux, Switzerland, 2 pages, 2003.

U. Seger, S. Gawad, A. Scheer, P. Renaud. *Towards single-cell-controlled electroporation in a microfluidic device*, µTAS, Nara, Japan, pp.797-798, 2002.

U. Seger, A. Scheer, S. Gawad, P. Renaud. *Impedance monitoring of single-cell electroporation in a microfluidic device*, NanoTech, Montreux, Switzerland, 2 pages, 2002.

Supervision of Student Projects

R. Tornay, *Software-controlled real-time sorting of individual cells in flow*, Diploma Project, 2004/2005.

S. Schnydrig, *Temperature detection in microfluidic systems – Study of thermal side-effects of dielectrophoresis*, Semester Project (Collaboration with EPFL, LBCH, Prof. R. Freitag), 2004.

M. Tonteling, *Capture, immersion and electropermeabilisation of single cells*, Semester Project, 2003/2004.

F. Declercq, *nDEP-based electronic detection of cells captured in microfluidic devices*, Semester Project, 2003/2004.

A. Hmamda, *Optical real-time detection of electropermeabilisation*, Diploma Project, 2003.

N. Demierre, *DEPDEF: A dielectrophoretic deflection filter for biological matter*, Semester Project (Collaboration with EPFL, LCPPM, Prof. H. Vogel), 2003.

V. Gfeller, *Design and fabrication of a pulse generator for electroporation of individual cells in microchannels*, Semester Project, 2002.